Very long baseline interferometry of radio-loud active galactic nuclei, the multimessenger connection

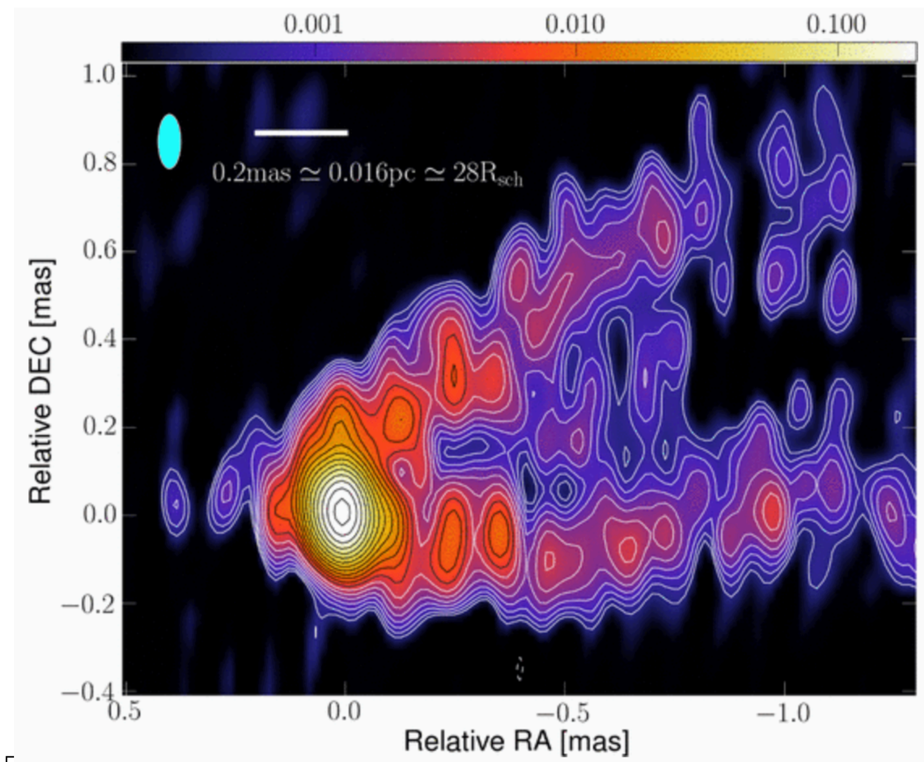

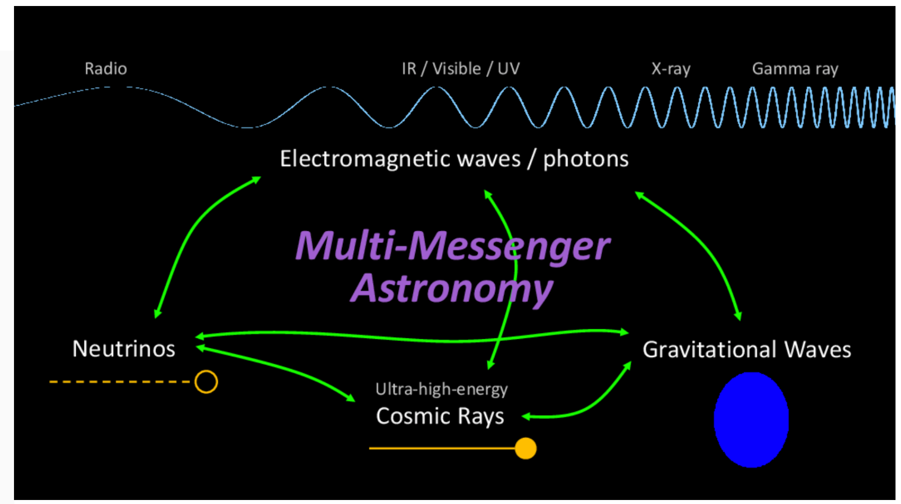

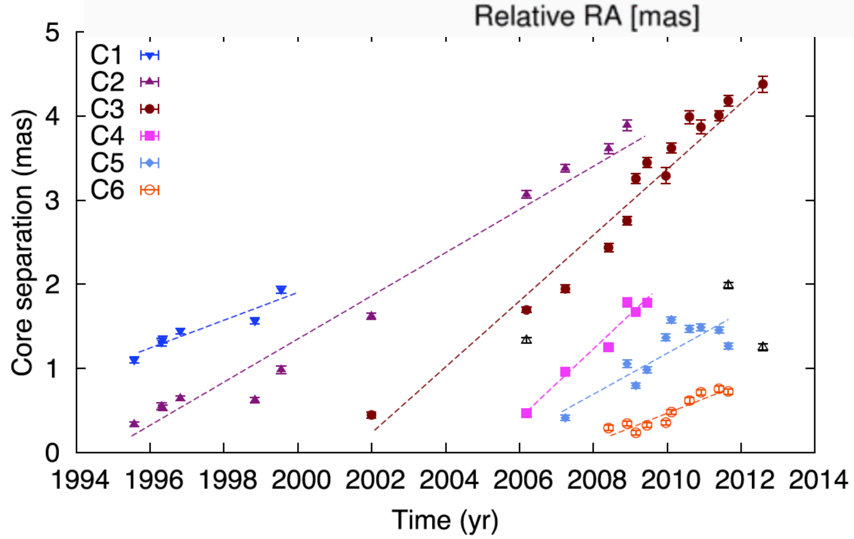

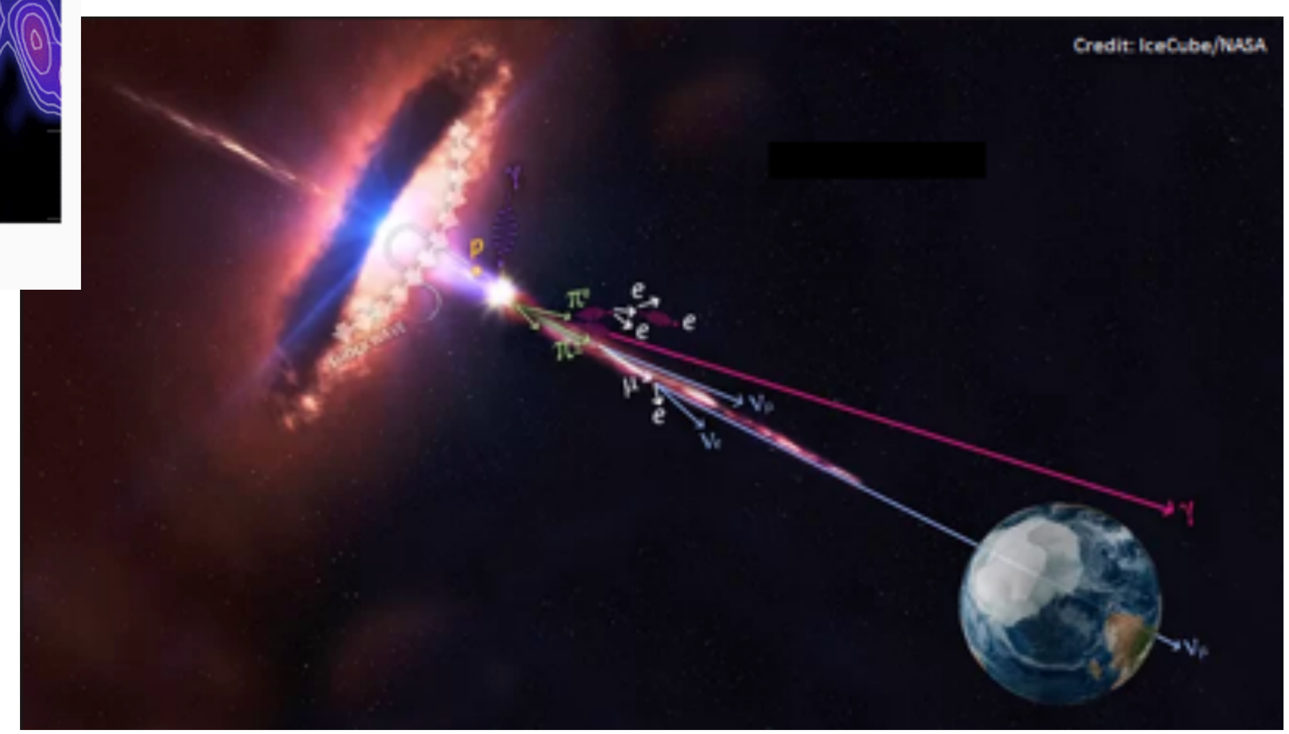

Emma Kun
Konkoly Observatory, Budapest, Hungary
20 May 2022, CRC ring lecture series

Active galactic nuclei

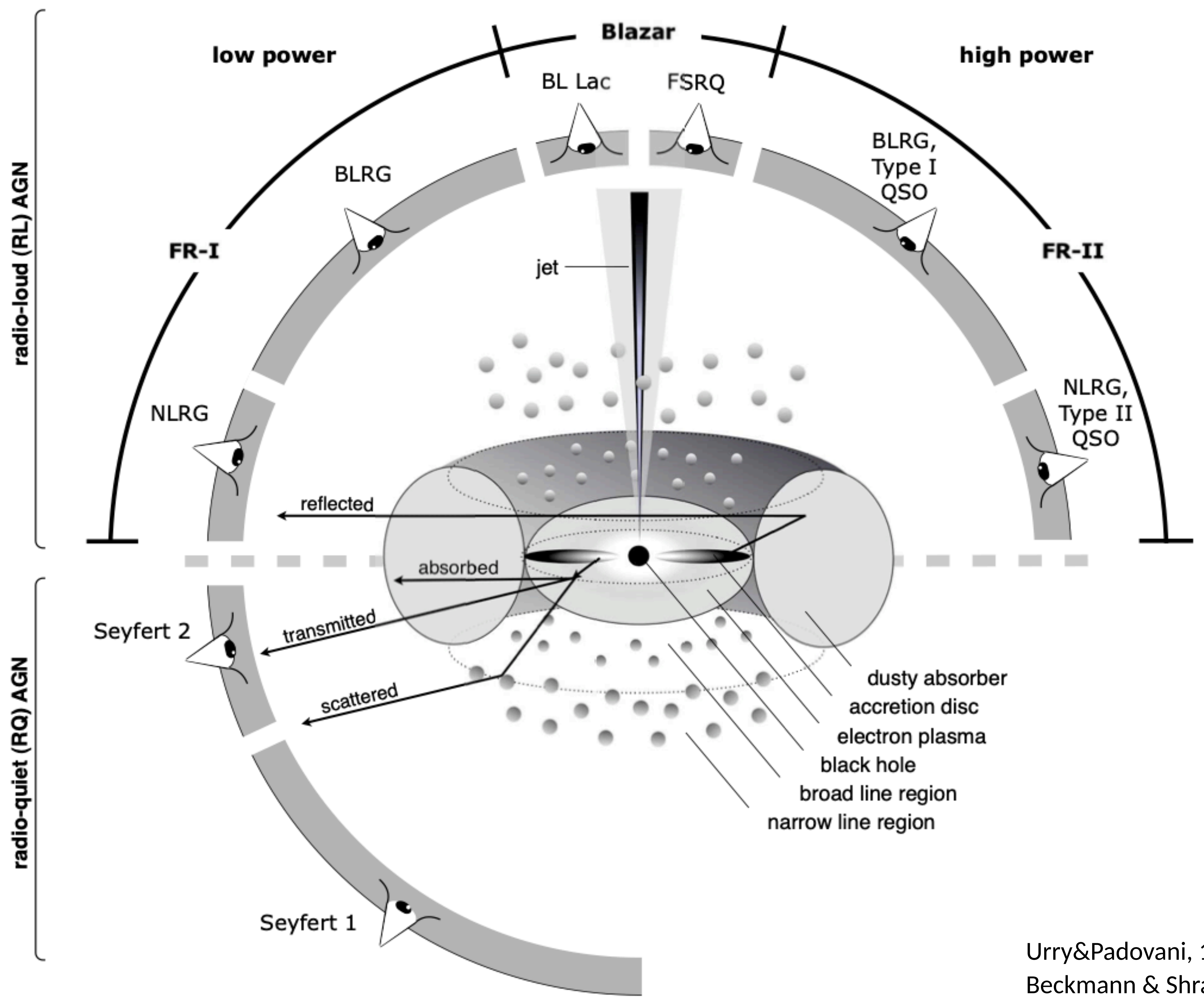

Urry&Padovani, 1995, PASP,107, 803
Beckmann & Shrader, 2012
illustration by Marie-Luise Menzel, 2012

The continuum spectrum of AGN

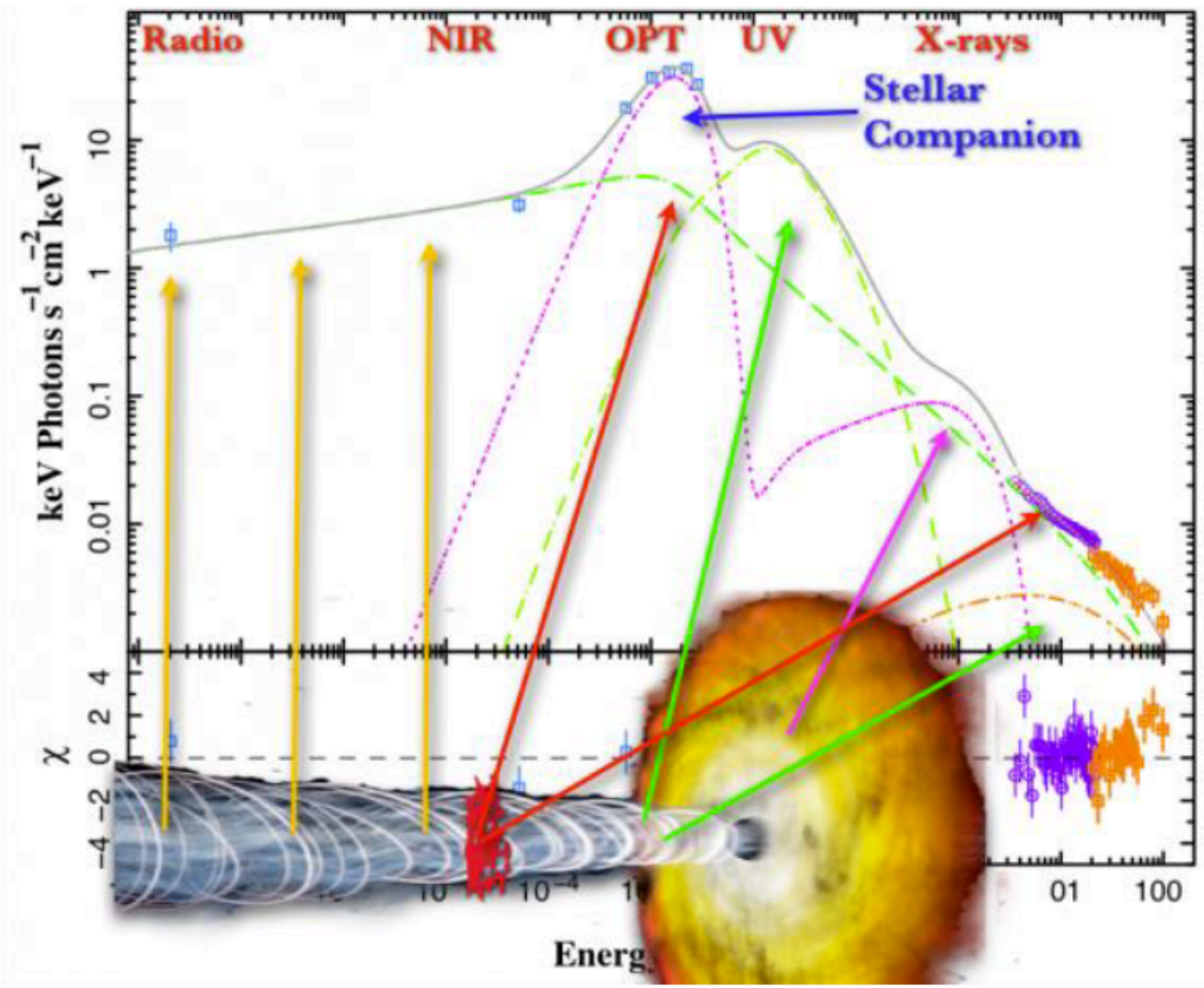

Schematic overview of a broadband jet model and the various components contributing to the spectral energy distribution (Migliari et al. 2007).

Relativistic jets

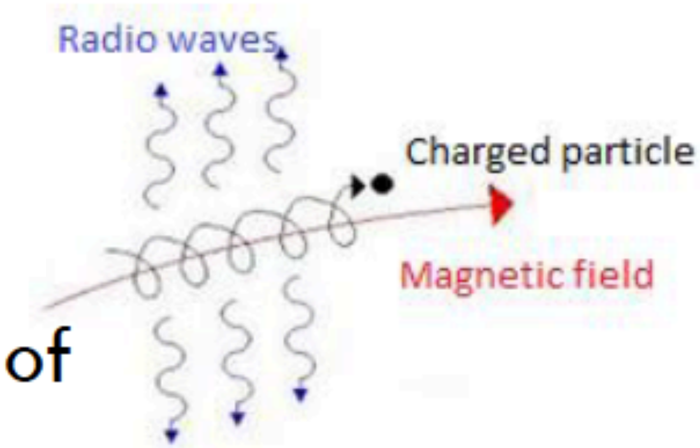

Blandford–Znajek-effect

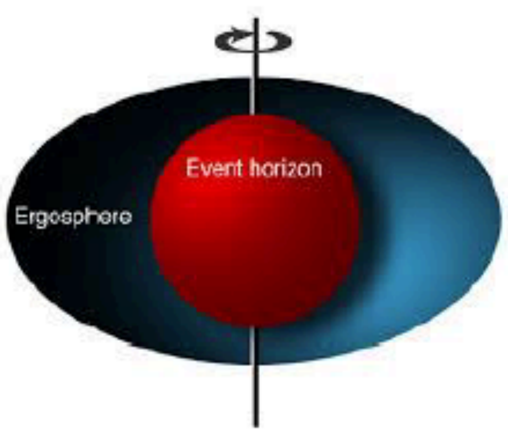

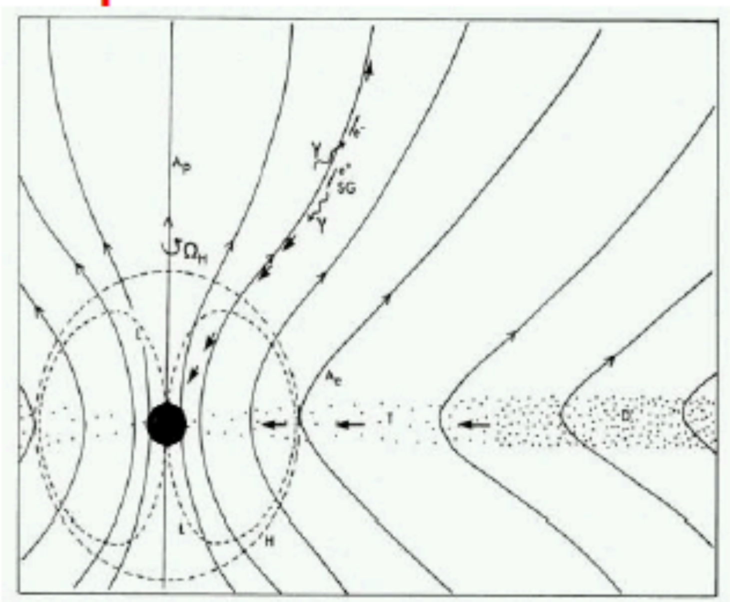

Critical frecquency of synchrotron radiation:

$$\upsilon_{c,e^-} = \frac{3}{4\pi}\frac{eB\chi}{m_{0,e^-}c}\gamma^2 = 16{,}1 \times \left(\frac{B\chi}{\mu G}\right)\left(\frac{E}{GeV}\right)^2 \text{ MHz}$$

B_χ=0,1μG, E=10GeV → $\upsilon_{c,e^-} \approx 160$ MHz

The collimated jets are observed as radio loud AGN

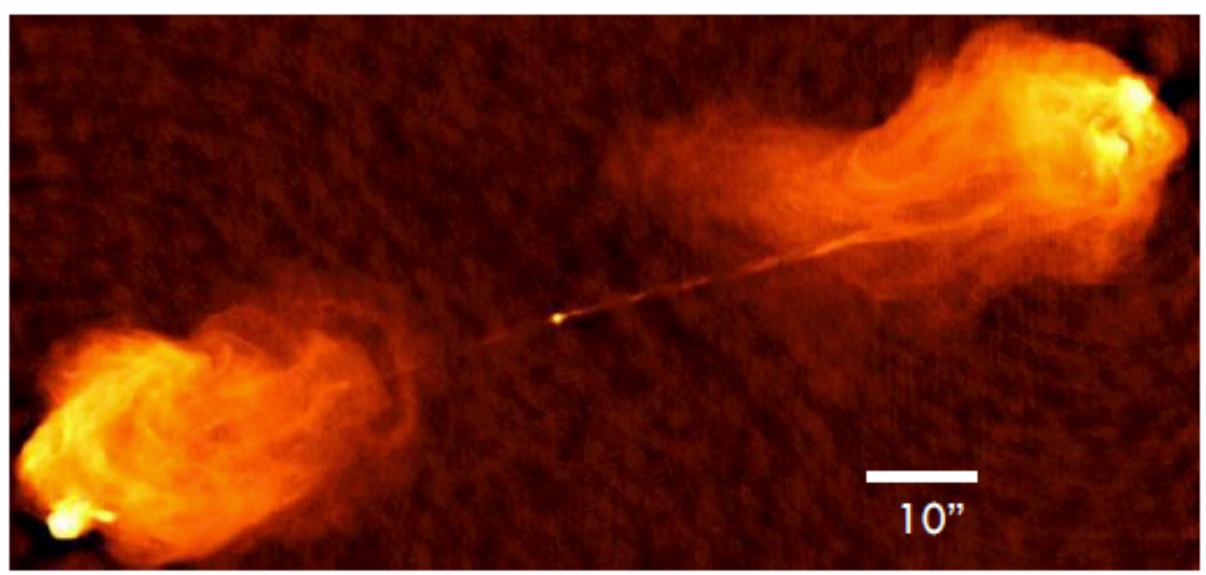

The Cygnus–A AGN at 5GHz (VLA)
The source-distance is 760 mega-lightyear (z=0,056, scale 1,096kpc/”)
National Radio Astronomy Observatory (NRAO)

Apparent superluminal motion

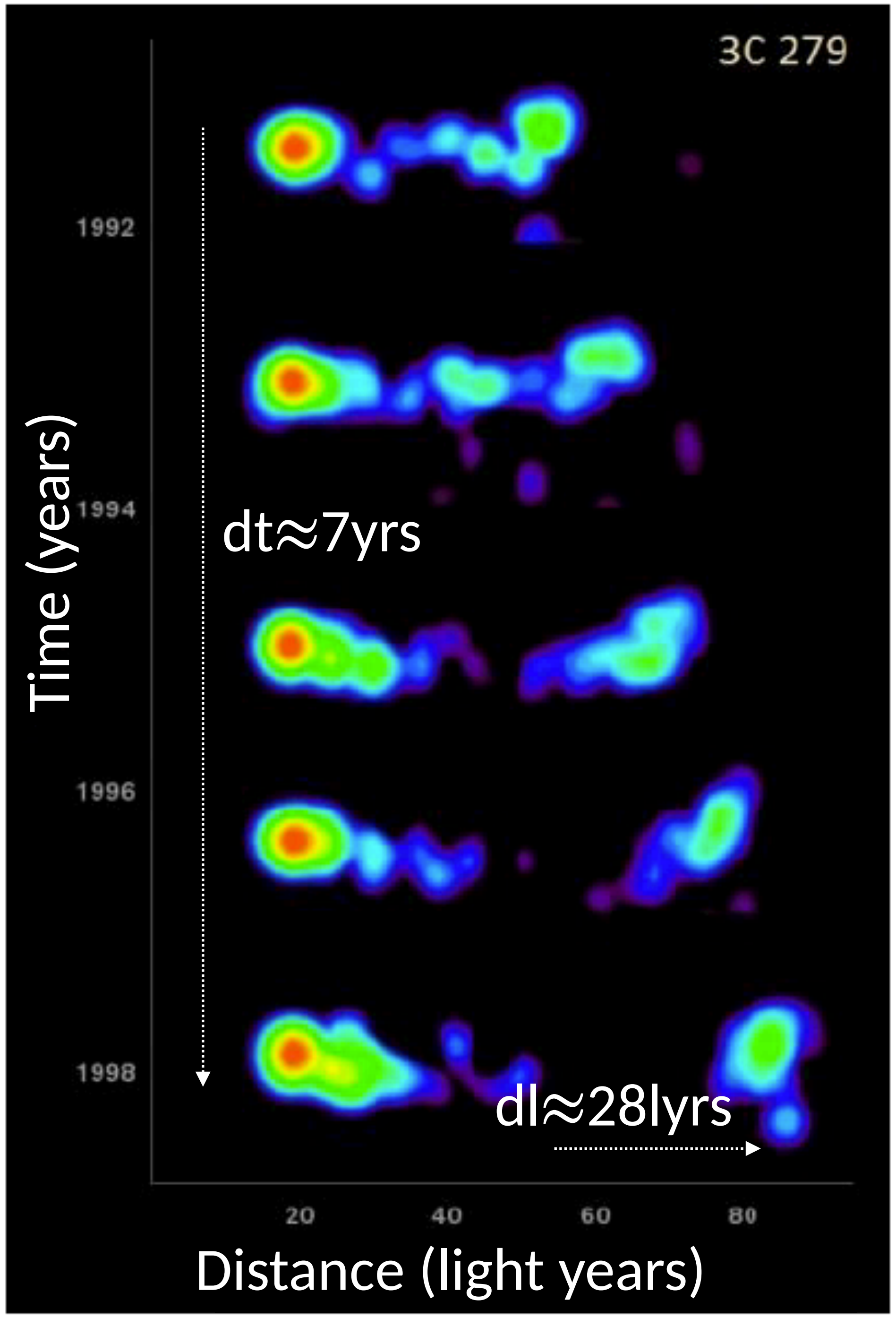

Jet moving with apparent superluminal speed.
Source : NRAO

Due to projection effects in relativistic jets

$$\beta_{app} = \frac{\beta \sin \iota}{1 - \beta \cos \iota}$$

β_{app}: apparent speed (in unit of c)
β: jet speed (in unit of c)
ι: „inclination” angle

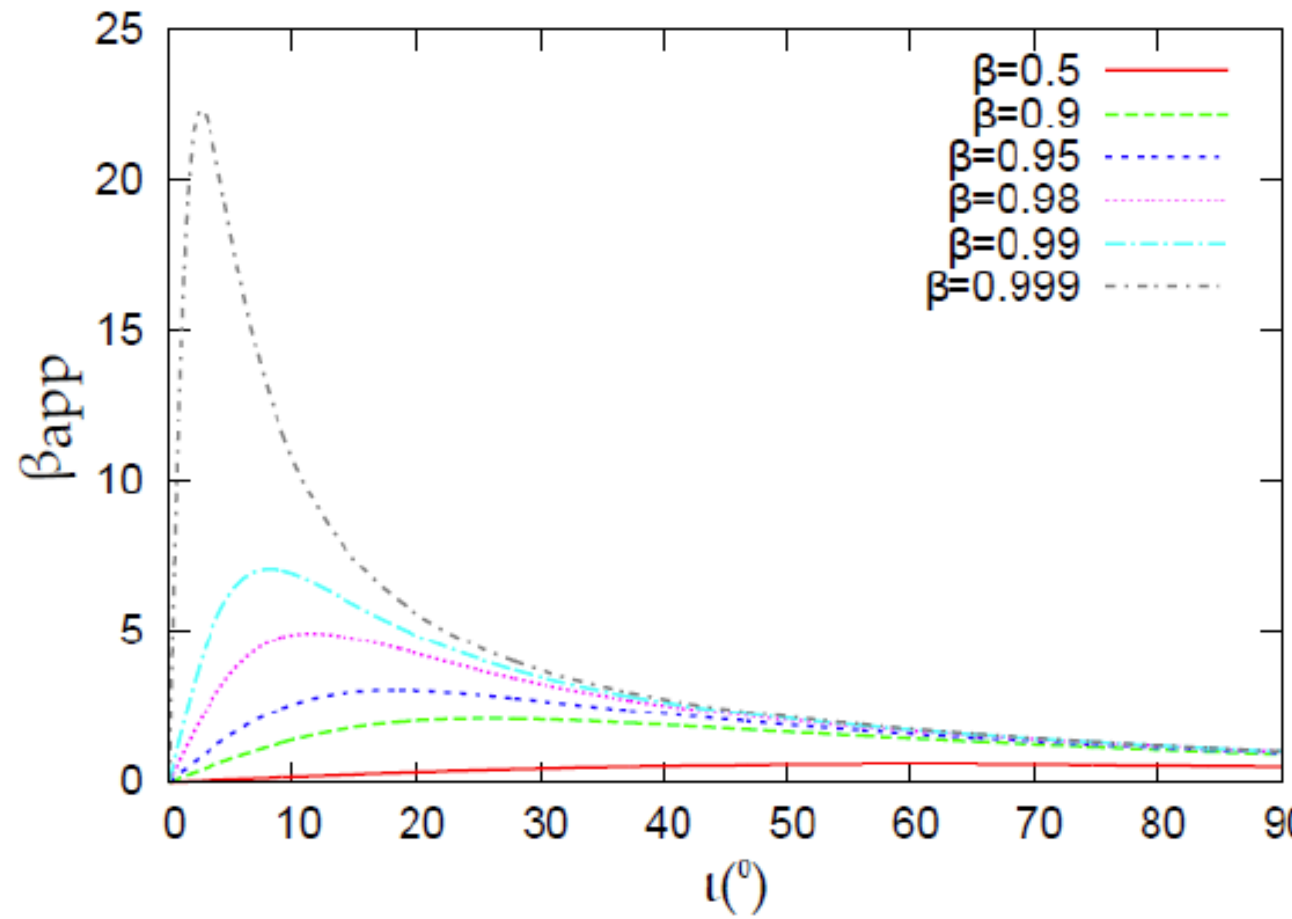

$dl/dt \approx 4c$ (impossible according to first postulate of the special relativity)

Relativistic beaming

- The synchrotron radiation is beamed within a cone having half-opening angle $\sim 1/\gamma$ ($\gamma = 1/(1-\beta^2)^{1/2}$ Lorentz factor)

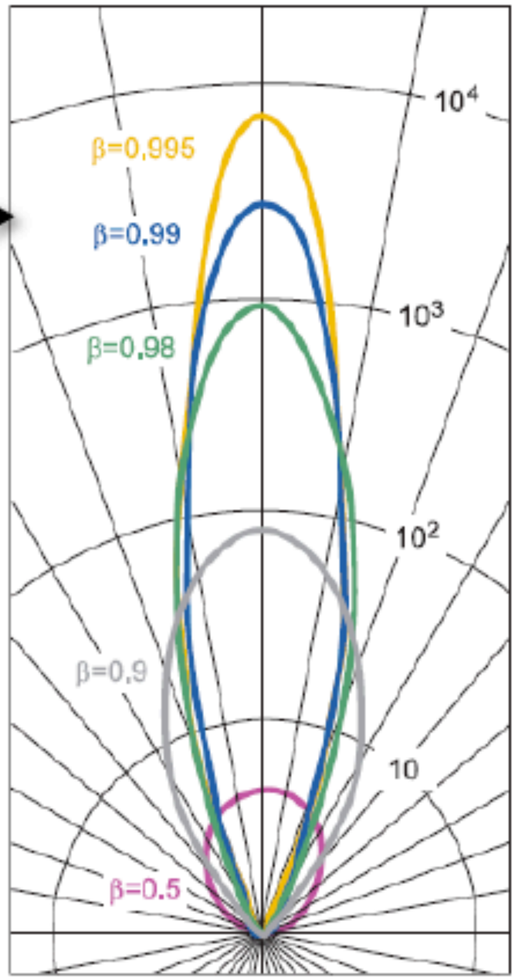

The apparent luminosity $L = L_0 \delta^n$ as function of the jetspeed and line-of-sight angle.
/Kellerman et al., 2007/

- $F_{obs}(\upsilon)$ apparent spectral flux density:

$$F_{obs}(\upsilon) = F(\upsilon)\delta^{\,n-\alpha}$$

(Jansky, $1\,Jy = 10^{-26}\ W/m^2/Hz$)

$\delta = 1/[\gamma(1-\beta\cos\iota)]$ Doppler factor,
α: spectral index,
n: jetgeometric factor

- Intrinsic flux density: $F(\upsilon) \sim \upsilon^{+\alpha}$
- Depending on the α spectral index, the continuum spectrum can be
  - inverted: $\alpha > 0$ (optically thick)
  - flat: $-0{,}5 < \alpha < 0$ (optically thick)
  - steep: $\alpha < -0{,}5$ (optically thin)
- The ratio of the Doppler beaming and debeaming

$$R = \left(\frac{1+\beta\cos\iota}{1-\beta\cos\iota}\right)^{(n+\alpha)}$$

E.g..: $\beta = 0{,}992$, $\iota = 7^0$, $n = 2$, $\alpha = -0{,}05 \rightarrow R = 13000$

- Only the approaching jet is seen if the jet is relativistic, and has small inclination

Relativistic beaming

(relativistic aberration, time dilatation, blue- or redshifting)

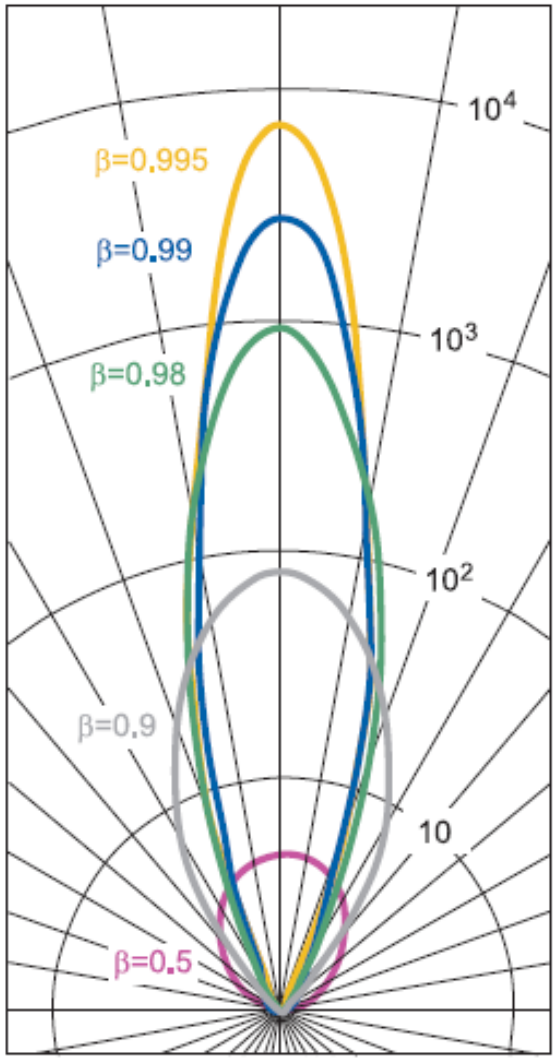

Light-house effect: the brightness of the light-source depends on the angle under which we sees its beam

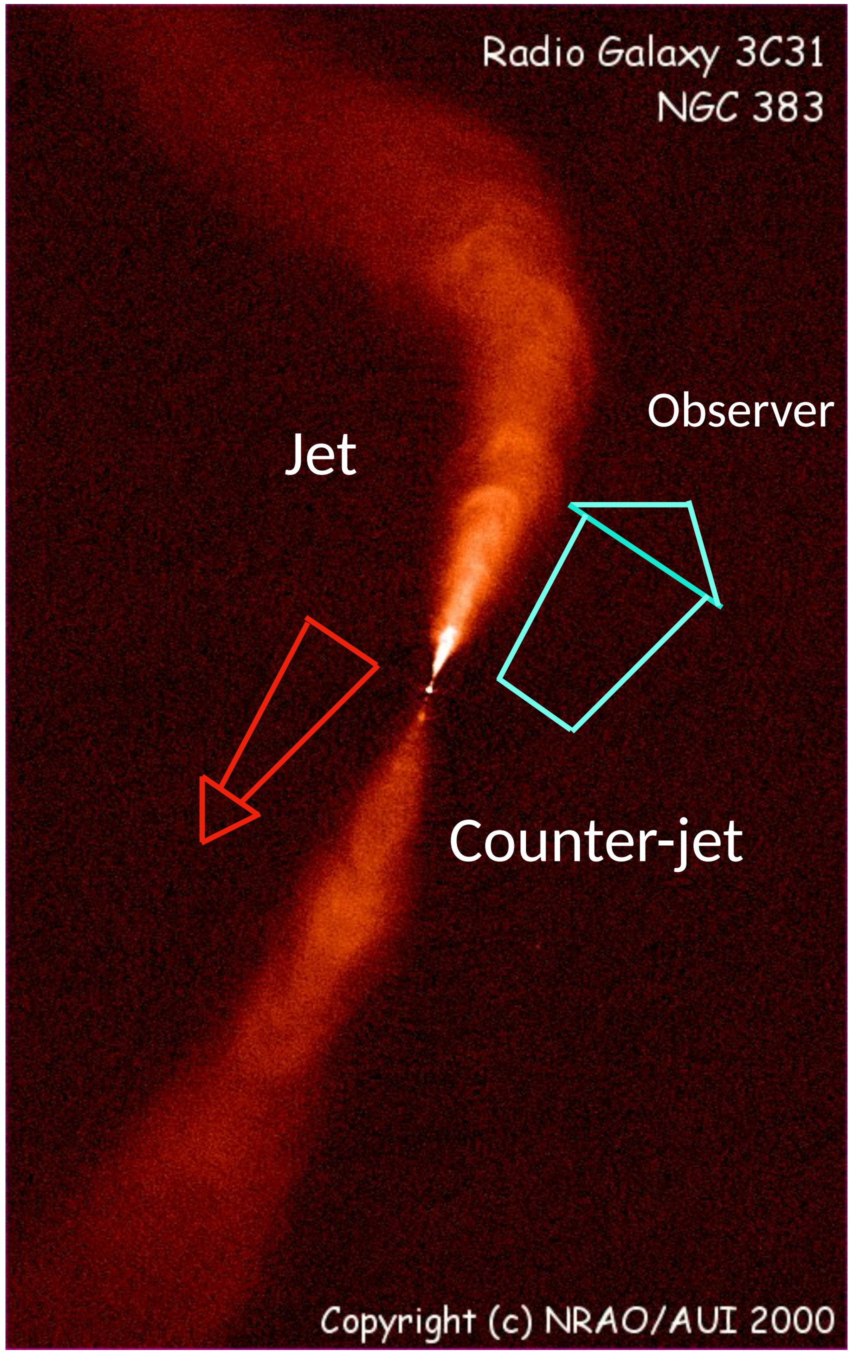

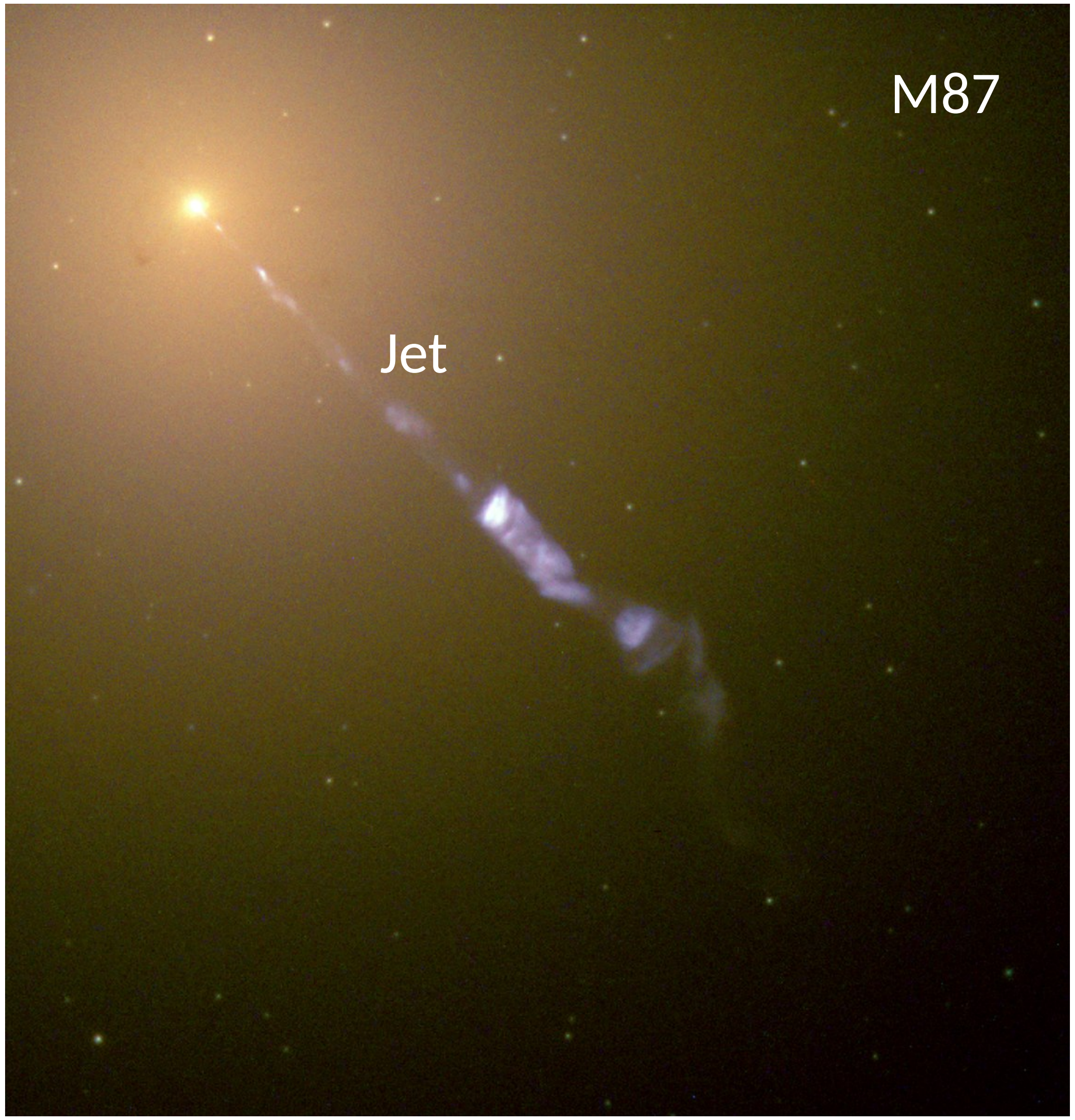

If the line-of-sight angle (inclination) is small (a few degrees, or smaller):
-> The jet is largely boosted
-> The counter-jet is largely de-boosted

With VLBI we see a core+jet structure

The continuum radio spectrum of AGN

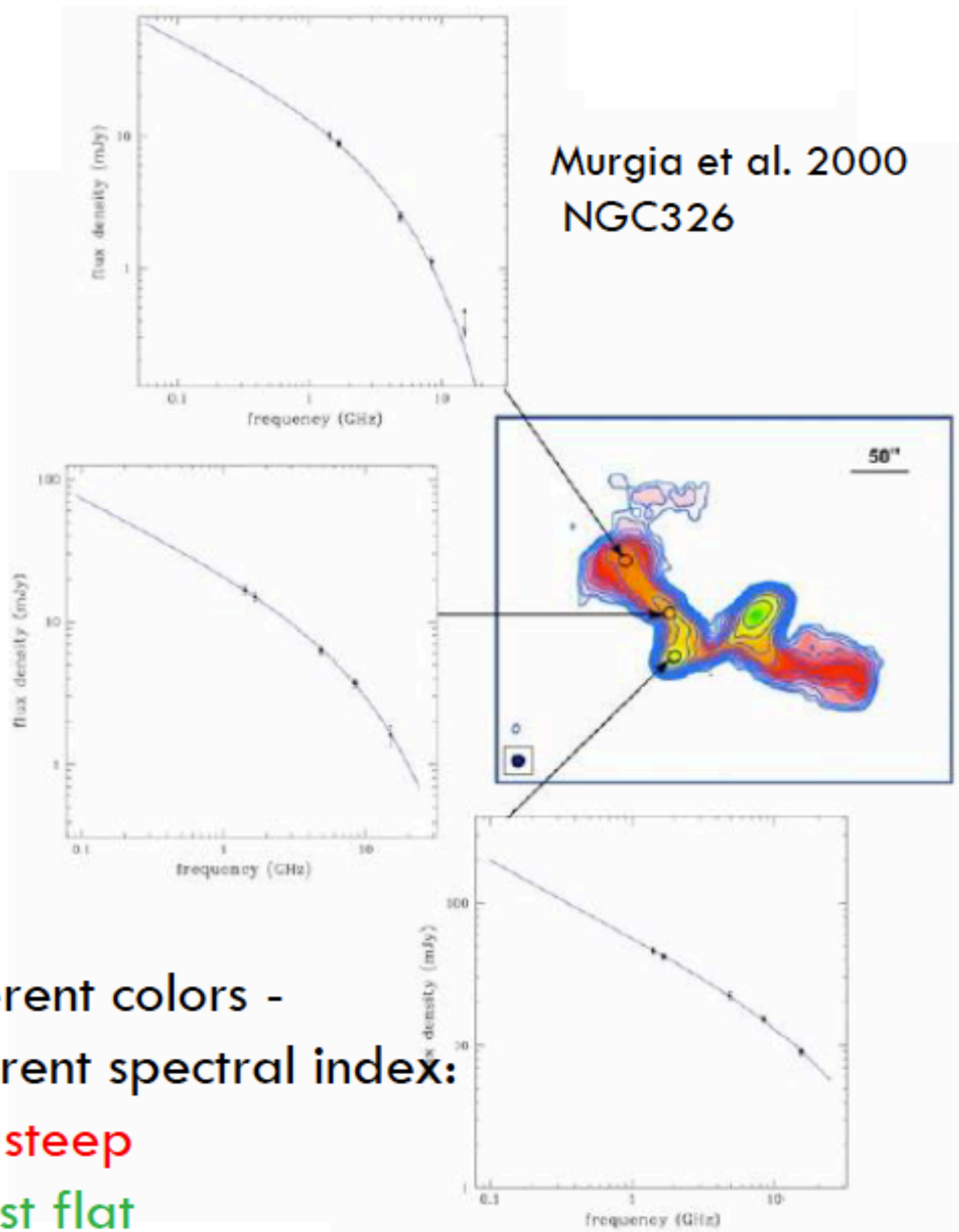

Murgia et al. 2000
NGC326

Different colors -
different spectral index:
very steep
almost flat

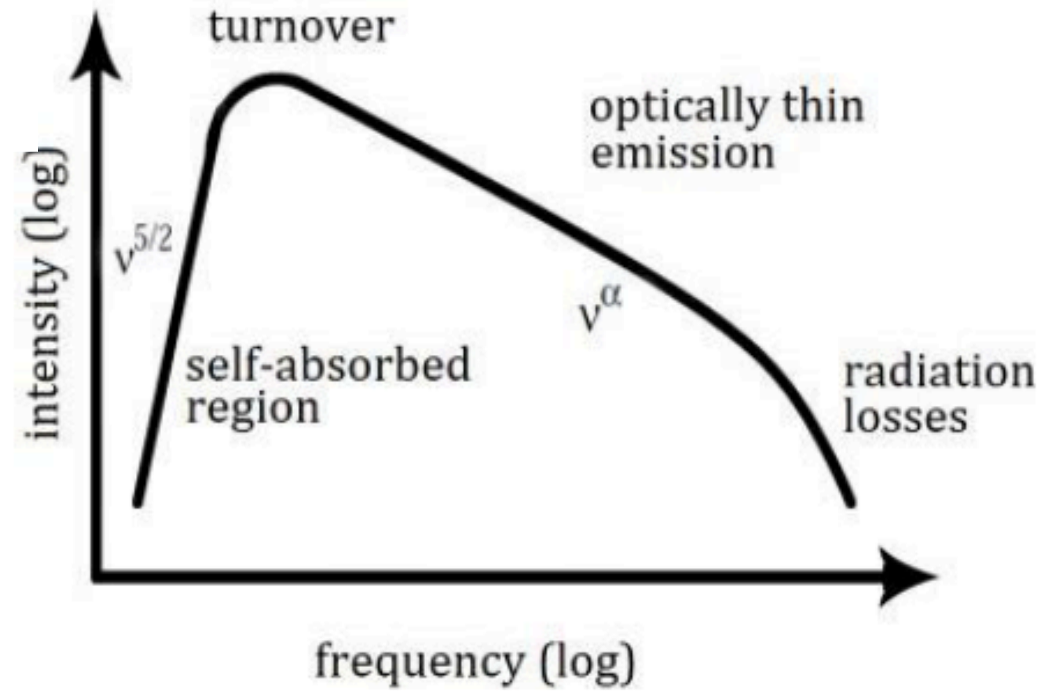

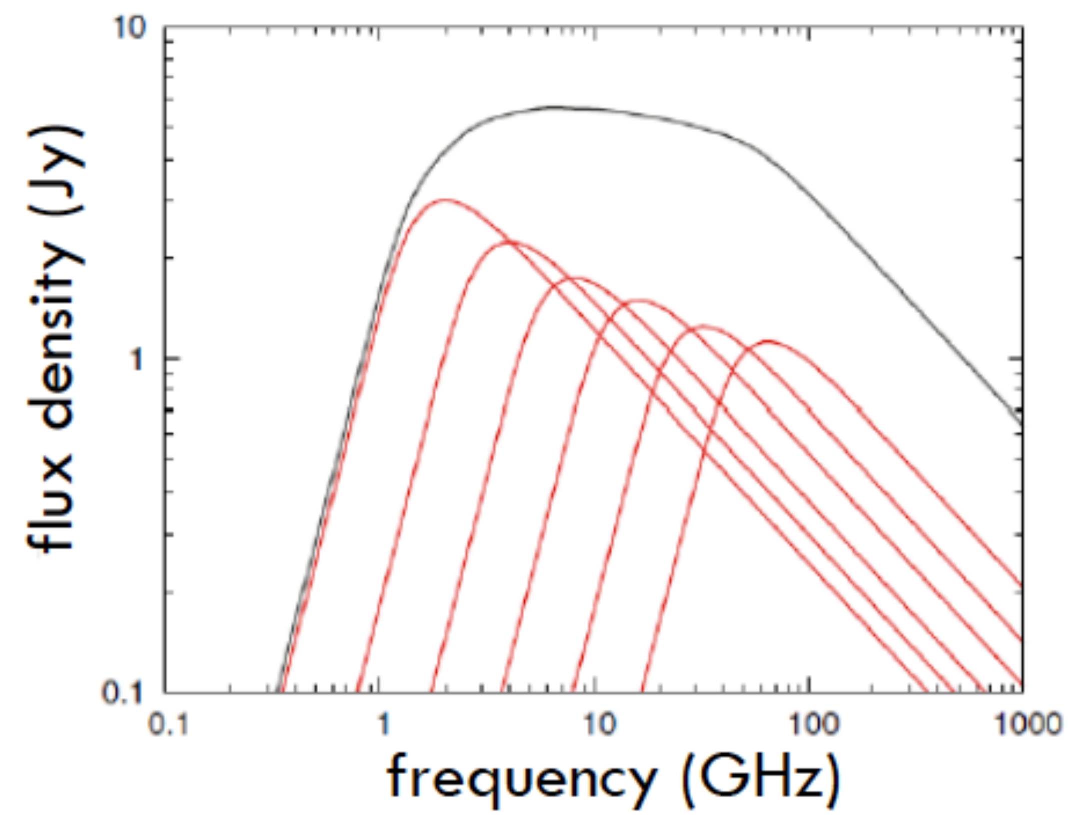

Flat spectrum is due to energetic electrons, with high Lorentz factors

Single-dish radio telescopes

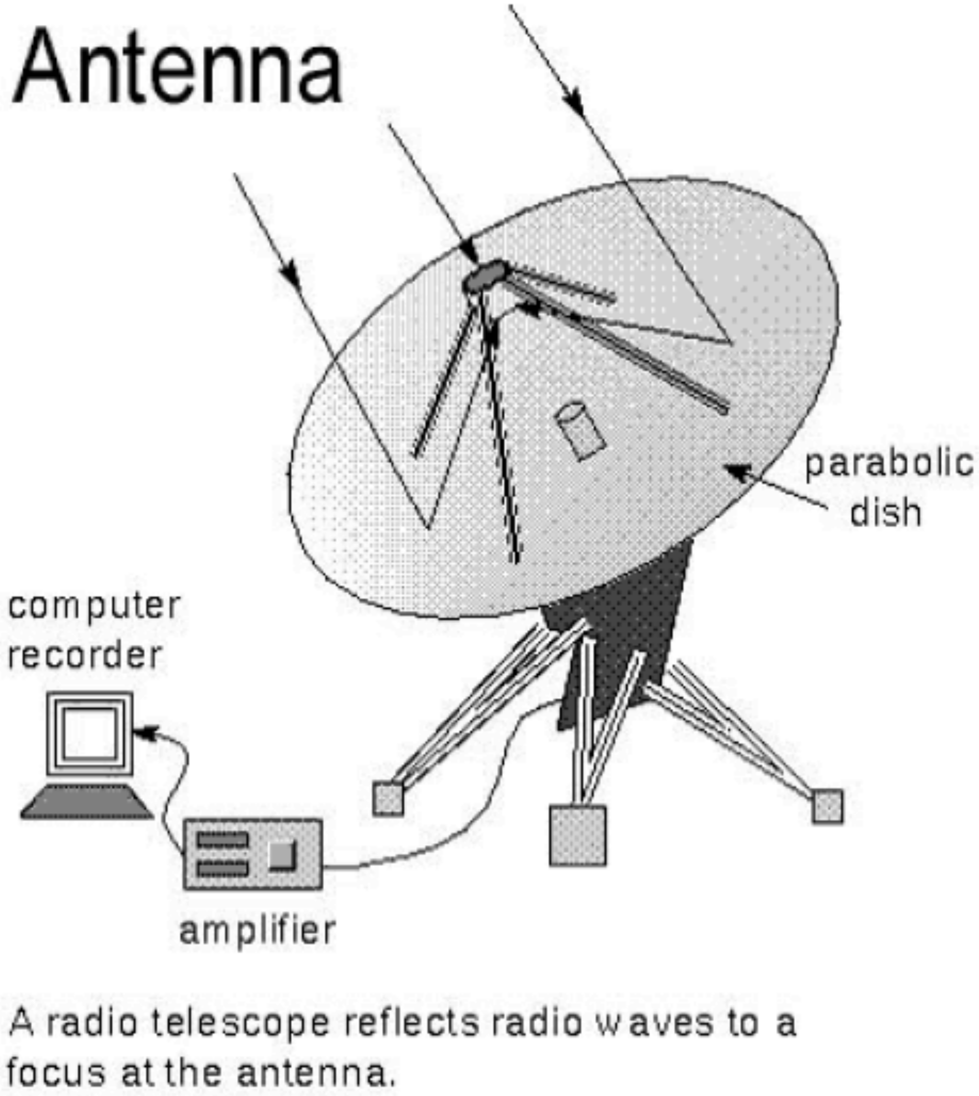

Paraboloid antennas: movable dish to follow the source, focusable radiation, weak signals can be amplified, diameter~sensitivity

Diffraction, antenna-beam

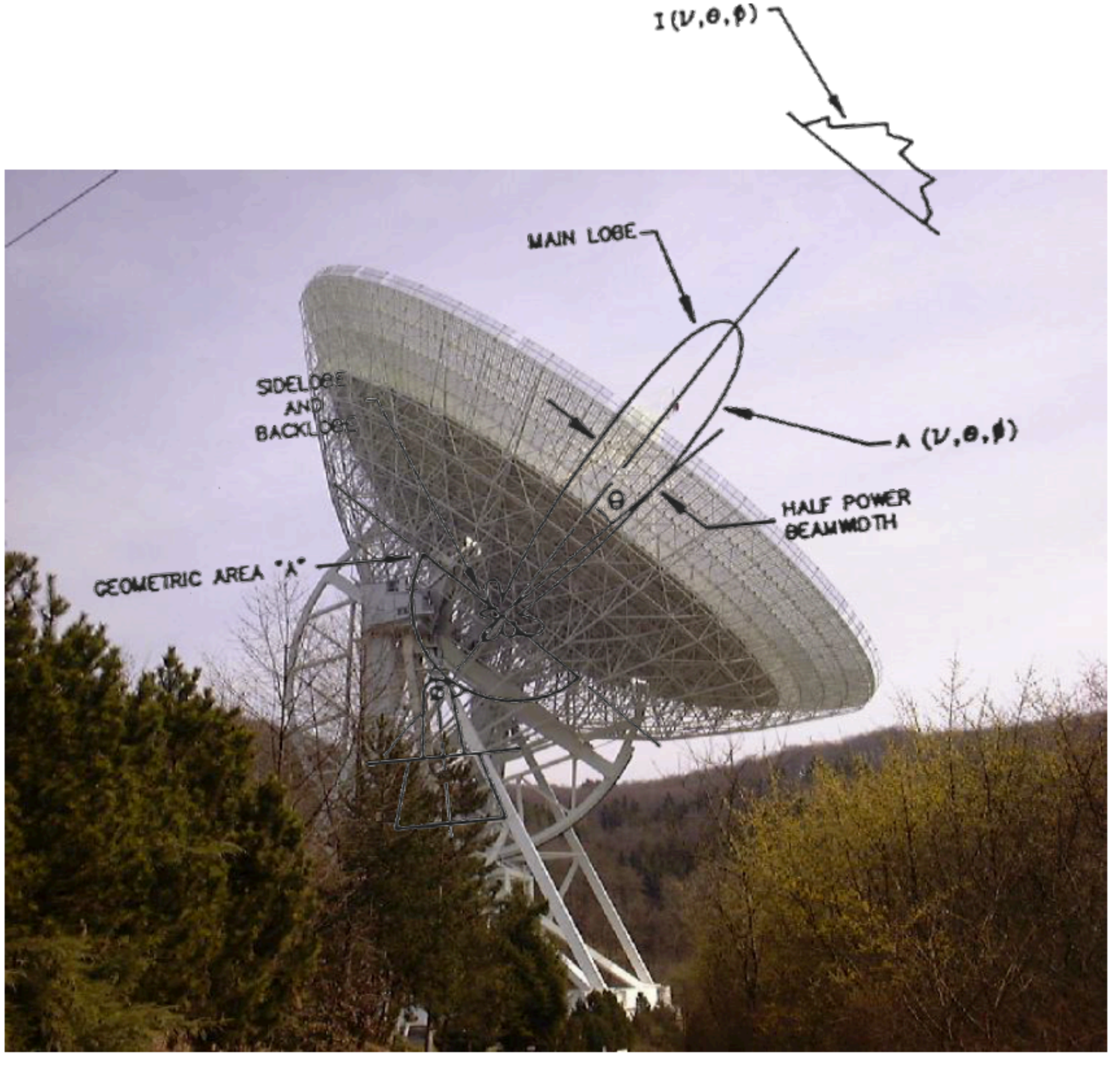

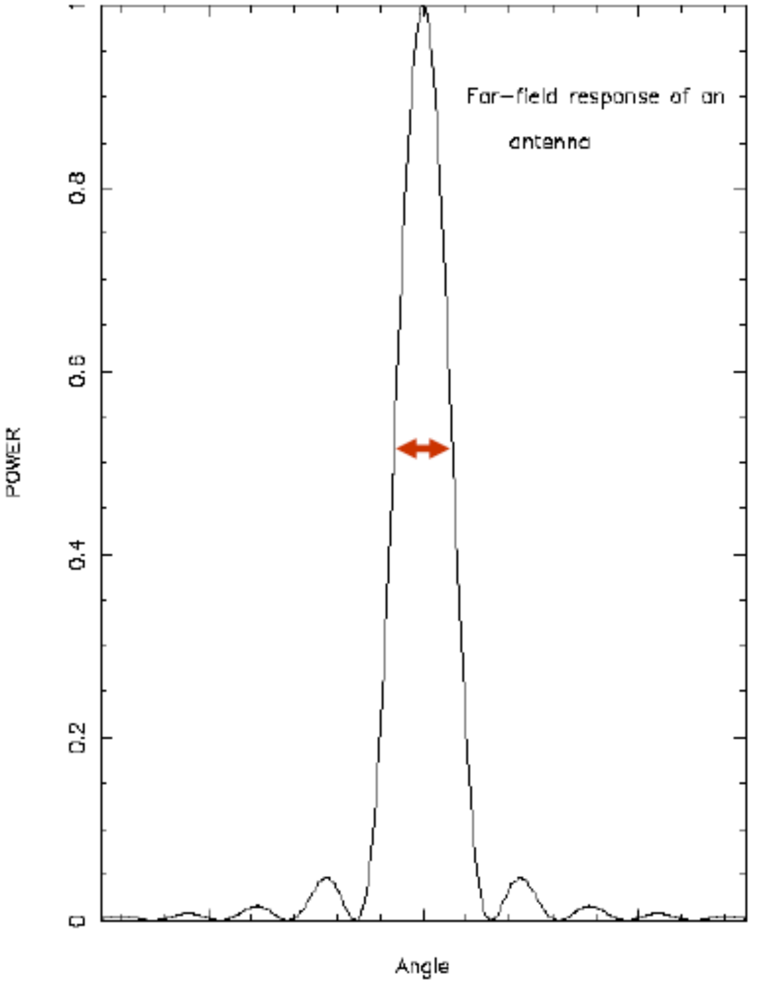

Diffraction pattern caused by the finite size of the aperture main lobe+side lobes

Half-power beamwidth: $\theta = 1.22\lambda/D$

Solid angle: $\Omega = \lambda^2/A$

Gain: $G = 4\pi/\Omega$

D: diameter of the dish

λ: wavelength of observation

A: surface of the dish

Diffraction, antenna beam

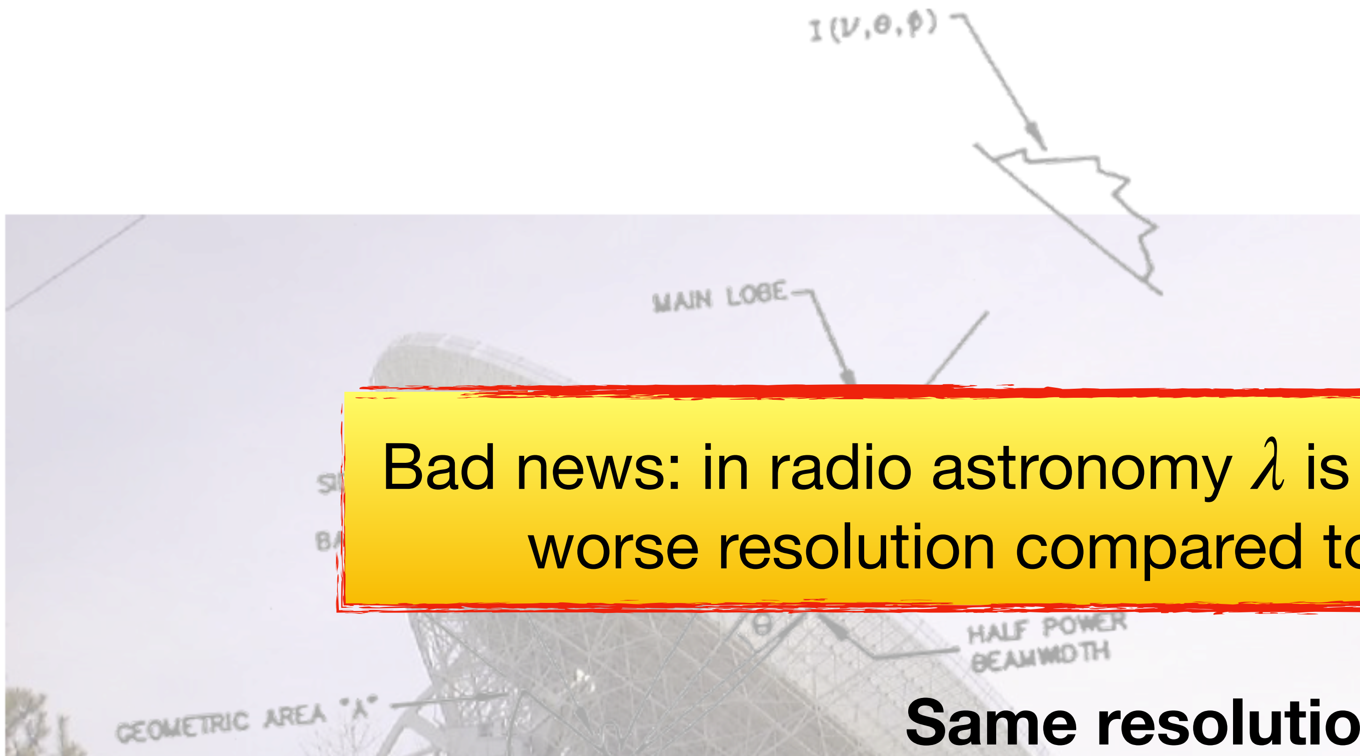

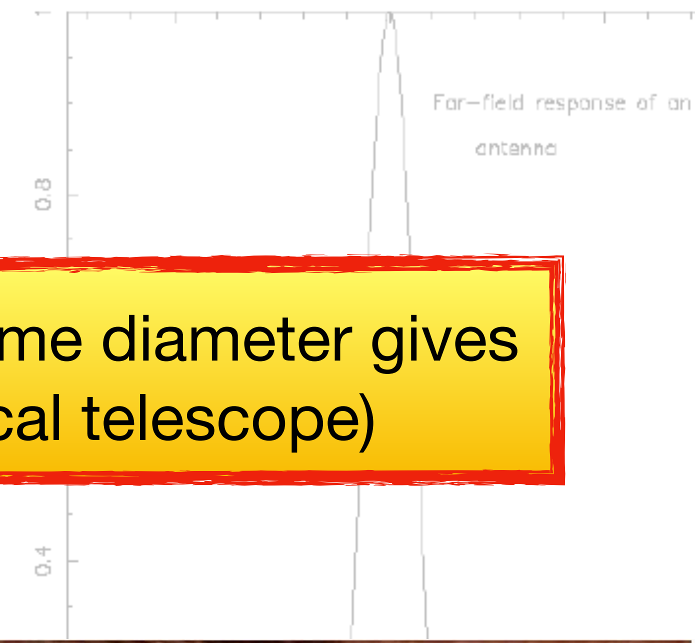

Bad news: in radio astronomy λ is large (same diameter gives worse resolution compared to an optical telescope)

Same resolution!

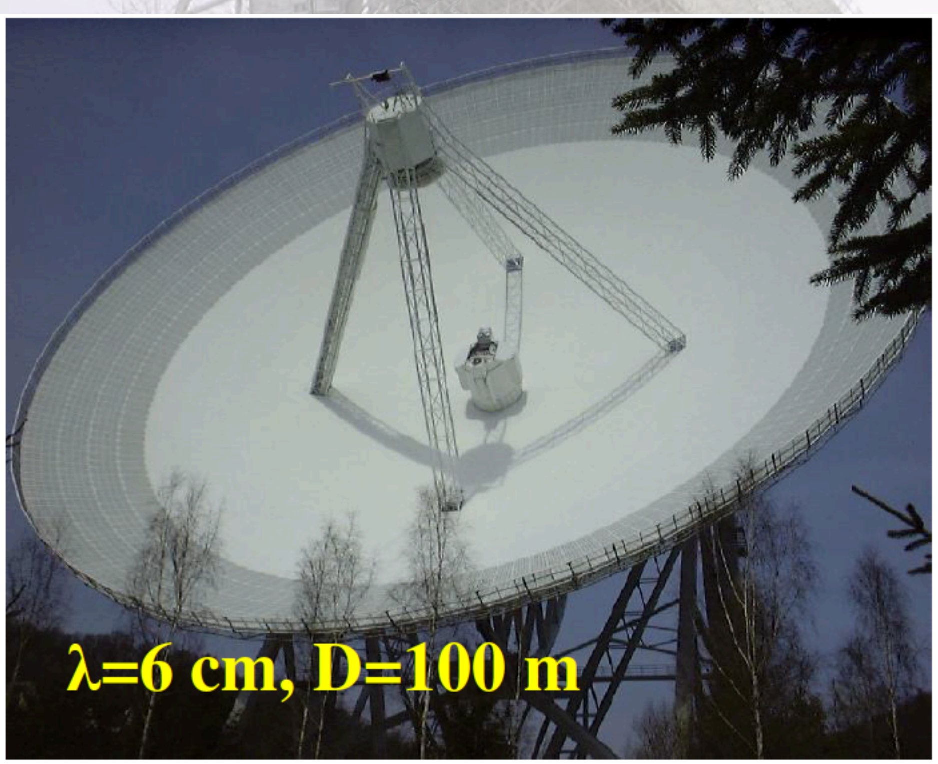

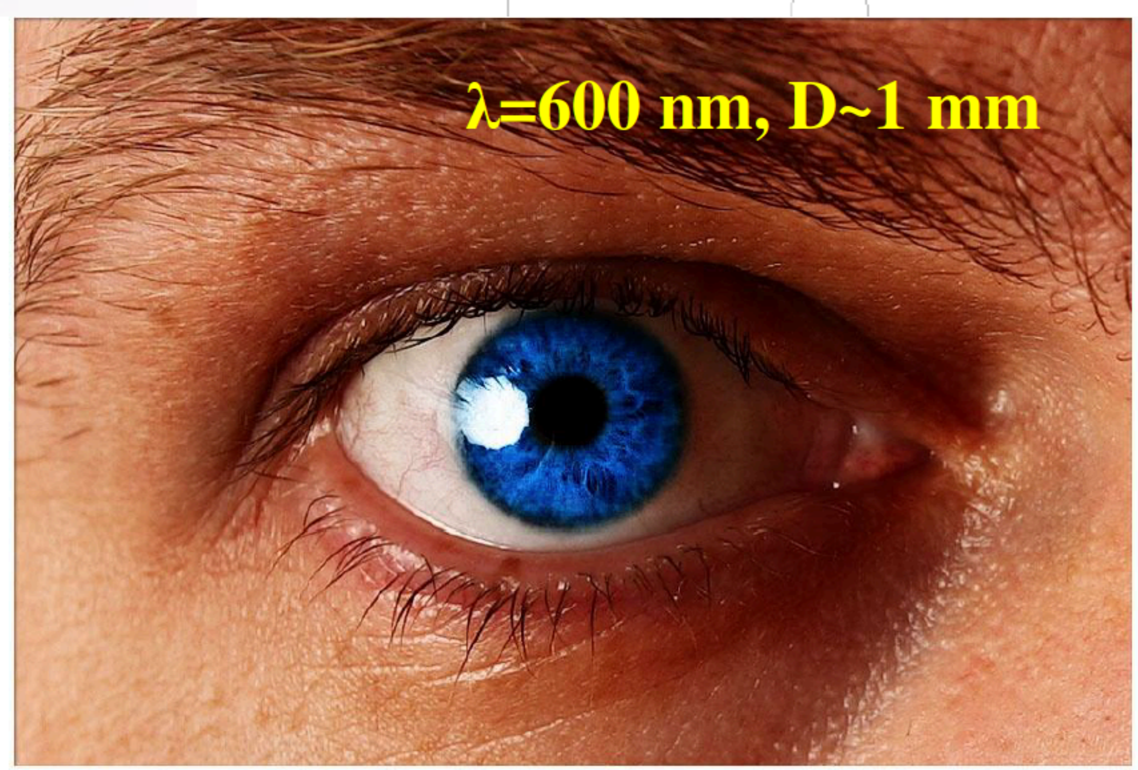

by

ire

Half

Soli

Gain: $G = 4\pi/\Omega$

λ: wavelength of observation

A: surface of the dish

Diffraction, antenna beam

Bad news: in radio astronomy λ is large (same diameter gives worse resolution compared to an optical telescope)

Good news: in radio astronomy *D* can be thousands of kilometers (we build that large dishes?? ofc. no…)

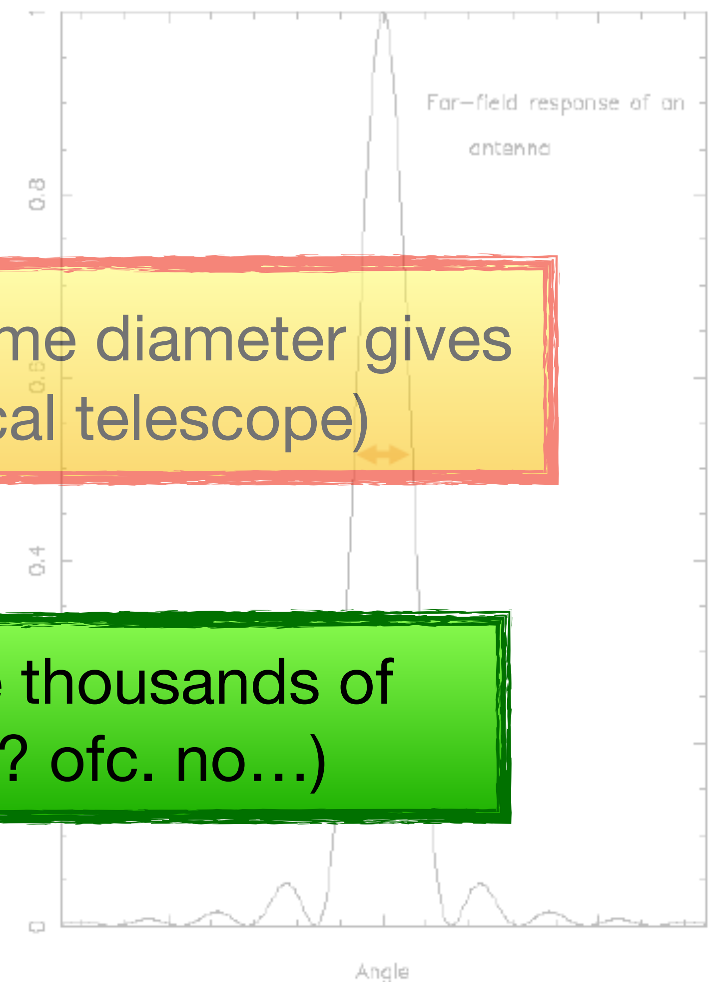

Diffraction pattern caused by the finite size of the aperture main lobe+side lobes

Half-power beamwidth: $\theta = 1.22\lambda/D$

Solid angle: $\Omega = \lambda^2/A$

Gain: $G = 4\pi/\Omega$

D: diameter of the dish

λ: wavelength of observation

A: surface of the dish

Solution: Very Long Baseline Interferometry (VLBI)

Stations of the Very Long Baseline Array (NRAO) in US

$$\theta \sim \frac{\lambda\,(\sim mm - m)}{D\,(\sim 1000\,km)}$$

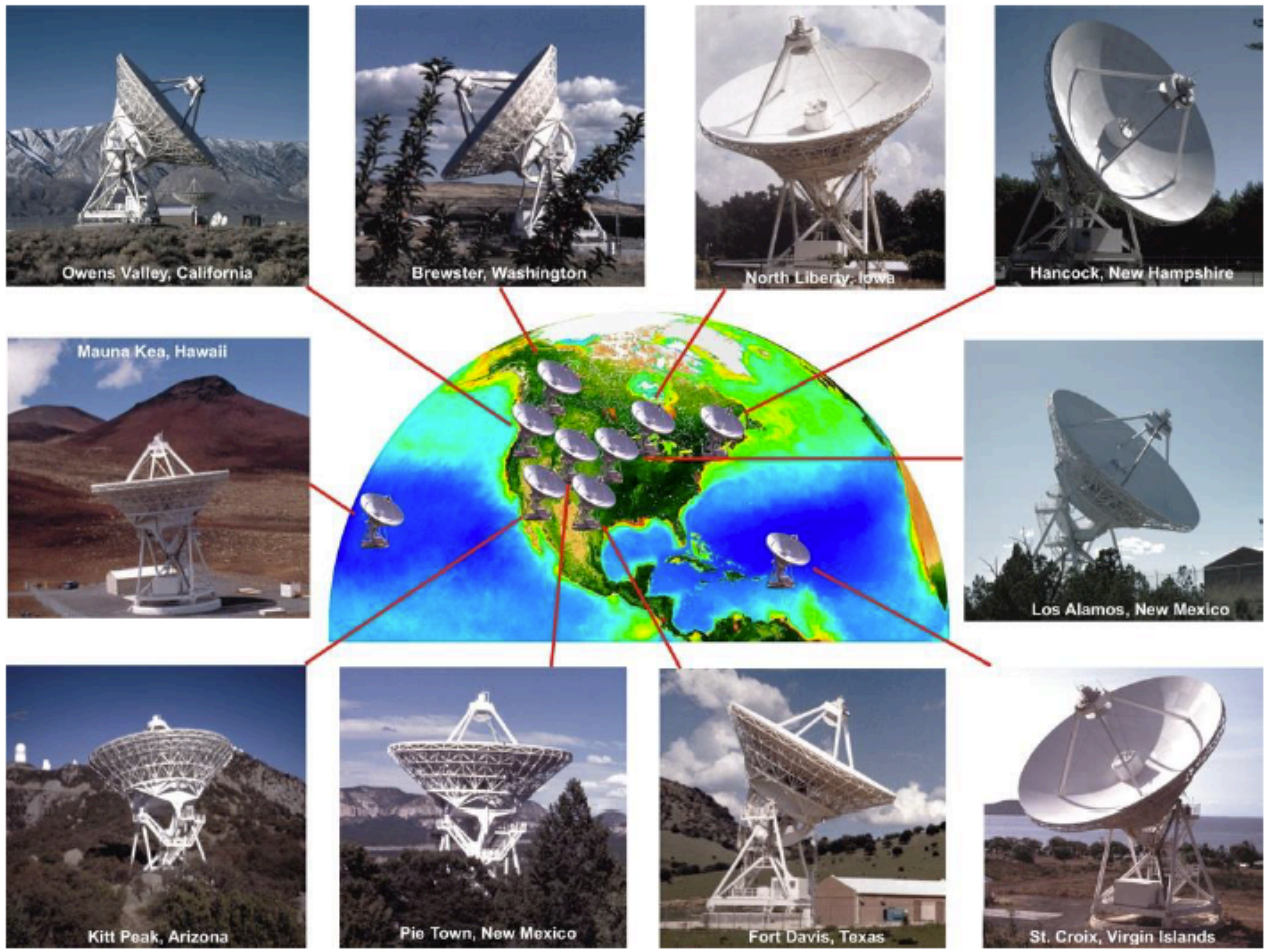

Wavelength (cm)	90	50	21	18	13	6	4	2	1	0,7	0,3
θ_{HPBW} milliarcsecs	22	12	5	4,3	3,2	1,4	0,85	0,47	0,32	0,17	0,12

In VLBI not the diameter of the dishes rather the baseline between them counts

$\theta \sim \frac{\lambda\ (\sim mm - m}{D\ (\sim 1000\ km}$

Distances between locations

—	SC	HN	NL	FD	LA	PT	KP	OV	BR	MK	EB	AR	GB	Y27
SC	—	2853	3645	4143	4458	4579	4839	5460	5767	8611	6822	238	2708	4532
HN	2853	—	1611	3105	3006	3226	3623	3885	3657	7502	5602	2748	829	3198
NL	3645	1611	—	1654	1432	1663	2075	2328	2300	6156	6734	3461	1064	1640
FD	4143	3105	1654	—	608	564	744	1508	2345	5134	8084	3922	2354	515
LA	4458	3006	1432	608	—	236	652	1088	1757	4970	7831	4246	2344	226
PT	4579	3226	1663	564	236	—	417	973	1806	4795	8014	4365	2551	52
KP	4839	3623	2075	744	652	417	—	845	1913	4466	8321	4623	2939	441
OV	5460	3885	2328	1508	1088	973	845	—	1214	4015	8203	5255	3323	1025
BR	5767	3657	2300	2345	1757	1806	1913	1214	—	4398	7441	5585	3326	1849
MK	8611	7502	6156	5134	4970	4795	4466	4015	4398	—	10328	8434	7028	4835
EB	6822	5602	6734	8084	7831	8014	8321	8203	7441	10328	—	6911	6335	8008
AR	238	2748	3461	3922	4246	4365	4623	5255	5585	8434	6911	—	2545	4317
GB	2708	829	1064	2354	2344	2551	2939	3323	3326	7028	6335	2545	—	2516
Y27	4532	3198	1640	515	226	52	441	1025	1849	4835	8008	4317	2516	—

Wavelength (cm)	...	0,7	0,3
θ_{HPBW} milliarcsecs	...32	0,17	0,12

sub-mas resolutions are routinely done
1mas =1/3,600,000 degrees!

(the apparent separation of your car's headlights, as seen by an astronaut on the Moon)

Very Large Array (NRAO)

Very Large Array (NRAO)

Very Large Array (NRAO)

Very Large Array (NRAO)

Table 3.1.1: Configuration Properties

Configuration	A	B	C	D
B_{max} (km[1])	36.4	11.1	3.4	1.03
B_{min} (km[1])	0.68	0.21	0.035[5]	0.035
Band	**Synthesized Beamwidth θ_{HPBW}**(arcsec)[1,2,3]			
74 MHz (4)	24	80	260	850
350 MHz (P)	5.6	18.5	60	200
1.5 GHz (L)	1.3	4.3	14	46
3.0 GHz (S)	0.65	2.1	7.0	23
6.0 GHz (C)	0.33	1.0	3.5	12
10 GHz (X)	0.20	0.60	2.1	7.2
15 GHz (Ku)	0.13	0.42	1.4	4.6
22 GHz (K)	0.089	0.28	0.95	3.1
33 GHz (Ka)	0.059	0.19	0.63	2.1
45 GHz (Q)	0.043	0.14	0.47	1.5
Band	**Largest Angular Scale θ_{LAS}**(arcsec)[1,4]			
74 MHz (4)	800	2200	20000	20000
350 MHz (P)	155	515	4150	4150
1.5 GHz (L)	36	120	970	970
3.0 GHz (S)	18	58	490	490
6.0 GHz (C)	8.9	29	240	240
10 GHz (X)	5.3	17	145	145
15 GHz (Ku)	3.6	12	97	97
22 GHz (K)	2.4	7.9	66	66
33 GHz (Ka)	1.6	5.3	44	44
45 GHz (Q)	1.2	3.9	32	32

arcsec scale

typically kpc-scale

Australia Telescope Compact Array (ATCA)

22m radio telescopes (6)

Multi-Element Radio Linked Interferometer Network MERLIN

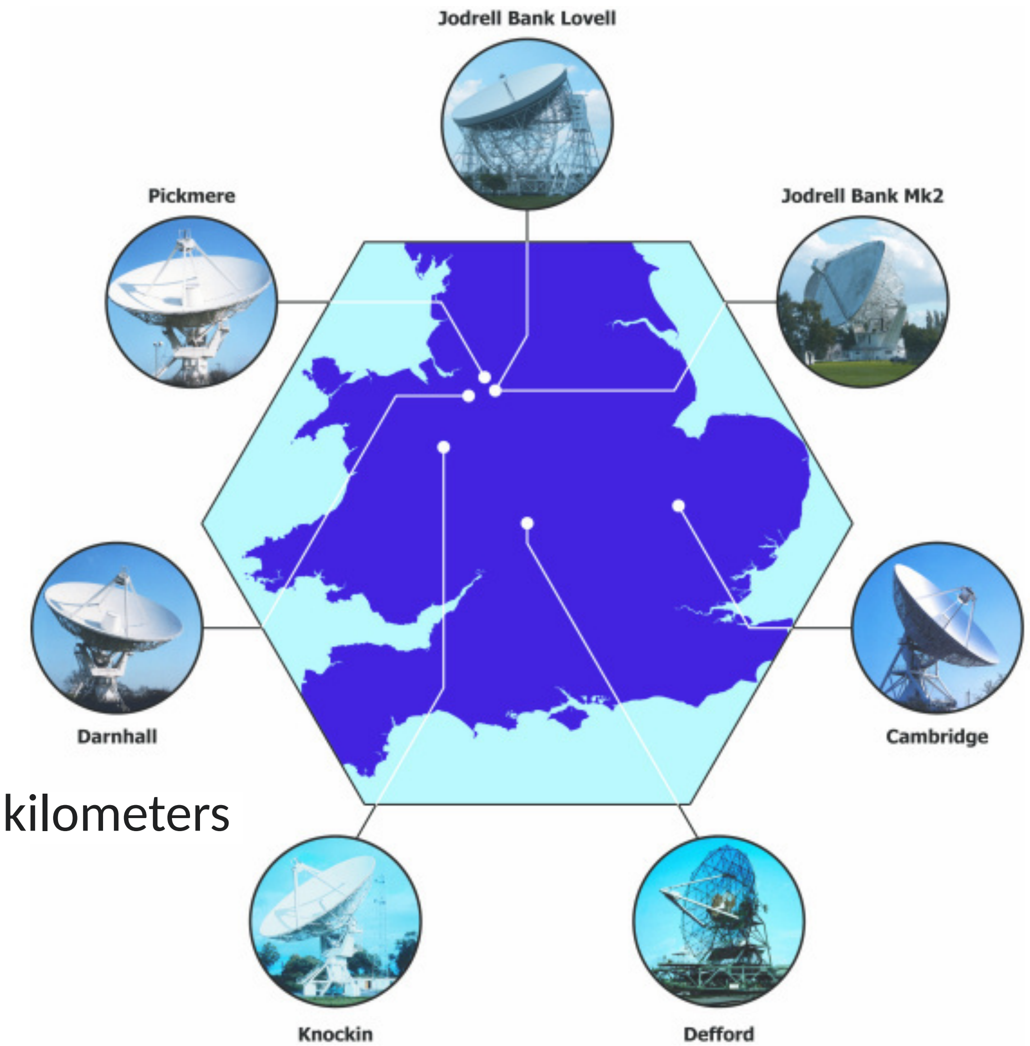

Westerbork Synthesis Radio Telescope

25-meter radio telescopes deployed in a linear array arranged on a 2.7 kilometers

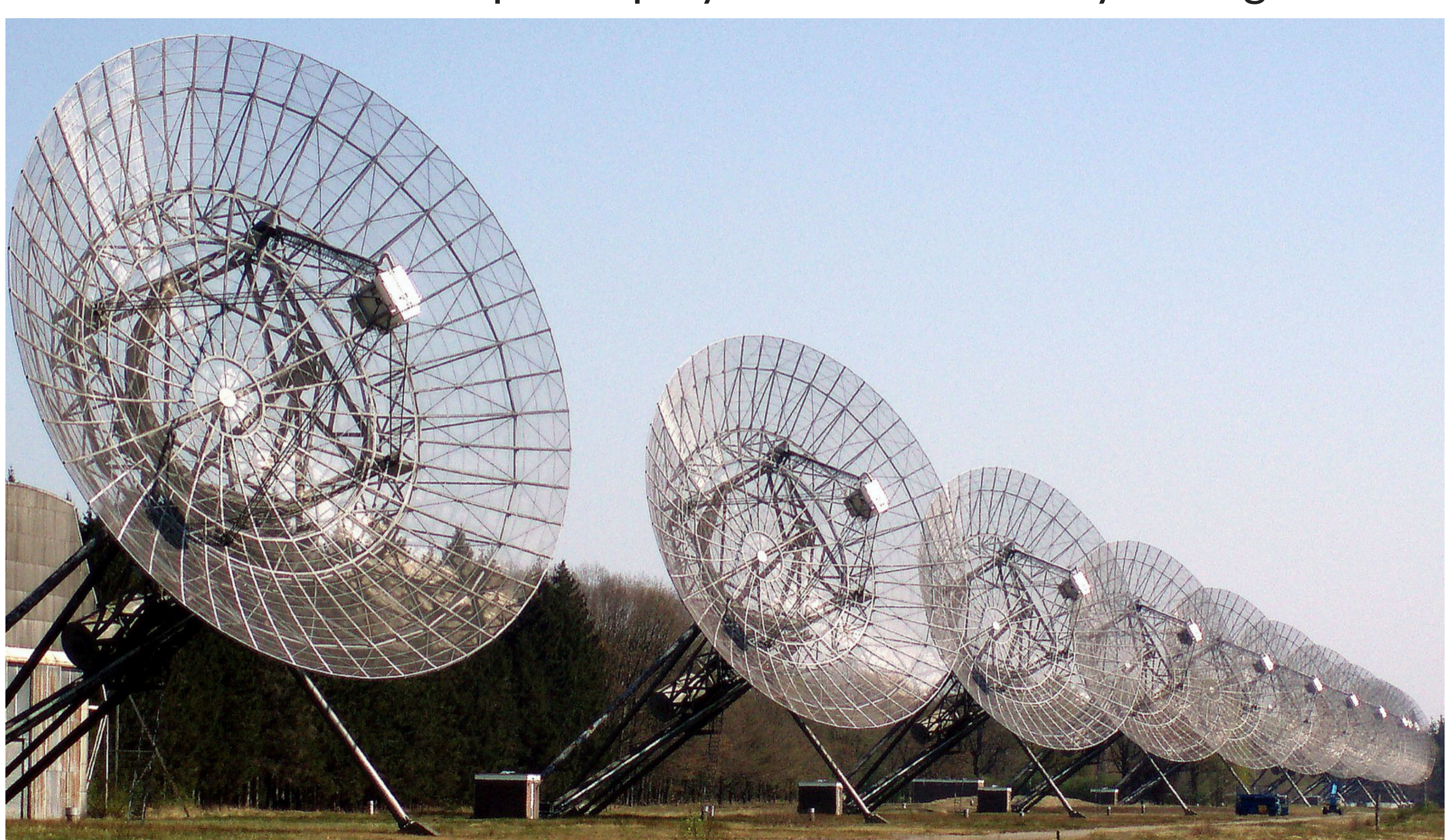

Space VLBI: (VSOP)

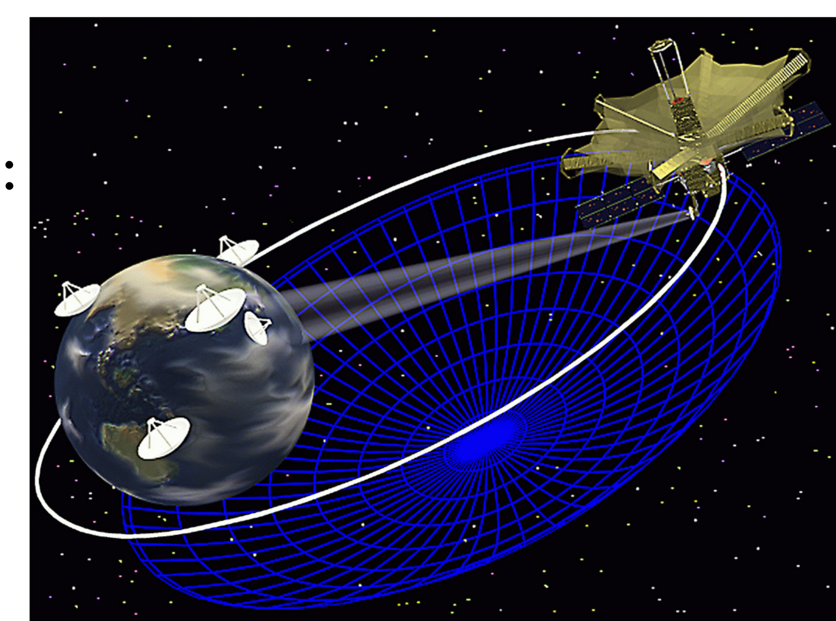

Basics of the very long baseline interferometry (VLBI)

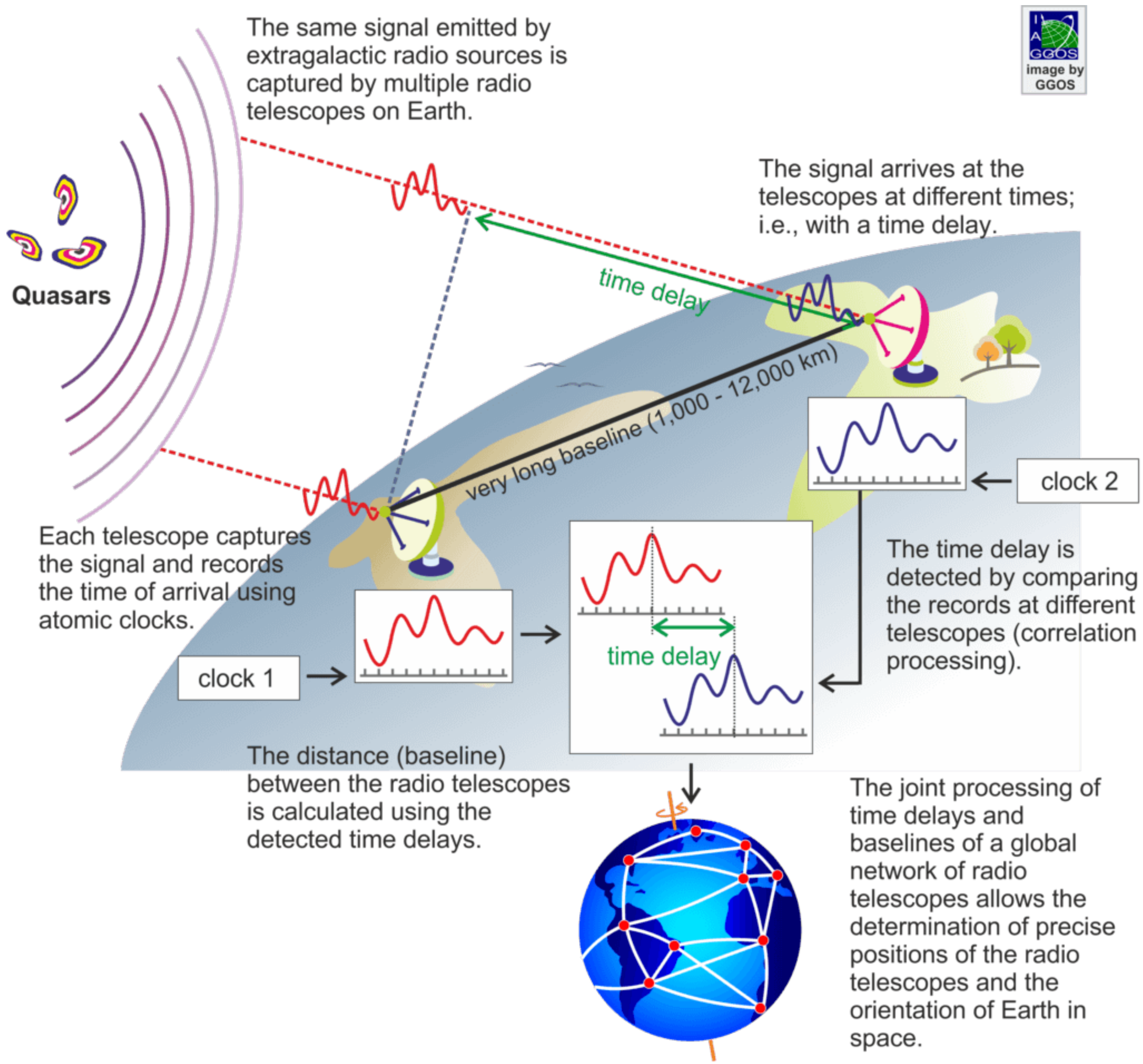

Parsec-scale modelling the surface brightness of AGN jets

- Monitoring of jets in Active galactic nuclei with VLBA Experiments, MOJAVE (Lister et al. 2009-)
- Since 1994 they observed and analyzed 447 bright radio-loud AGNs based on 15 GHz VLBA data
- Calibrated uv-visibilities are public!
  (no need of fringe fitting, amplitude and phase calibration, yeyy!)
- We can do the imaging of these sources and model the surface brightness distribution of their jets (DIFMAP, Pearson&Taylor, 1994, BAAS, 26, 987).
- 2D Gaussian (circular or elliptic base) components
- Fitted parameters:
  - ⋆ Integrated flux density (Jansky, 1Jy=10-26 W/Hz/m2)
  - ⋆ Position relative to the VLBI core (mas)
  - ⋆ Size (mas)

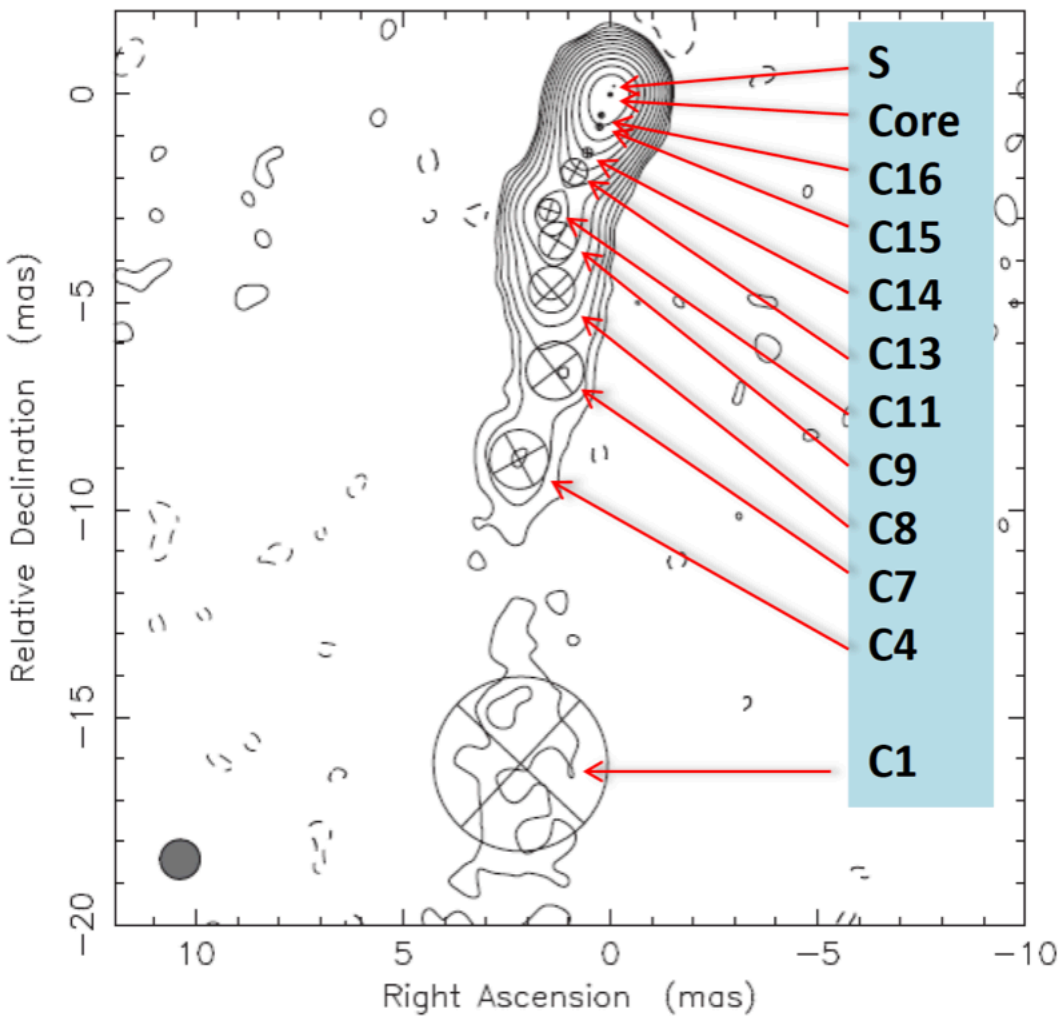

z=0.302

Planck18, 1mas->4.44pc

Jet structure of S5 1928+738

Kun et al, 2014, MNRAS, 445, 1370

MOJAVE database (>447 sources!)

0003+380 (S4 0003+38)	0003-066 (NRAO 005)	0006+061 (TXS 0006+061)	0007+106 (III Zw 2)	0010+405 (4C +40.01)
0011+189 (RGB J0013+191)	0012+610 (4C +60.01)	0014+813 (S5 0014+813)	0015-054 (PMN J0017-0512)	0016+731 (S5 0016+73)
0019+058 (PKS 0019+058)	0026+346 (B2 0026+34)	0027+056 (PKS 0027+056)	0035+413 (B3 0035+413)	0035-252 (OB -259)
0041+341 (GB6 J0043+3426)	0044+566 (GB6 J0047+5657)	0048-071 (OB -082)	0048-097 (PKS 0048-09)	0055+300 (NGC 315)
0059+581 (TXS 0059+581)				

0106+013 (4C +01.02)	0106+612 (TXS 0106+612)	0106+678 (4C +67.04)	0108+388 (S4 0108+38)	0109+224 (S2 0109+22)
0109+351 (B2 0109+35)	0110+318 (4C +31.03)	0111+021 (UGC 00773)	0112-017 (UM 310)	0113-118 (PKS 0113-118)
0116-219 (OC -228)	0118-272 (OC -230.4)	0119+041 (PKS 0119+041)	0119+115 (PKS 0119+11)	0122-003 (UM 321)
0125+487 (GB6 J0128+4901)	0128+554 (TXS 0128+554)	0130-171 (OC -150)	0133+388 (B3 0133+388)	0133+476 (DA 55)
0134+579 (TXS 0134+579)	0136+176 (PKS 0136+176)	0138-097 (PKS 0139-09)	0141+268 (TXS 0141+268)	0142-278 (OC -270)
0149+218 (PKS 0149+21)	0149+710 (TXS 0149+710)	0151+081 (GB6 J0154+0823)	0153+744 (S5 0153+744)	0159+723 (S5 0159+723)

0200+304 (IVS B0200+30A)	0201+113 (PKS 0201+113)	0202+149 (4C +15.05)	0202+319 (B2 0202+31)	0202-172 (PKS 0202-17)
0203-120 (PMN J0206-1150)	0208+106 (IVS B0208+106)	0210+515 (TXS 0210+515)	0212+735 (S5 0212+73)	0214+083 (PMN J0217+0837)
0215+015 (OD 026)	0219+428 (3C 66A)	0221+067 (4C +06.11)	0224+671 (4C +67.05)	0229+131 (4C +13.14)
0234+285 (4C +28.07)	0235+164 (PKS 0235+164)	0237-027 (PKS 0237-027)	0238+711 (S5 0238+711)	0238-084 (NGC 1052)
0239+843 (WN B0239.6+8423)	0241+622 (TXS 0241+622)	0248+430 (B3 0248+430)	0250+320 (IVS B0250+320)	0250-225 (OD -283)
0256+075 (OD 94.7)				

Common Name:	TXS 0506+056
B1950 Name:	0506+056
J2000 Name:	J0509+0541
R.A. and Dec. (J2000):	5h9m25.964s +5d41'35.334"
AGN Class:	ISP BL Lac
Redshift:	0.3365 (2018ApJ...854L..32P)
Luminosity Distance:	1762 Mpc ; 4.78 pc/mas
Radio Spectrum:	Flat
Gamma-ray Association	LAT: Y, EGRET: Y, TeV: Y
Kpc-scale morphology:	Core
Jet Speed:	Maximum: 51 ± 6 µas/y ; 1.07 ± 0.14 c Median: N/A ; based on 5 moving features Lister et al. 2021, ApJ,923,30
Separation Versus Time Plot:	PNG PS

MOJAVE 15 GHz [Total intensity movie] | [Polariz. movie]

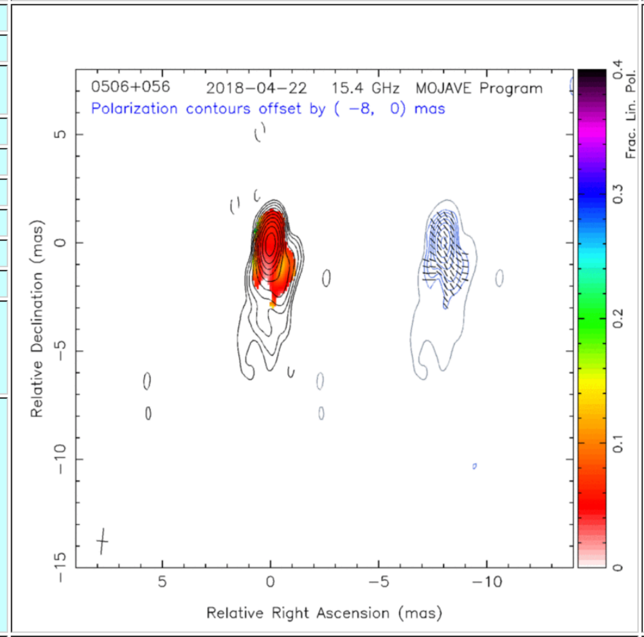

VLBA 1.4 GHz: NRAO Archive

TXS 0506+056

Image Not Available

Stacked epoch 15 GHz VLBA images:
Uniform weight: [PS] [GIF]
Natural weight: [PS] [GIF]
Circular Beam : [PS] [GIF]
Tapered Beam: [PS] [GIF]
Pushkarev et al. 2017 : FITS

Rotation Measure Map: | Not available |

Spectral Index Map: | Not available |

VLBA 23 GHz: RRIFD Database

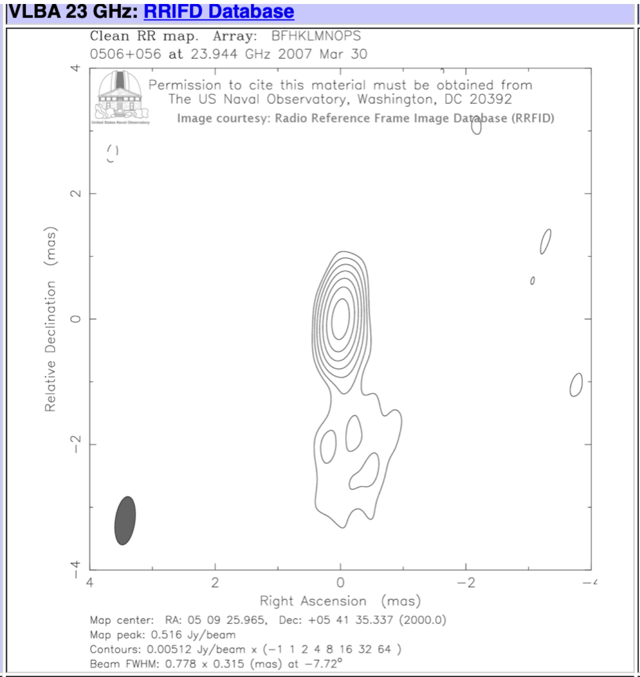

Kpc-scale: Healey et al. 2007, ApJS 171, 61

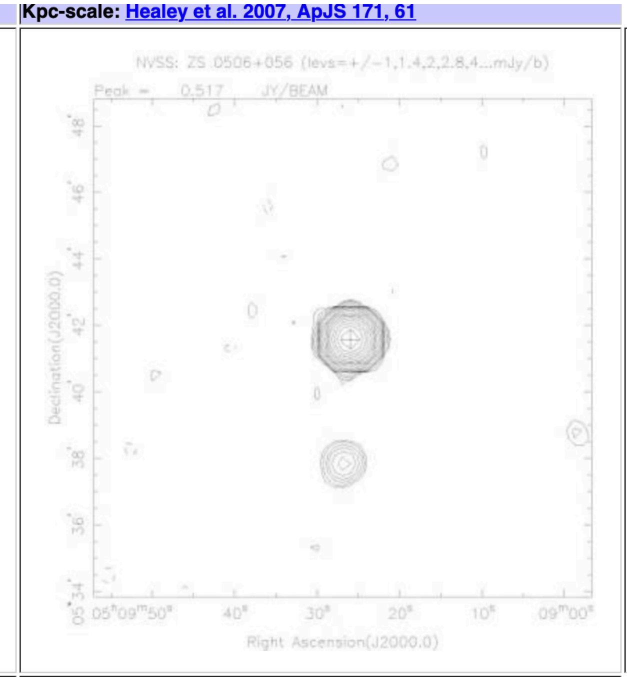

Fermi LAT and 15 GHz VLBA Light Curves

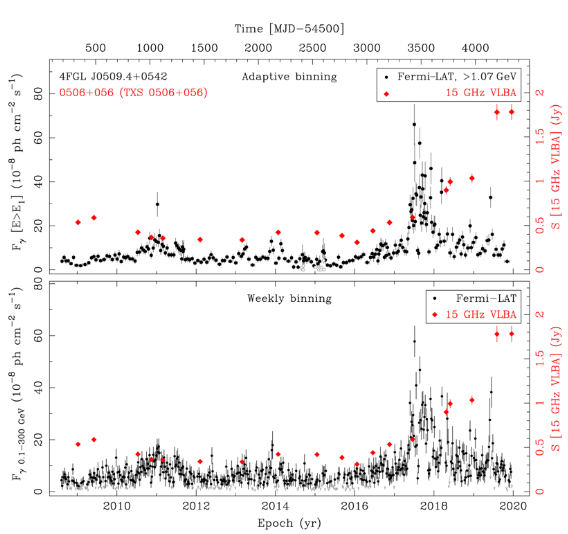

VLBA 43 GHz:

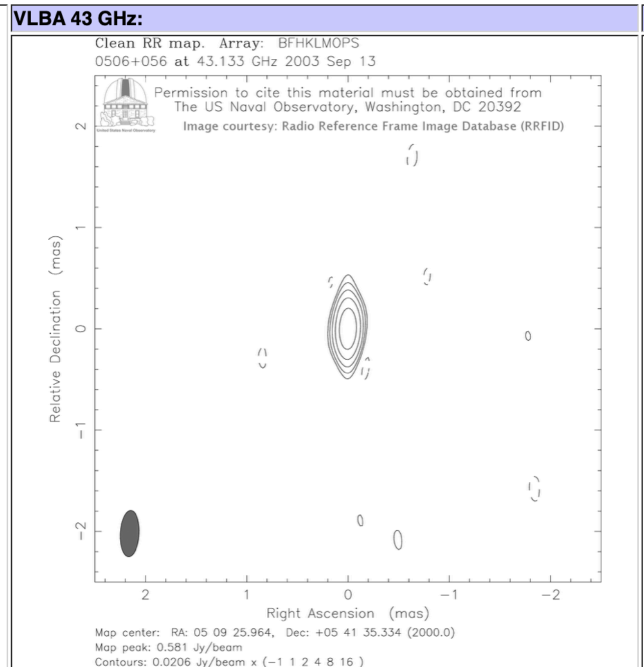

Multiepoch Radio Spectrum:

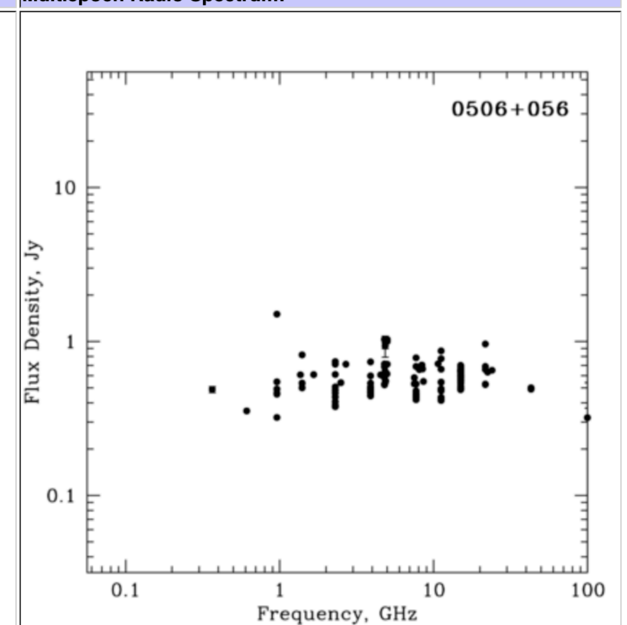

Common Name:	TXS 0506+056
B1950 Name:	0506+056
J2000 Name:	J0509+0541
R.A. and Dec. (J2000):	5h9m25.964s +5d41'35.334"
AGN Class:	ISP BL Lac
Redshift:	0.3365 (2018ApJ...854L..32P)
Luminosity Distance:	1762 Mpc ; 4.78 pc/mas
Radio Spectrum:	Flat
Gamma-ray Association	LAT: Y, EGRET: Y, TeV: Y
Kpc-scale morphology:	Core
	Maximum: 51 ± 6 μas/y ; 1.07 ± 0.14 c

MOJAVE 15 GHz [Total intensity movie] | [Polariz. movie]

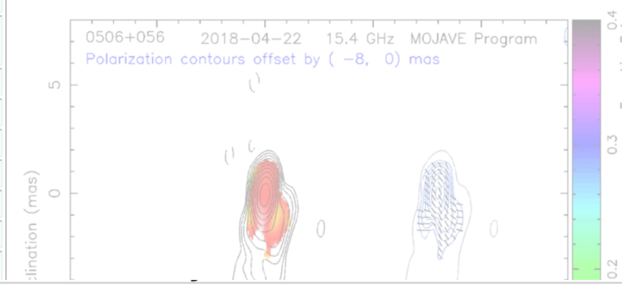

VLBA 1.4 GHz: NRAO Archive

Image Not

Epoch (Y-M-D)	VLBA Code	VLBA I (mJy)	VLBA P (mJy)	VLBA P (%)	VLBA EVPA (deg.)	I Image (Nat. Weight)	Tapered I Image	Tapered I Image (Widefield)	Visibility Data	Stokes I Radplot	Pol. Image
2022-02-24 *	BL286AH										
2021-08-07	BL286AA	1082	18	1.6	126	FITS PNG PS	FITS PNG PS	PNG PS	uvf	PNG PS	PNG PS
2021-03-02	BL273J	1584	43	2.7	139	FITS PNG PS	FITS PNG PS	PNG PS	uvf	PNG PS	PNG PS
2020-12-24	BL229BL	2029	55	2.7	148	FITS PNG PS	FITS PNG PS	PNG PS	uvf	PNG PS	PNG PS
2020-08-01	BL229BH	2084	21	1.0	84	FITS PNG PS	FITS PNG PS	PNG PS	uvf	PNG PS	PNG PS
2020-06-13	BL229BF	2159	30	1.4	82	FITS PNG PS	FITS PNG PS	PNG PS	uvf	PNG PS	PNG PS
2020-05-08	BL273E1	2307	23	1.0	66	FITS PNG PS	FITS PNG PS	PNG PS	uvf	PNG PS	PNG PS
2020-04-09	BL273E	2324	52	2.2	38	FITS PNG PS	FITS PNG PS	PNG PS	uvf	PNG PS	PNG PS
2020-02-16	BL273D	2191	39	1.8	38	FITS PNG PS	FITS PNG PS	PNG PS	uvf	PNG PS	PNG PS
2019-12-17	BL273C	2130	32	1.5	59	FITS PNG PS	FITS PNG PS	PNG PS	uvf	PNG PS	PNG PS
2019-08-04	BL273A	1789	8.8	0.5	117	FITS PNG PS	FITS PNG PS	PNG PS	uvf	PNG PS	PNG PS
2018-12-16	BL229AT	1010	22	2.1	18	FITS PNG PS	FITS PNG PS	PNG PS	uvf	PNG PS	PNG PS
2018-05-31	BL229AO	975	31	3.2	33	FITS PNG PS	FITS PNG PS	PNG PS	uvf	PNG PS	PNG PS
2018-04-22	BL229AN	896	42	4.7	34	FITS PNG PS	FITS PNG PS	PNG PS	uvf	PNG PS	PNG PS
2017-06-17	BL229AI	588	12	2.0	12	FITS PNG PS	FITS PNG PS	PNG PS	uvf	PNG PS	PNG PS
2016-11-18	BL193BM	533	7.8	1.5	13	FITS PNG PS	FITS PNG PS	PNG PS	uvf	PNG PS	PNG PS
2016-06-16	BL193BG	436	6.4	1.5	38	FITS PNG PS	FITS PNG PS	PNG PS	uvf	PNG PS	PNG PS
2016-01-22	BL193BB	307	4.3	1.4	12	FITS PNG PS	FITS PNG PS	PNG PS	uvf	PNG PS	PNG PS
2015-09-06	BL193AW	382	7.4	1.9	159	FITS PNG PS	FITS PNG PS	PNG PS	uvf	PNG PS	PNG PS
2015-01-18	BL193AQ	420	8.5	2.0	16	FITS PNG PS	FITS PNG PS	PNG PS	uvf	PNG PS	PNG PS
2014-01-25	BL193AE	420	9.8	2.3	161	FITS PNG PS	FITS PNG PS	PNG PS	uvf	PNG PS	PNG PS
2013-02-28	BL178BA	338	8.6	2.5	31	FITS PNG PS	FITS PNG PS	PNG PS	uvf	PNG PS	PNG PS
2012-02-06	BL178AG	342	4.6	1.3	26	FITS PNG PS	FITS PNG PS	PNG PS	uvf	PNG PS	PNG PS
2011-02-27	BL149DC	360	14	3.8	36	FITS PNG PS	FITS PNG PS	PNG PS	uvf	PNG PS	PNG PS
2010-11-13	BL149CW	376	13	3.4	38	FITS PNG PS	FITS PNG PS	PNG PS	uvf	PNG PS	PNG PS
2010-07-12	BL149CL	430	5.3	1.2	67	FITS PNG PS	FITS PNG PS	PNG PS	uvf	PNG PS	PNG PS
2009-06-03	BL149BM	598	4.2	0.7	165	FITS PNG PS	FITS PNG PS	PNG PS	uvf	PNG PS	PNG PS
2009-01-07	BL149BG	543	9.6	1.8	10	FITS PNG PS	FITS PNG PS	PNG PS	uvf	PNG PS	PNG PS

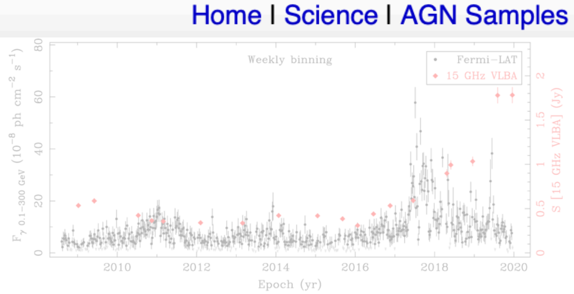

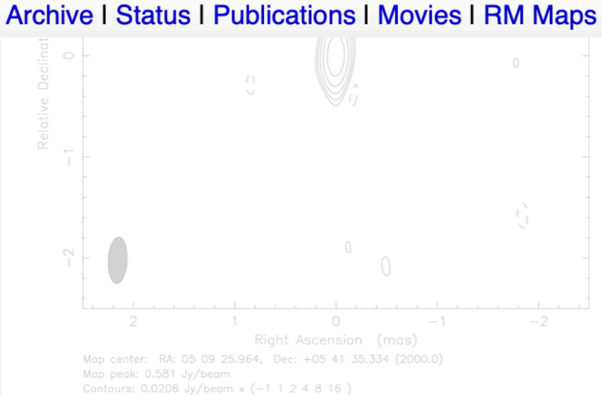

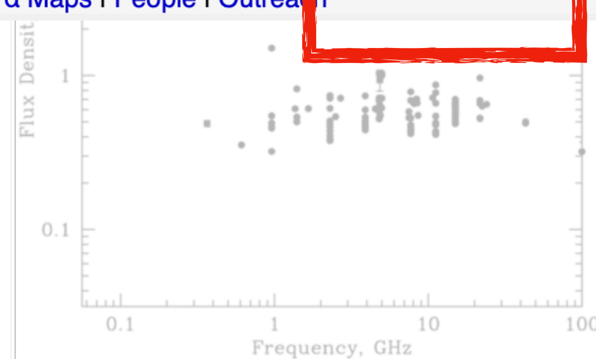

astrogeo.org

The Astrogeo VLBI FITS image database

The Astrogeo VLBI FITS image database contains **111,834** brightness distributions of **17432** compact radio sources, mainly active galaxy nuclea (AGN), generated by analyzing very long baseline interferometry (VLBI) surveys — dedicated radioastronomy observations of large lists of radio sources on networks of radio telescopes spread at distances of thousand kilometers. The primary database contents is not pictures, but **brightness distribution in a digital form**, specifically in FITS format, and calibrated visibility data, which makes it possible to use this database for scientific work. Derived quantities, such as visualization of images and estimates of the correlated flux density are also available.
The images were contributed by courtesy of many authors.

The database can be **searched** using one of these methods:

- Alphabetic list of source J2000-names
  Get alphabetic list
- Search by name
  Name: Get
- Search by position
  Right ascension: Declination: Get

In addition to brightness distribution, estimates of the correlated flux density from VLBI experiments for a number of sources are available. Currently, they are not included in the database and are not searched.

- Q-band correlated flux densities of 637 sources from the 43 GHz KVN Calibrator Survey
- K-band correlated flux densities of 551 sources from the 22 GHz VERA Fringe Survey
- K-band correlated flux densities of 68 sources from the 22 GHz experiment v230a at the LBA network.
- X-band correlated flux densities of 1101 sources from the 8.4 GHz LBA Calibrator survey observations.

J0509+0541

Sts	Dist	B1950 name	J2000 name	J2000.0 coordinates		Error	Image	Band	Flux (Jy)		PS map	PS rad plot	FITS map	FITS uv	Analyst
	deg			Right ascens.	Declination	mas	epoch		Tot	Unres					
C		0506+056	J0509+0541	05:09:25.9645	+05:41:35.333	0.12	1995.07.15	S	0.564	0.45	S_map_ps	S_rad_ps	S_map_fits	S_uf_fits	(yyk)
							1995.07.15	X	0.494	0.27	X_map_ps	X_rad_ps	X_map_fits	X_uf_fits	
							1996.06.05	C	0.482	0.33	C_map_ps	C_rad_ps	C_map_fits	C_uf_fits	(gur)
							2009.01.07	U	0.532	0.31	U_map_ps	U_rad_ps	U_map_fits	U_uf_fits	(moj)
							2009.06.03	U	0.580	0.33	U_map_ps	U_rad_ps	U_map_fits	U_uf_fits	(moj)
							2010.07.12	U	0.416	0.19	U_map_ps	U_rad_ps	U_map_fits	U_uf_fits	(moj)
							2010.10.23	X	0.375	0.18	X_map_ps	X_rad_ps	X_map_fits	X_uf_fits	(pet)
							2010.11.13	U	0.368	0.20	U_map_ps	U_rad_ps	U_map_fits	U_uf_fits	(moj)
							2010.12.26	X	0.346	0.17	X_map_ps	X_rad_ps	X_map_fits	X_uf_fits	(pet)
							2011.02.07	X	0.419	0.21	X_map_ps	X_rad_ps	X_map_fits	X_uf_fits	(pet)
							2011.02.27	U	0.346	0.20	U_map_ps	U_rad_ps	U_map_fits	U_uf_fits	(moj)
							2012.02.06	U	0.335	0.20	U_map_ps	U_rad_ps	U_map_fits	U_uf_fits	(moj)
							2012.03.15	X	0.381	0.23	X_map_ps	X_rad_ps	X_map_fits	X_uf_fits	(pet)
							2013.02.12	C	0.348	0.19	C_map_ps	C_rad_ps	C_map_fits	C_uf_fits	(pet)
							2013.02.12	X	0.346	0.18	X_map_ps	X_rad_ps	X_map_fits	X_uf_fits	
							2013.02.28	U	0.329	0.20	U_map_ps	U_rad_ps	U_map_fits	U_uf_fits	(moj)
							2013.05.07	X	0.434	0.25	X_map_ps	X_rad_ps	X_map_fits	X_uf_fits	(pet)
							2013.05.18	X	0.419	0.25	X_map_ps	X_rad_ps	X_map_fits	X_uf_fits	(pet)
							2014.01.25	U	0.418	0.24	U_map_ps	U_rad_ps	U_map_fits	U_uf_fits	(moj)

QSO S5 1928+738

Very Long Baseline Array (NRAO)/MOJAVE, 15 GHz

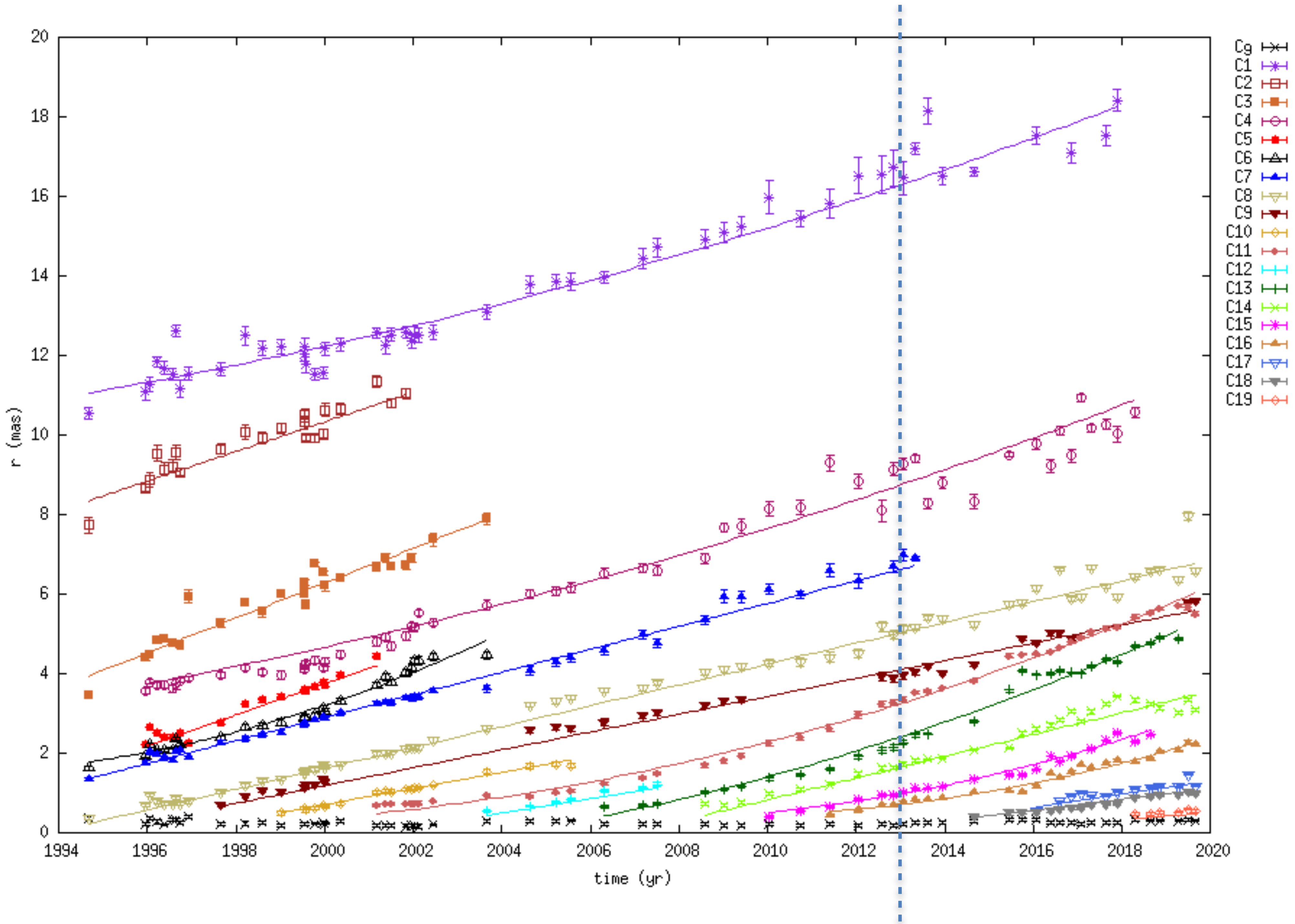

Kun, Gabányi, Karouzos, Britzen, Gergely, MNRAS, 2014, 445, 1370 in prep.

S5 1928+738

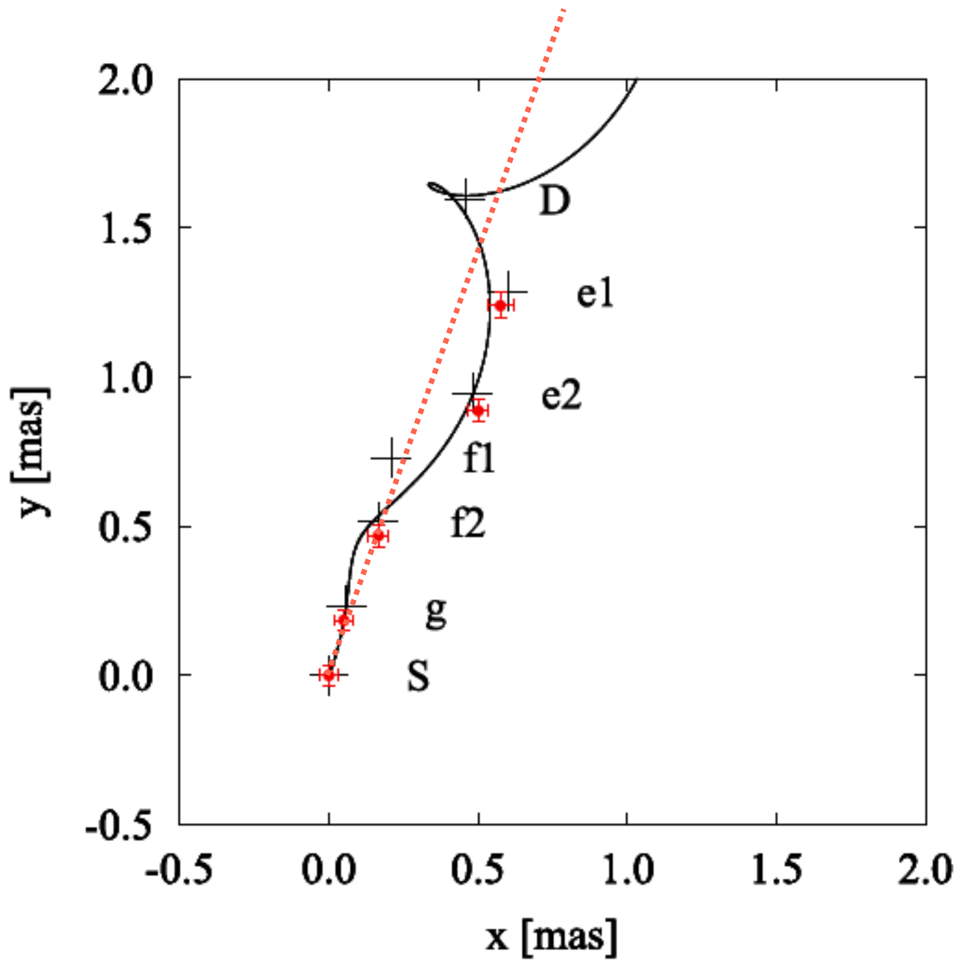

Flux density of the inner jet

Inclination angle of the symmetry axis of the inner jet

Position angle of the symmetry axis of the inner jet

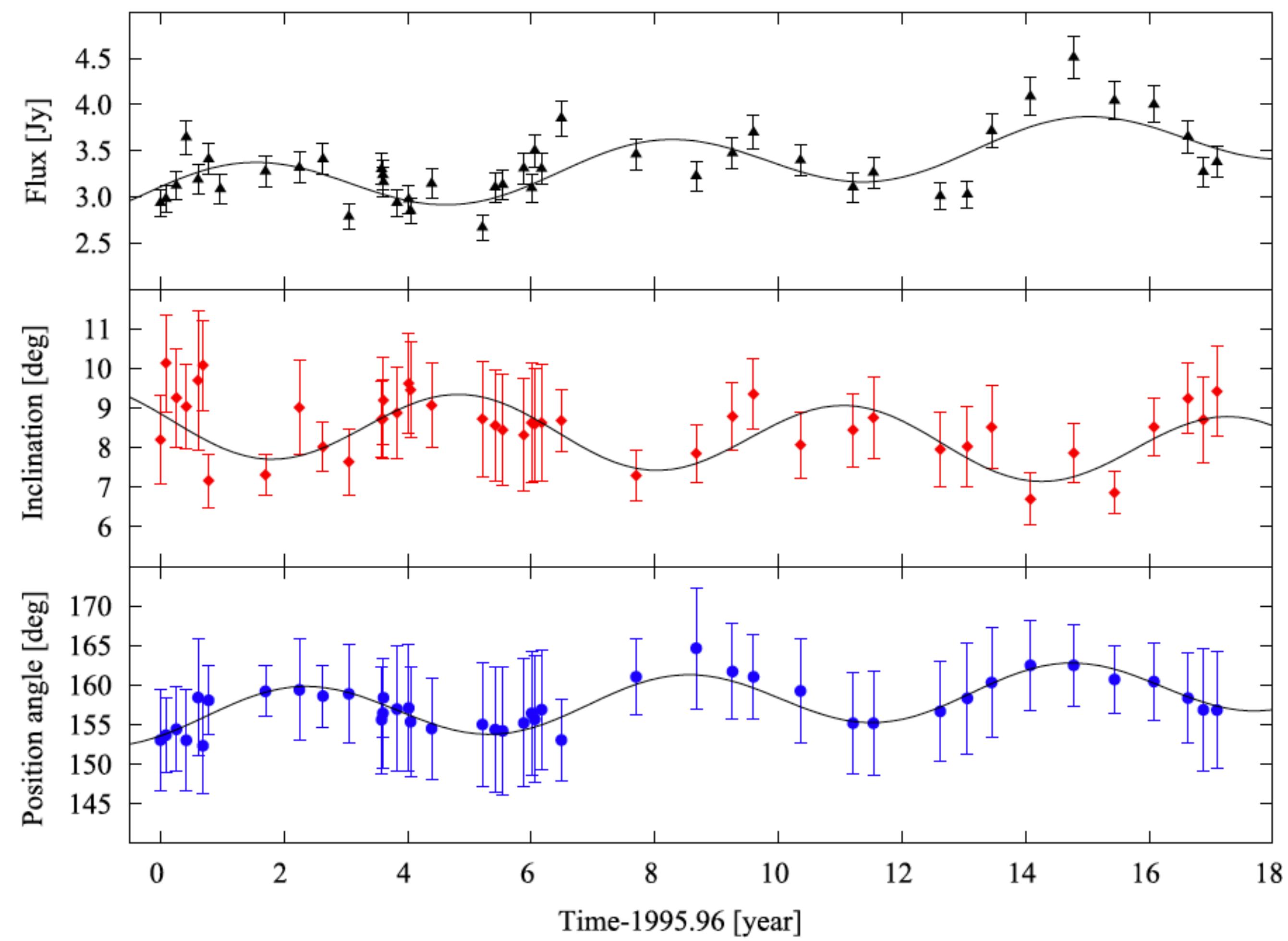

Binary parameters
of the putative SMBH binary:

Table 6. Binary parameters.

Total mass, m^a ($M_\odot$)	8.13×10^8
Orbital period, T (yr)	4.78 ± 0.14
Binary separation, r (pc)	0.0128 ± 0.0003
PN parameter, ε	≈ 0.003
Mass ratio, ν	[0.21 : 1/3]
Spin–orbit precession period, T_{SO} (yr)	4852 ± 646
Gravitational lifetime, T_{merger} (yr)	$(1.44 \pm 0.19) \times 10^6$

[a]independent result by Woo & Urry (2002).

QSO PG 1302-102

Very Long Baseline Array (NRAO)/MOJAVE, 15 GHz

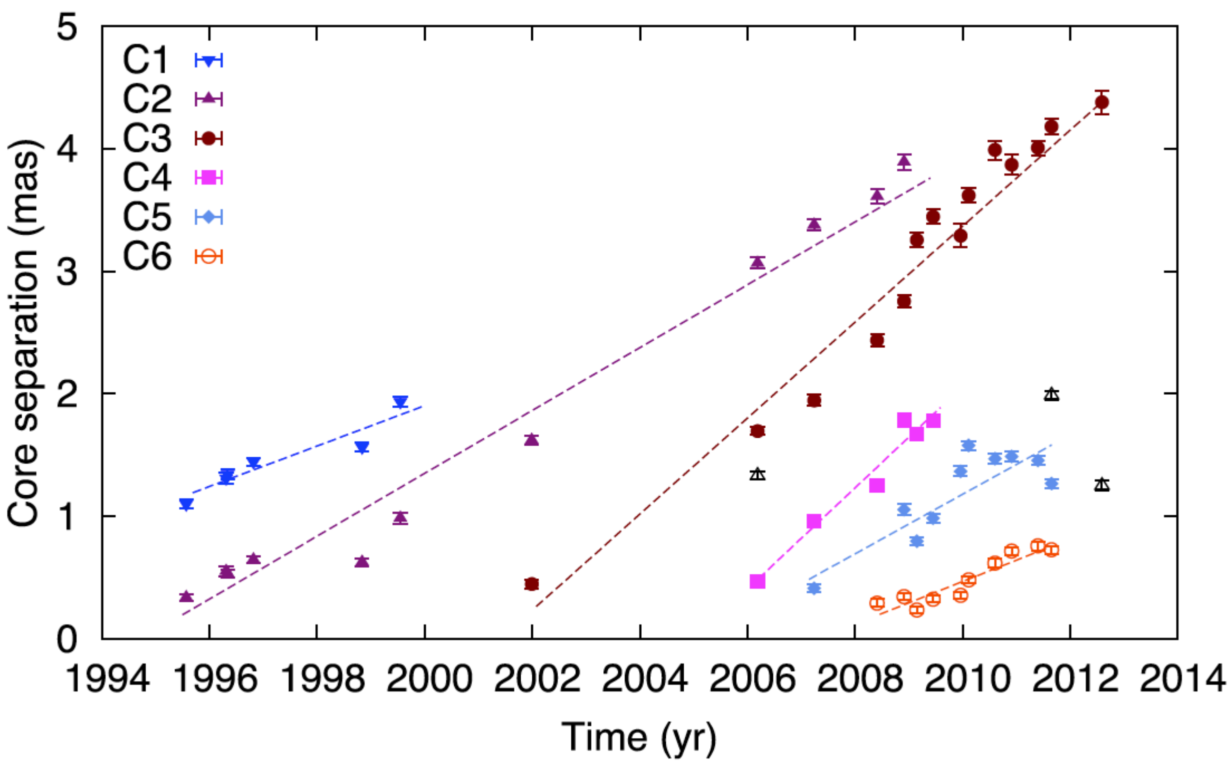

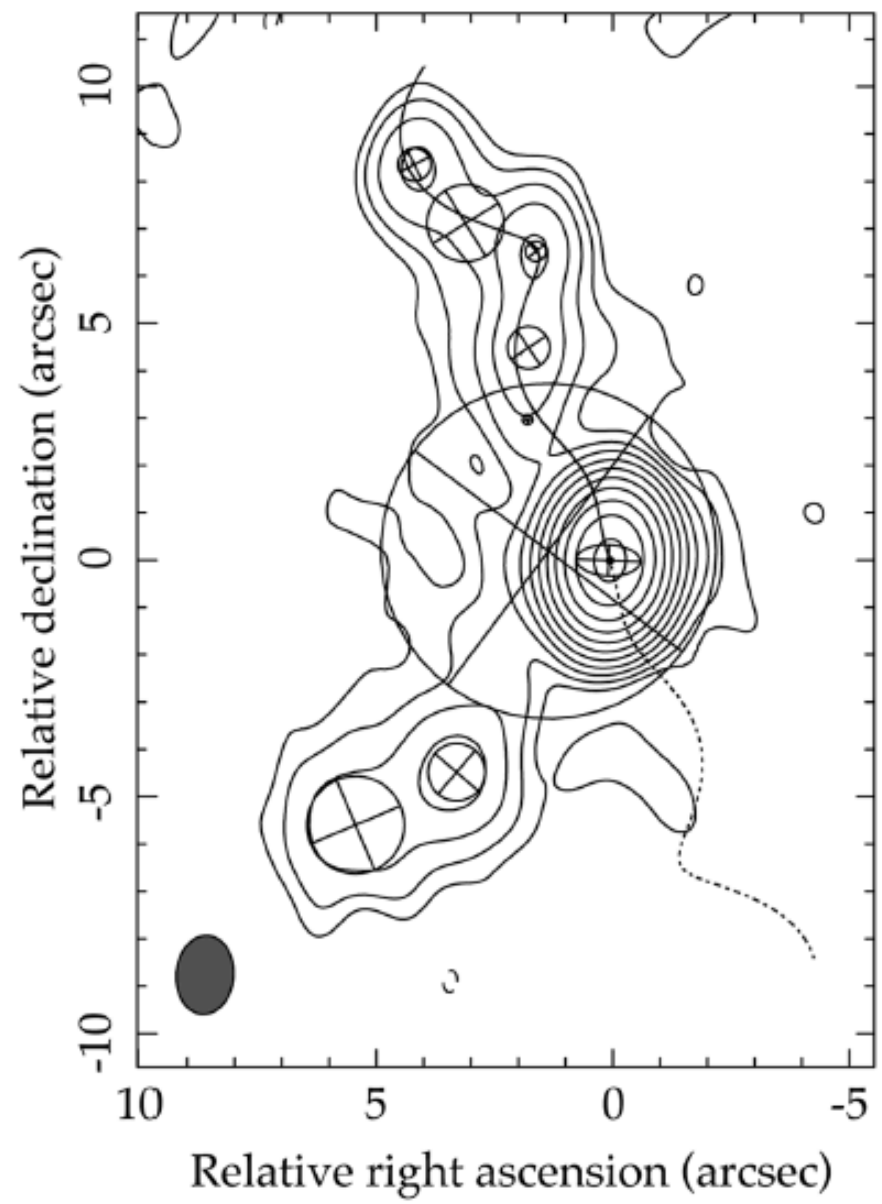

Very Large Array (NRAO), 1.4 GHz

Table 1. BBH parameters derived for PG 1302–102.

Total mass, m^* ($M_\odot$)	$\approx 4 \times 10^8$
Orbital period, T^* (yr)	4.0 ± 0.2
Binary separation, r^* (pc)	≈ 0.01
Post-Newtonian parameter, ε	≈ 0.002
Mass ratio, ν	$\nu > 0.08$
Spin–orbit precession period, T_{SO} (yr)	$<14\,100$
Gravitational lifetime, T_{GR} (yr)	$<7.2 \times 10^6$

Note. *Indicates parameters determined independently by Graham et al. (2015).

Kun, Frey, Gabányi, Britzen, Cseh, Gergely, MNRAS, 2015, 454, 1290

A blazar with oscillating jet components

S5 1803+784

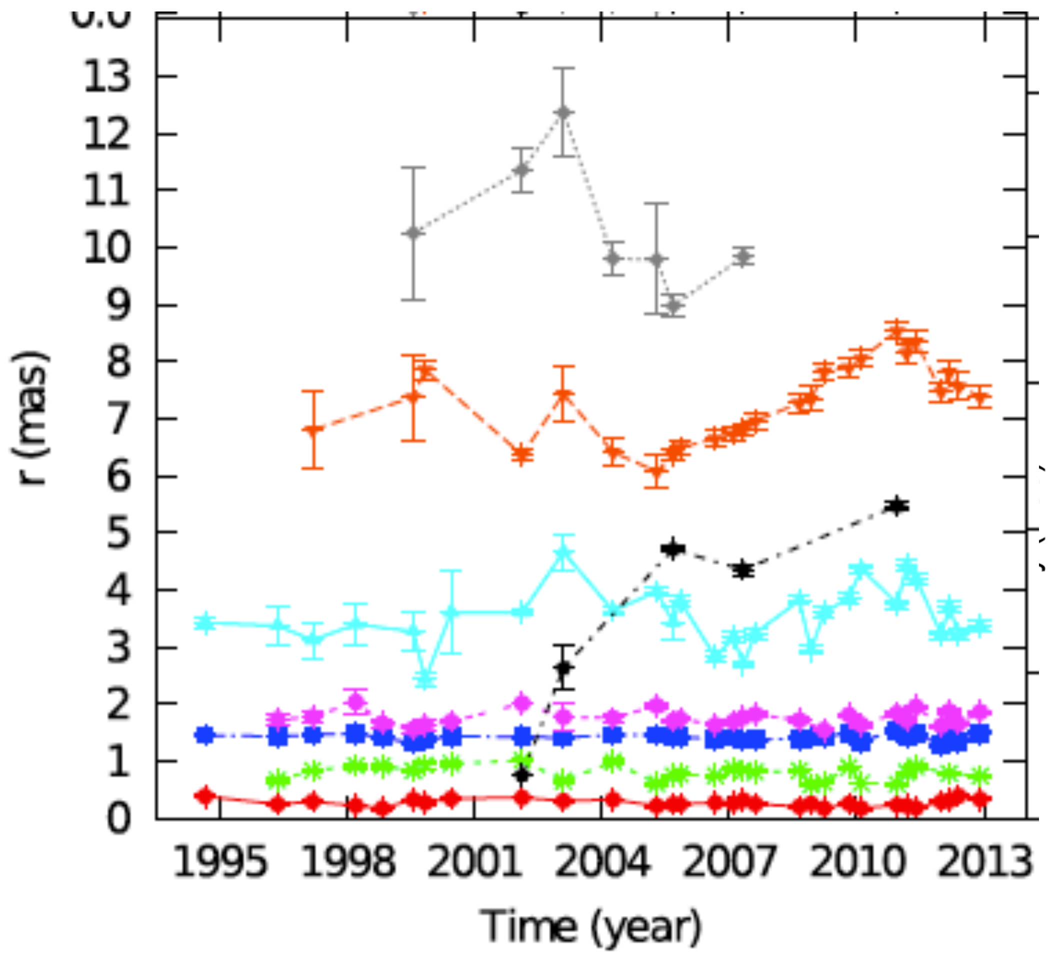

Very Long Baseline Array (NRAO)/MOJAVE, 15 GHz

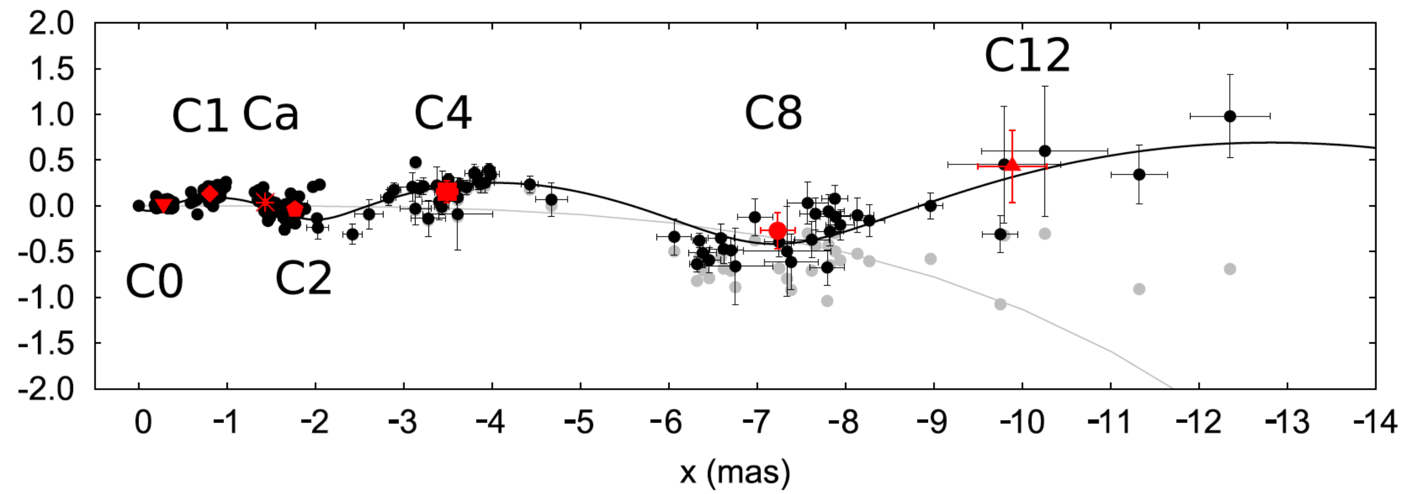

Quasi-stationary jet components

The jet components are regions of the jet flaring "lantern regions" that are apparently brighter due their strong Doppler boosting, most probably due to geometric reasons

Kun, Karouzos, Gabányi, Britzen, Kurtanidze, Gergely, MNRAS, 2018, 478, 359

The VLBI jet ridge-lines

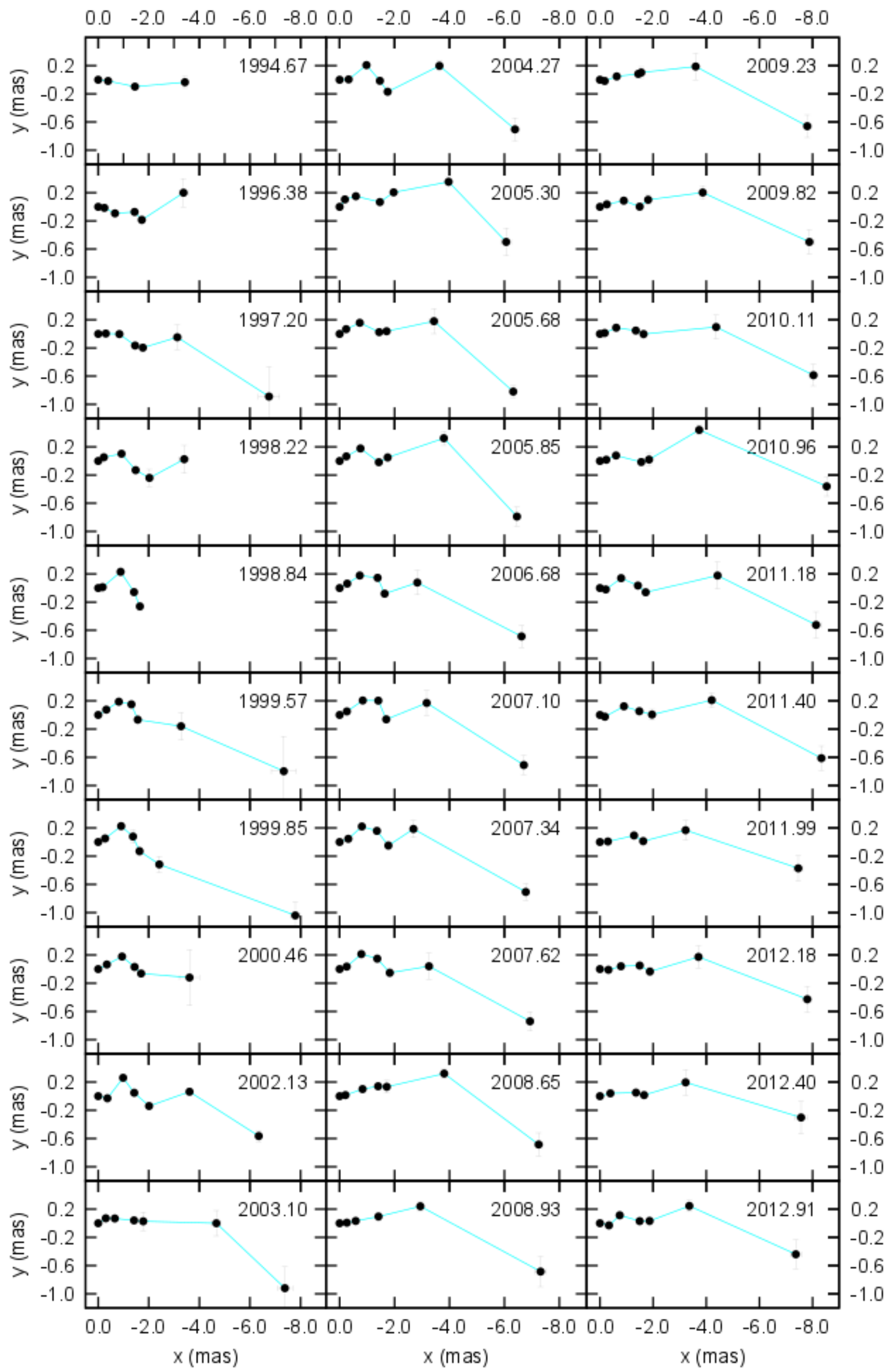

The average inclination angle of the jet
is only **~2 degrees** based on the VLBI data

VLBI jet structure of TXS 0506+056

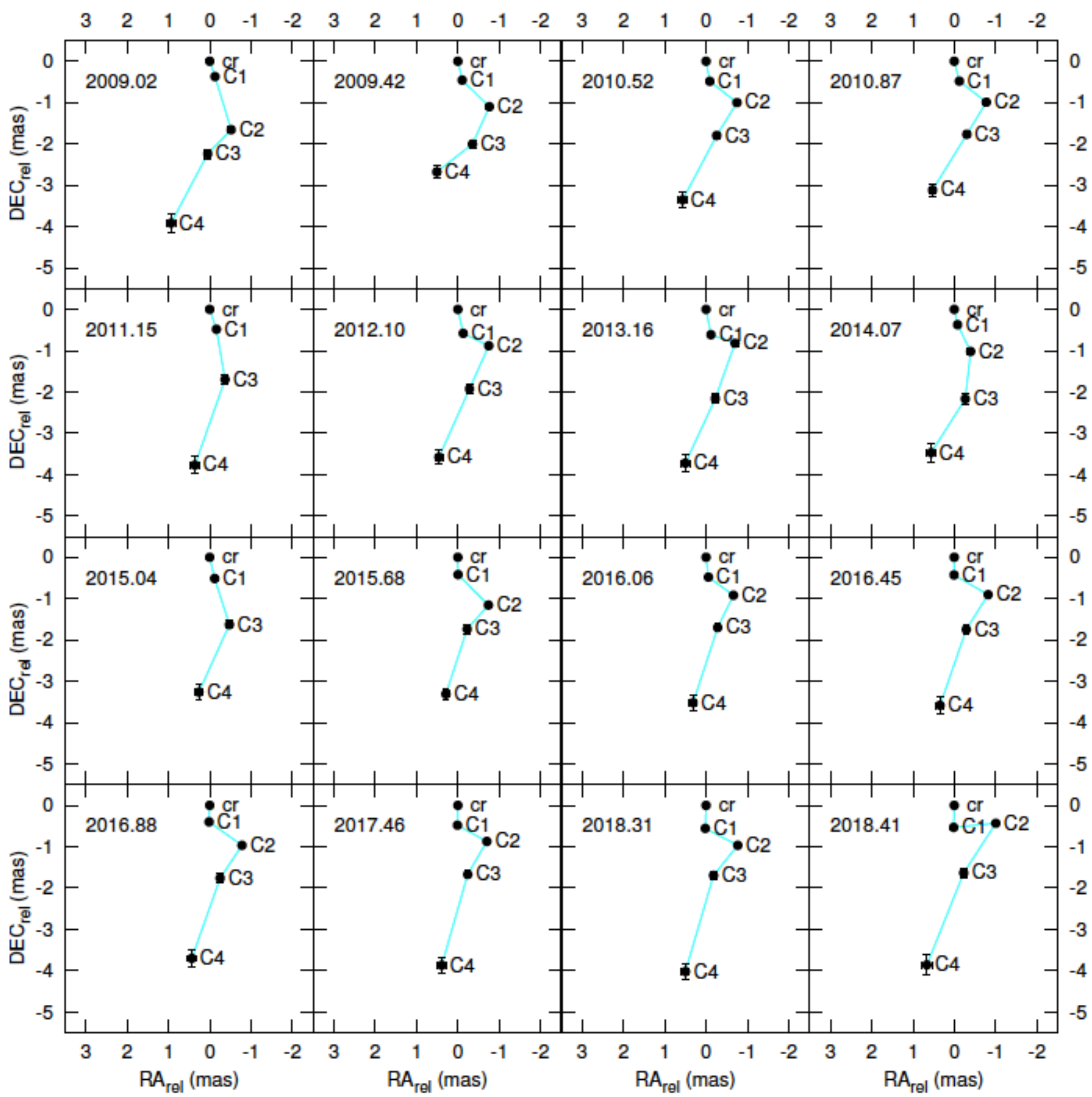

Very Long Baseline Array (NRAO)/MOJAVE

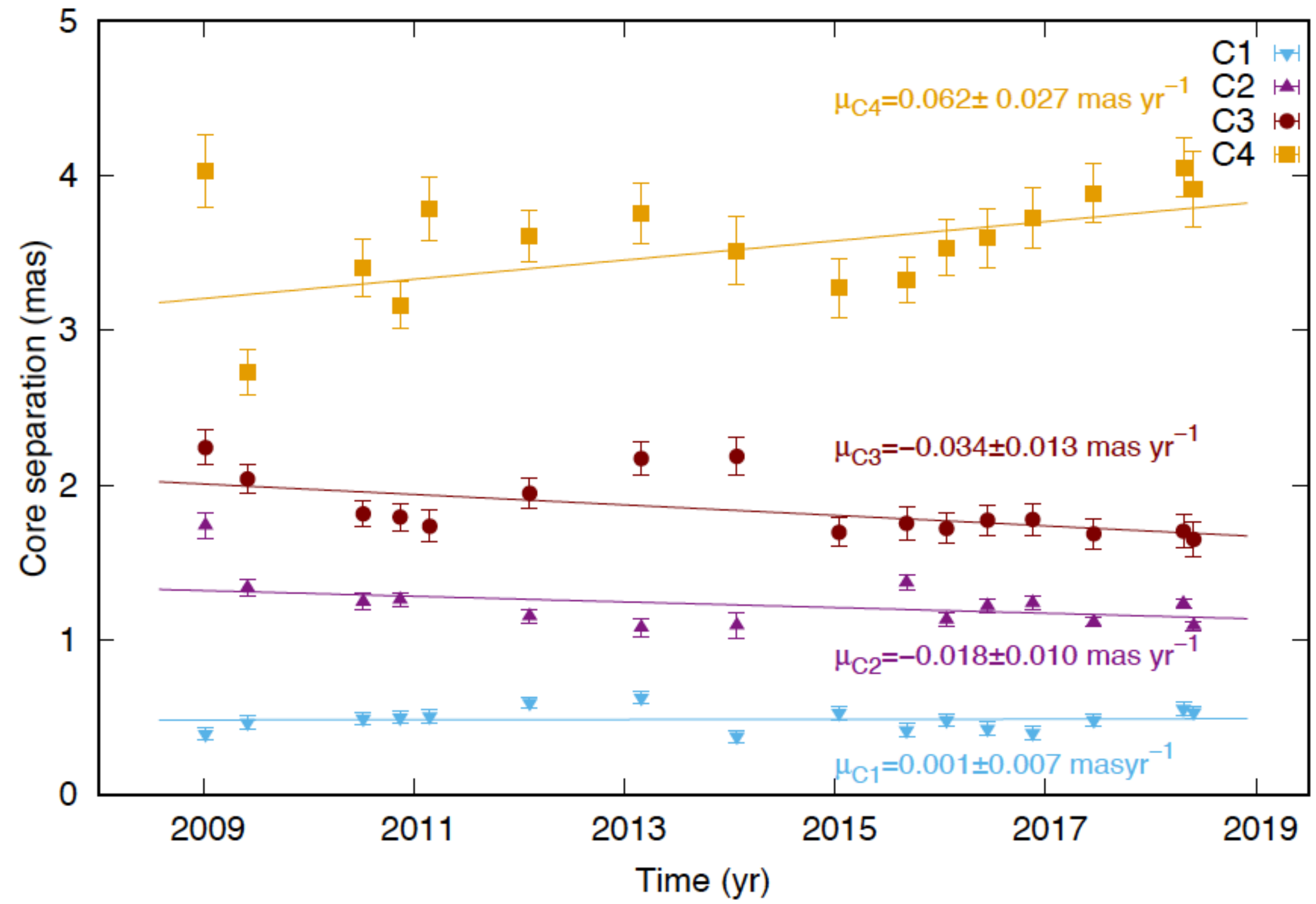

Quasi-stationary jet components

<u>The inclination angle should be pretty small, similarly to S5 1803+784</u>

Kun, Biermann, Gergely, MNRAS Letters, 2019, 483, 42

Radio brightening of TXS 0506+056

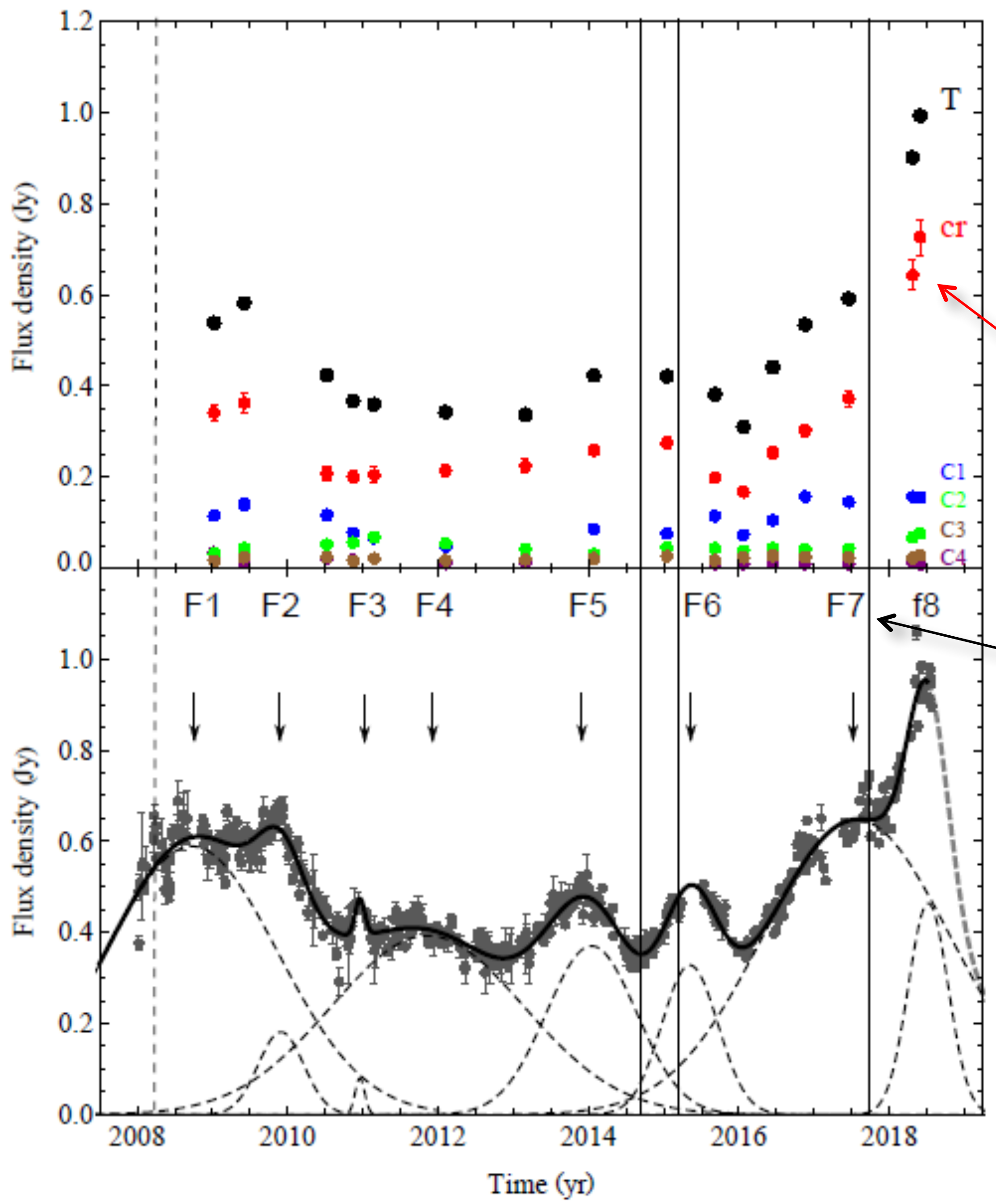

Flux density curve of the jet components (VLBA at 15 GHz)

VLBI core

IceCube-170922A, neutrino

Gaussian decomposition of the single dish flux density curves at 15 GHz measured with the OVRO 40m Telescope

The VLBI core is responsible for the abrupt radio brightening of the source

Kun, Biermann, Gergely, MNRAS Letters, 2019, 483, 42

Radio brightening of TXS 0506+056

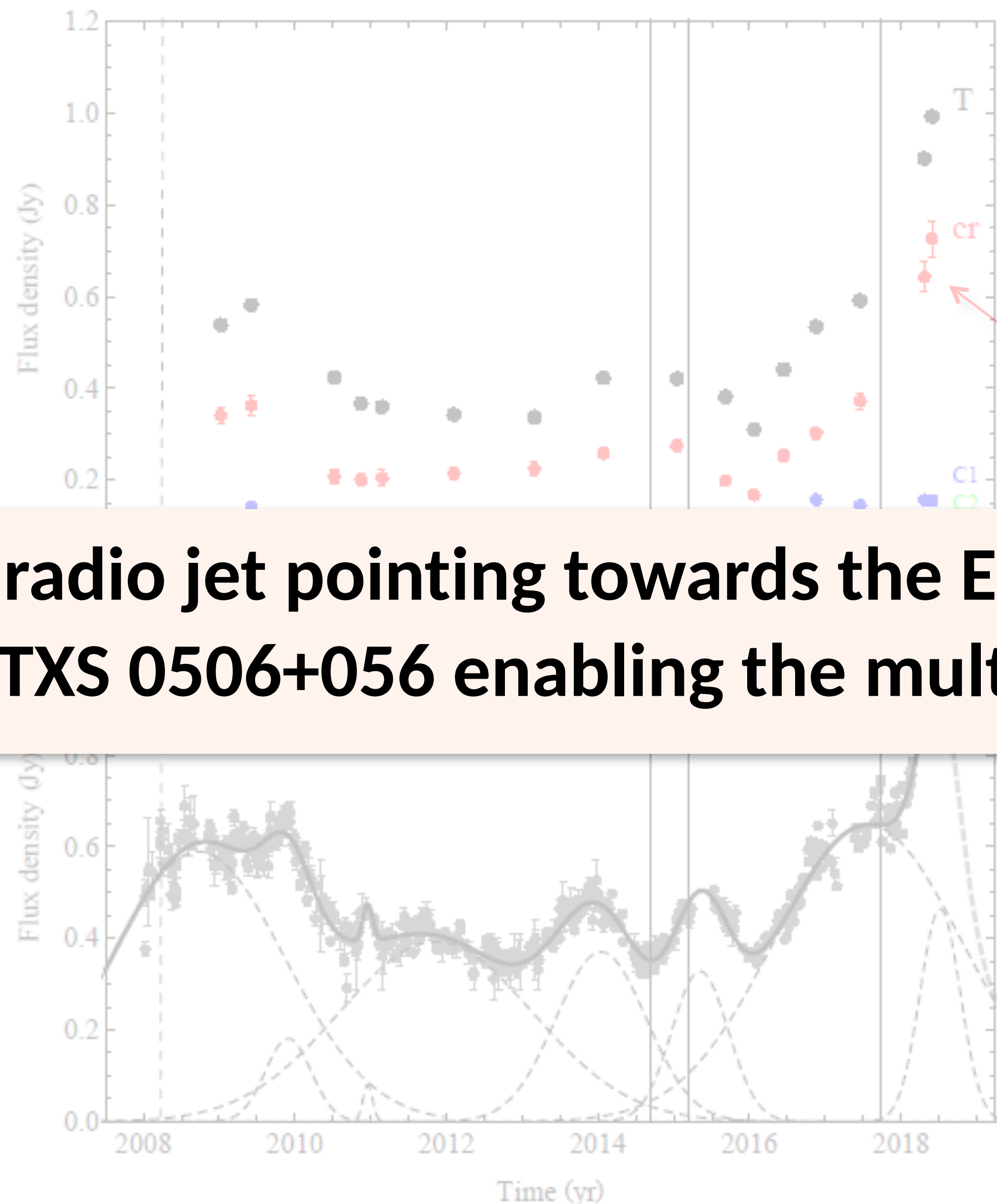

Flux density curve of the jet components (VLBA at 15 GHz)

The radio jet pointing towards the Earth is really a key property of TXS 0506+056 enabling the multimessenger observations.

Gaussian decomposition of the single dish flux density curves at 15 GHz measured with the OVRO 40m Telescope

The VLBI core is responsible for the abrupt radio brightening of the source

Kun, Biermann, Gergely, MNRAS Letters, 2019, 483, 42

The radio brightening of TXS 0506+056 continued…

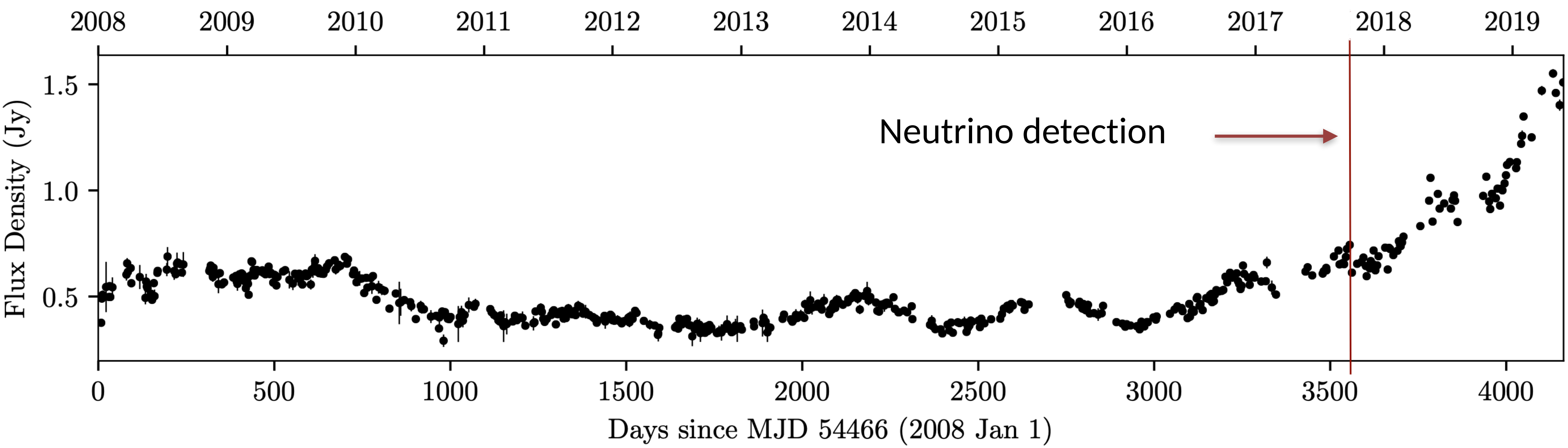

Multimessenger astronomy

A tool to observe the highest-energy phenomena in the Nature

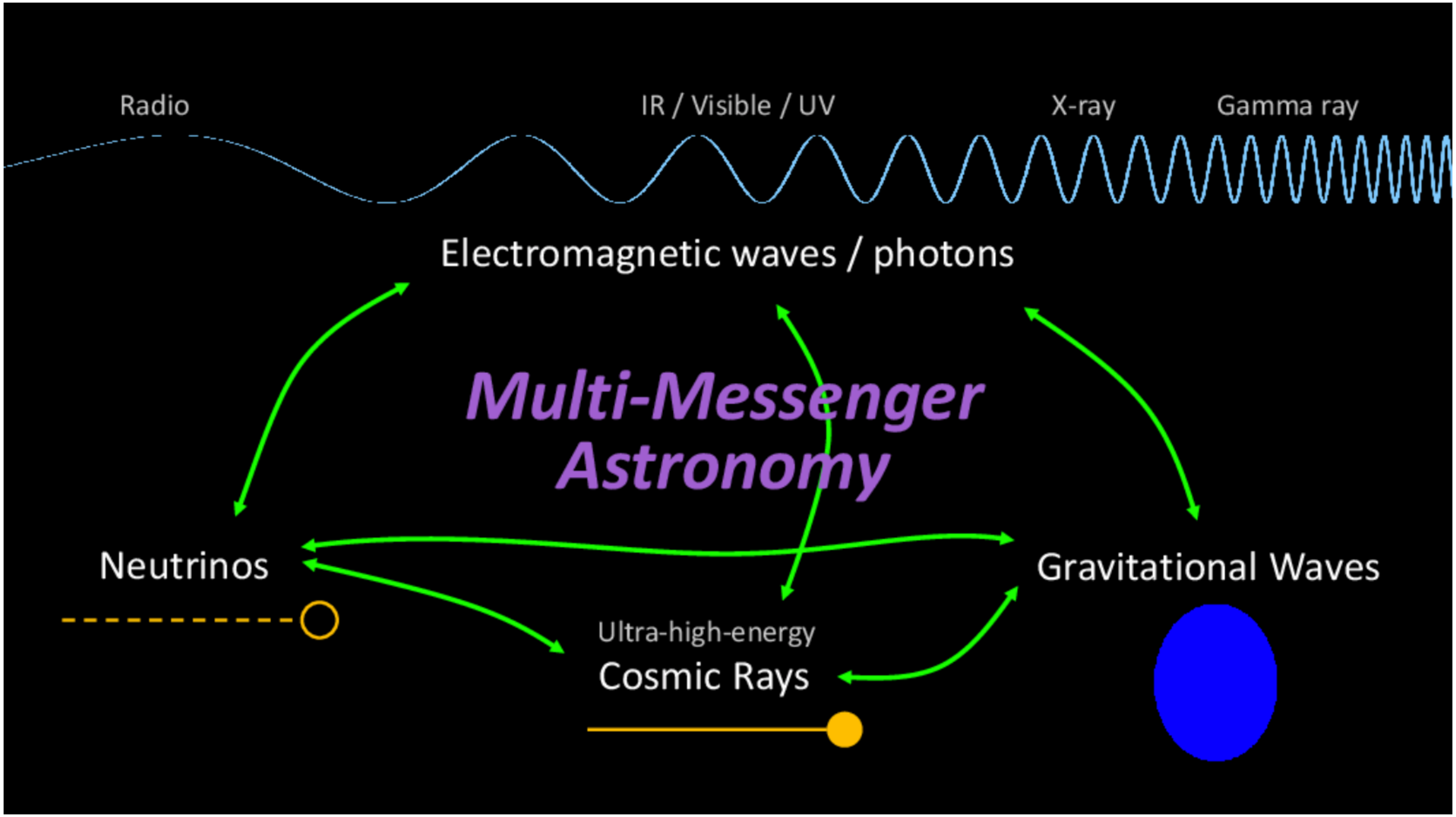

Multi-messenger observations of a binary neutron star merger

Abbott et al., 2017, ApJL, 848,12

GW170817

short GRB

Kilonova

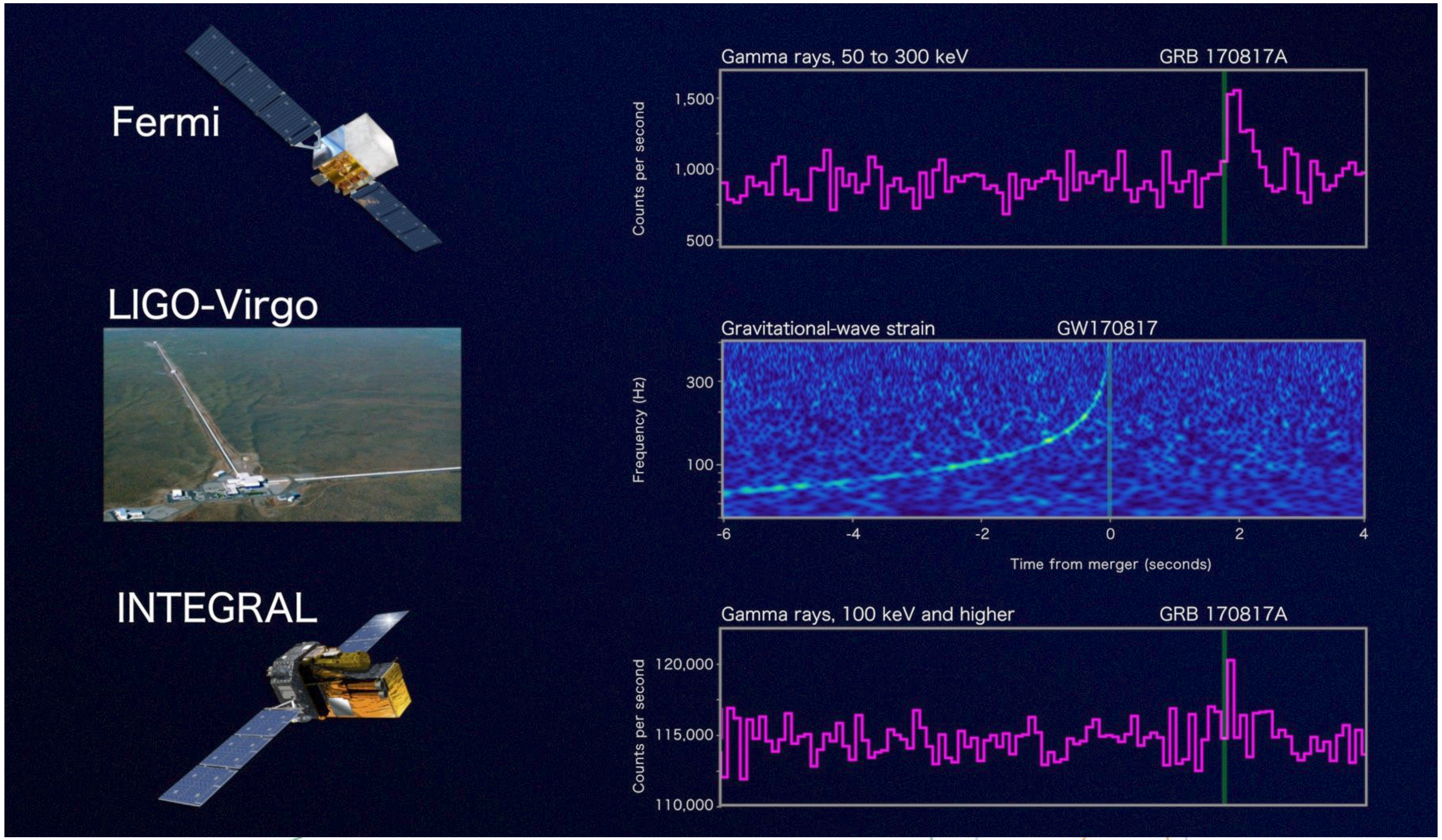

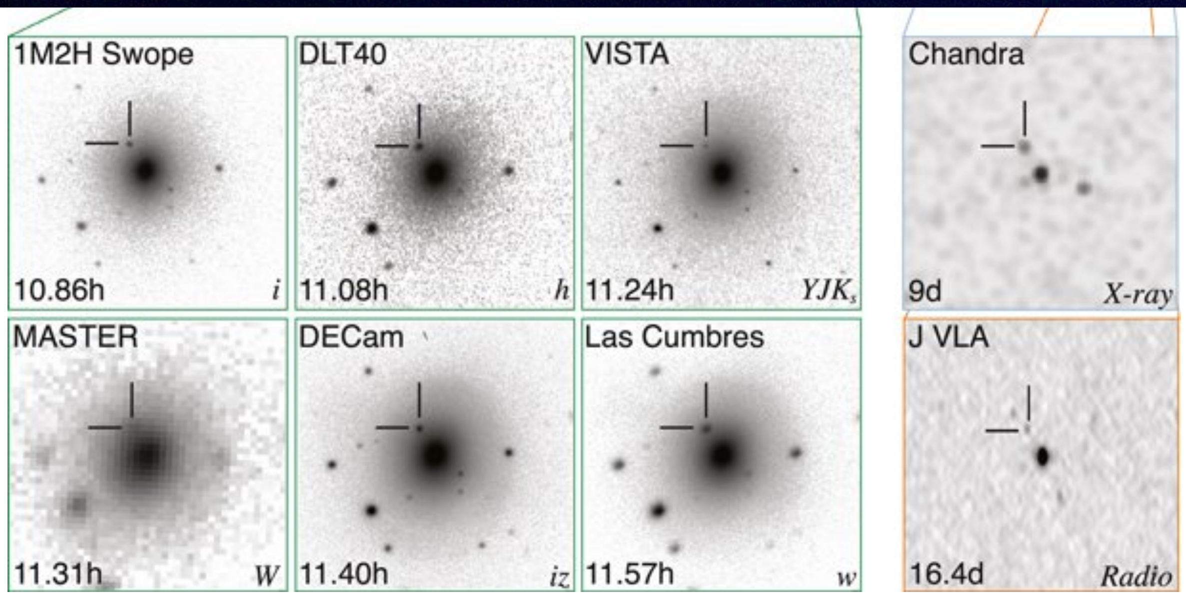

@LIGO, NASA's Goddard Space Flight Center, Caltech/MIT/LIGO Lab and ESA

Multi-messenger observations of a binary neutron star merger

Abbott et al., 2017, ApJL, 848,12

GW170817

short GRB

Kilonova

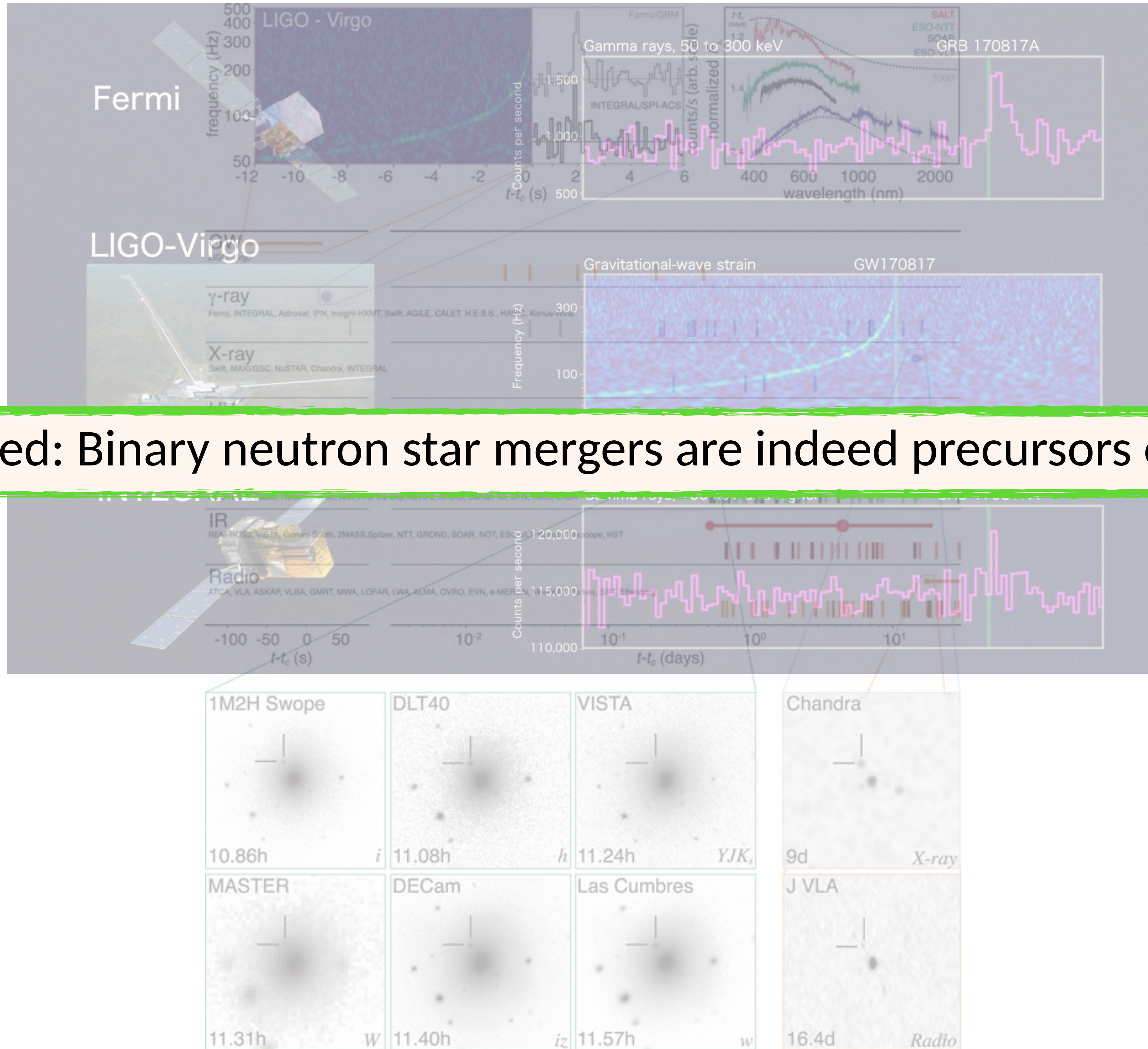

Lesson learned: Binary neutron star mergers are indeed precursors of short GRBs

@LIGO, NASA's Goddard Space Flight Center, Caltech/MIT/LIGO Lab and ESA

TXS 0506+056 — identified high-energy neutrino source (3.5 σ) IceCube-170922A

The IceCube Collaboration, Fermi-LAT, MAGIC, AGILE, ASAS-SN, HAWC, H.E.S.S, INTEGRAL, Kanata, Kiso, Kapteyn, Liverpool Telescope, Subaru, Swift/NuSTAR, VERITAS, and VLA/17B-403 teams, 2018, Science, 361, 6398

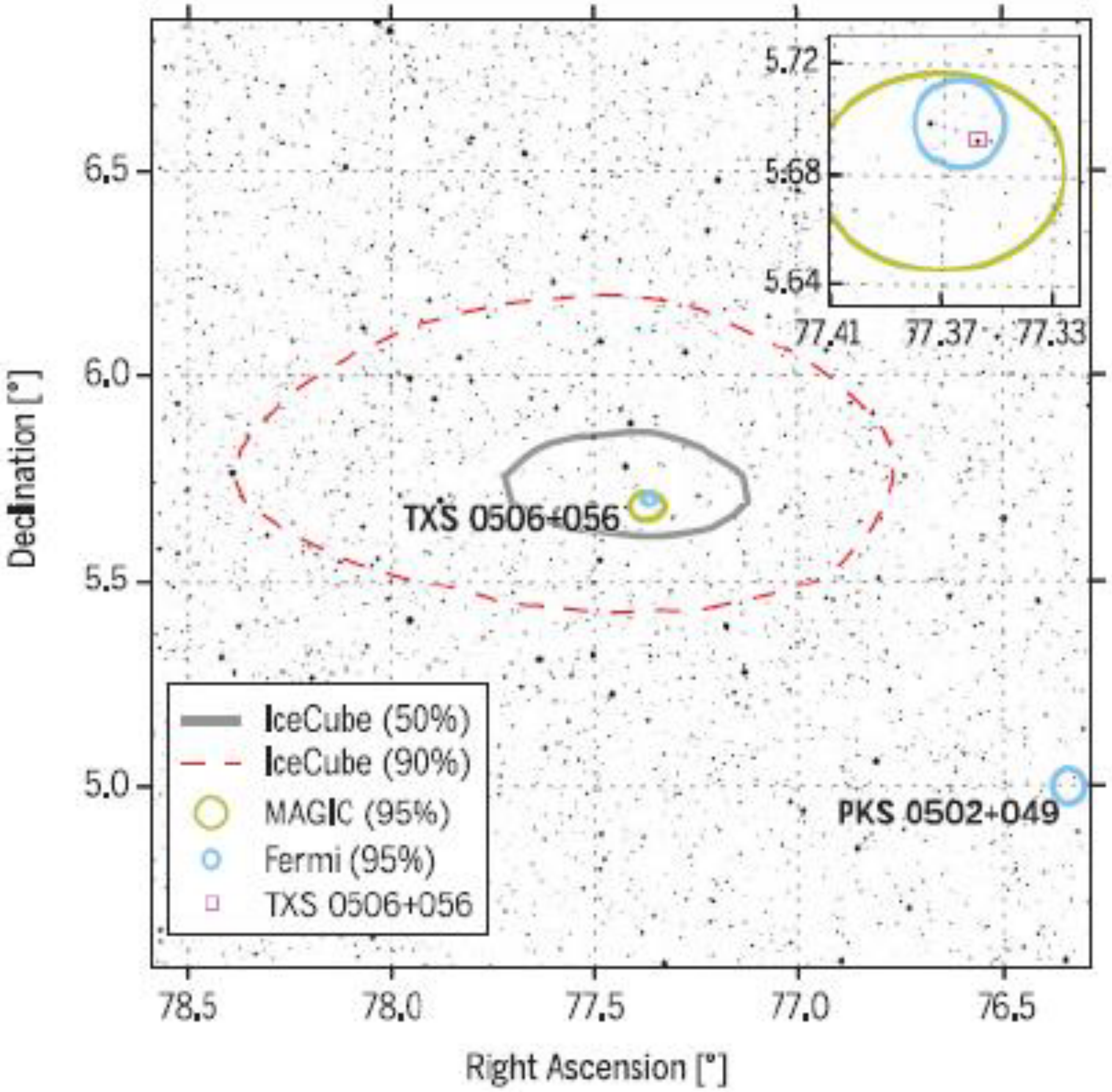

Multimessenger observations

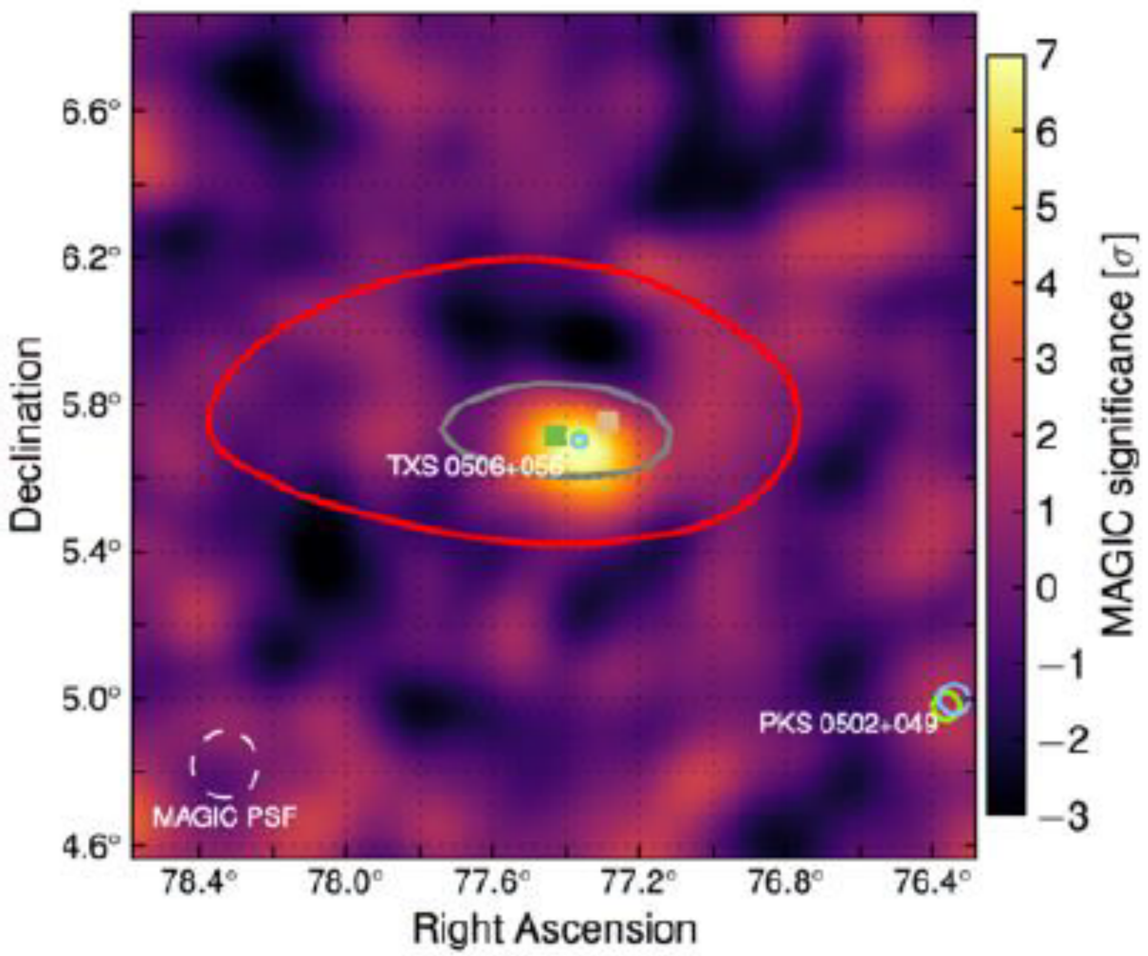

~300 TeV neutrino coincident with a γ-ray flare up to 400 GeV

TXS 0506-056 is a blazar (recently reclassified as a FSRQ), a class of the active galactic nuclei

TXS 0506+056 — identified high-energy neutrino source (3.5 σ) IceCube-170922A

The IceCube Collaboration, Fermi-LAT, MAGIC, AGILE, ASAS-SN, HAWC, H.E.S.S, INTEGRAL, Kanata, Kiso, Kapteyn, Liverpool Telescope, Subaru, Swift/NuSTAR, VERITAS, and VLA/17B-403 teams, 2018, Science, 361, 6398

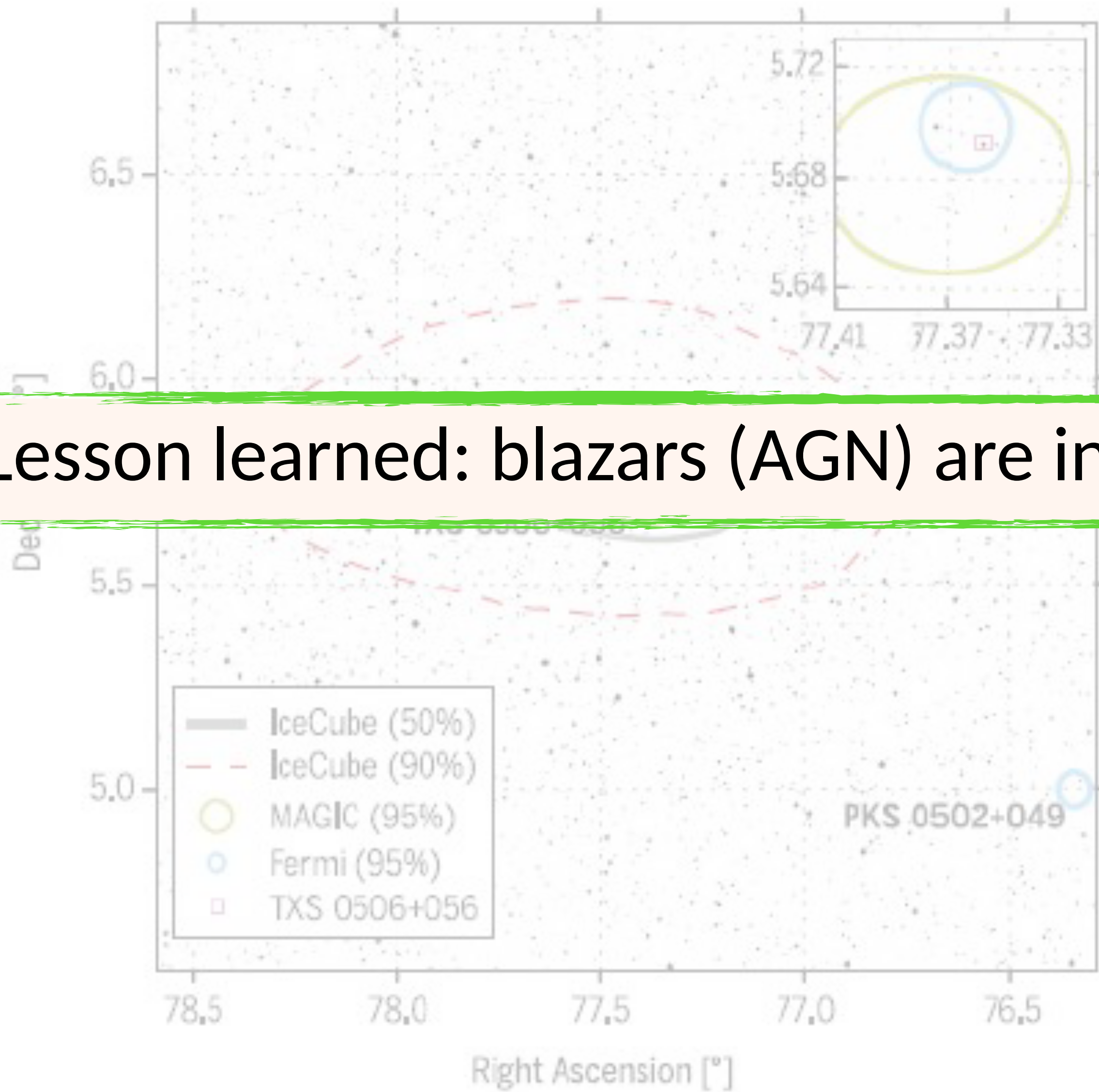

Multimessenger observations

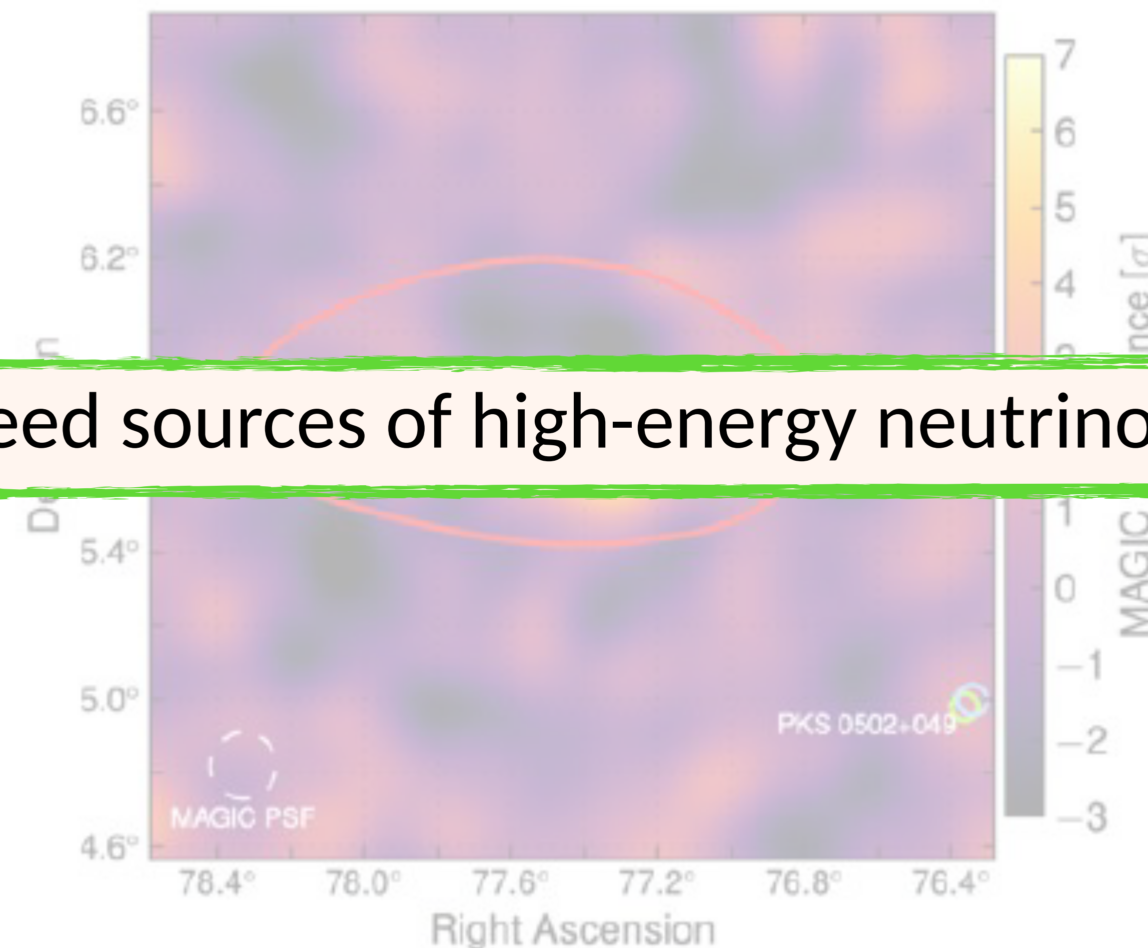

~300 TeV neutrino coincident with a γ-ray flare up to 400 GeV

Lesson learned: blazars (AGN) are indeed sources of high-energy neutrinos

TXS 0506-056 is a blazar (recently reclassified as a FSRQ), a class of the active galactic nuclei

Violent phenomena in the Universe

- active galactic nuclei (AGN)
- starburst galaxies
- tidal disruption events
- gamma-ray bursts
- merger of compact objects
- pulsars
- collapse of stellar cores
- …etc

they are able to accelerate particles

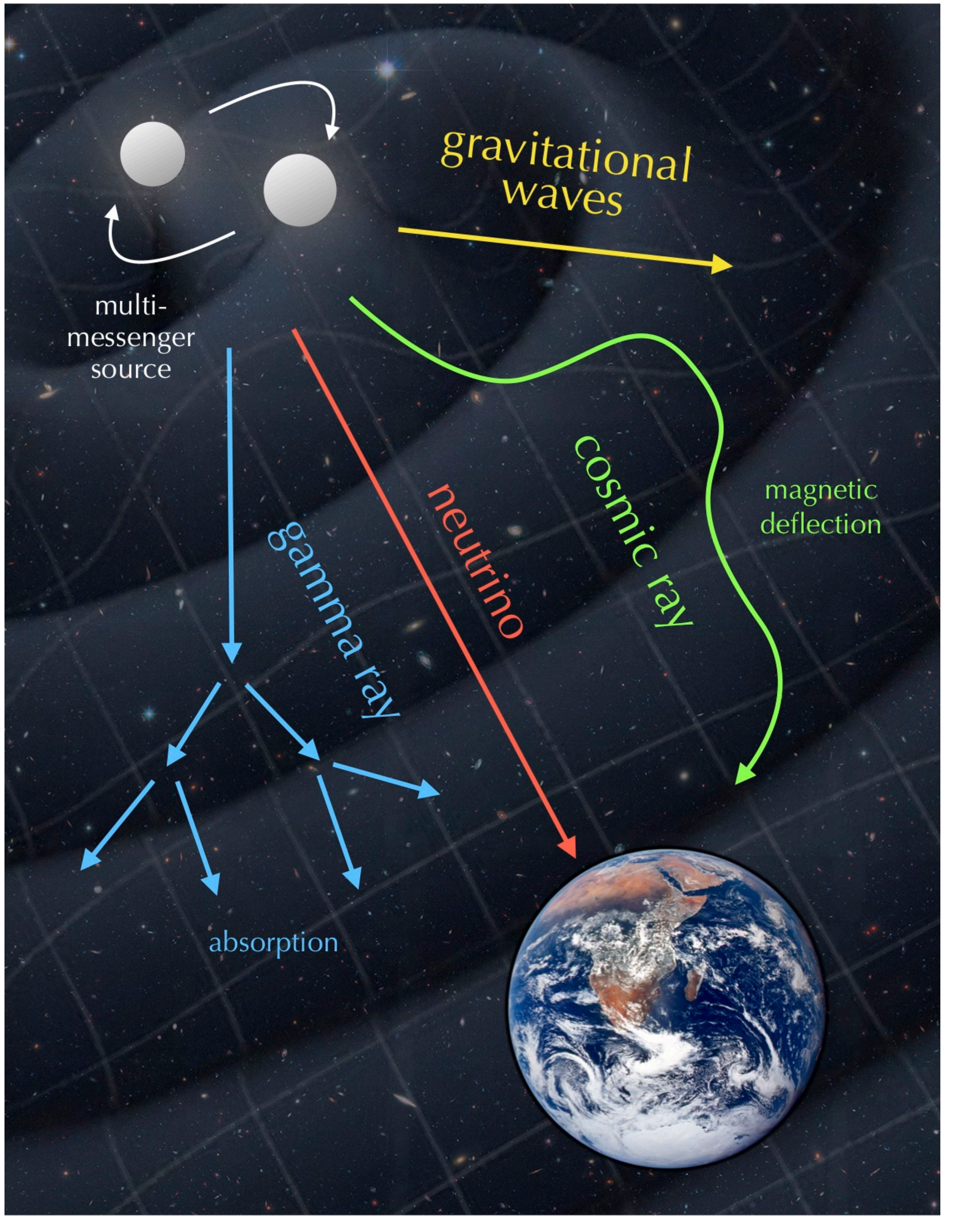

Cosmic-ray energy spectrum

Cosmic-rays

Charged particles (with intrinsic masses) from the Solar System, the Galaxy and beyond…

Protons (90%), heavier nuclei (9%), others (1%)

Oh-My-God particle (1991): 3x10^{11} GeV, 50 J

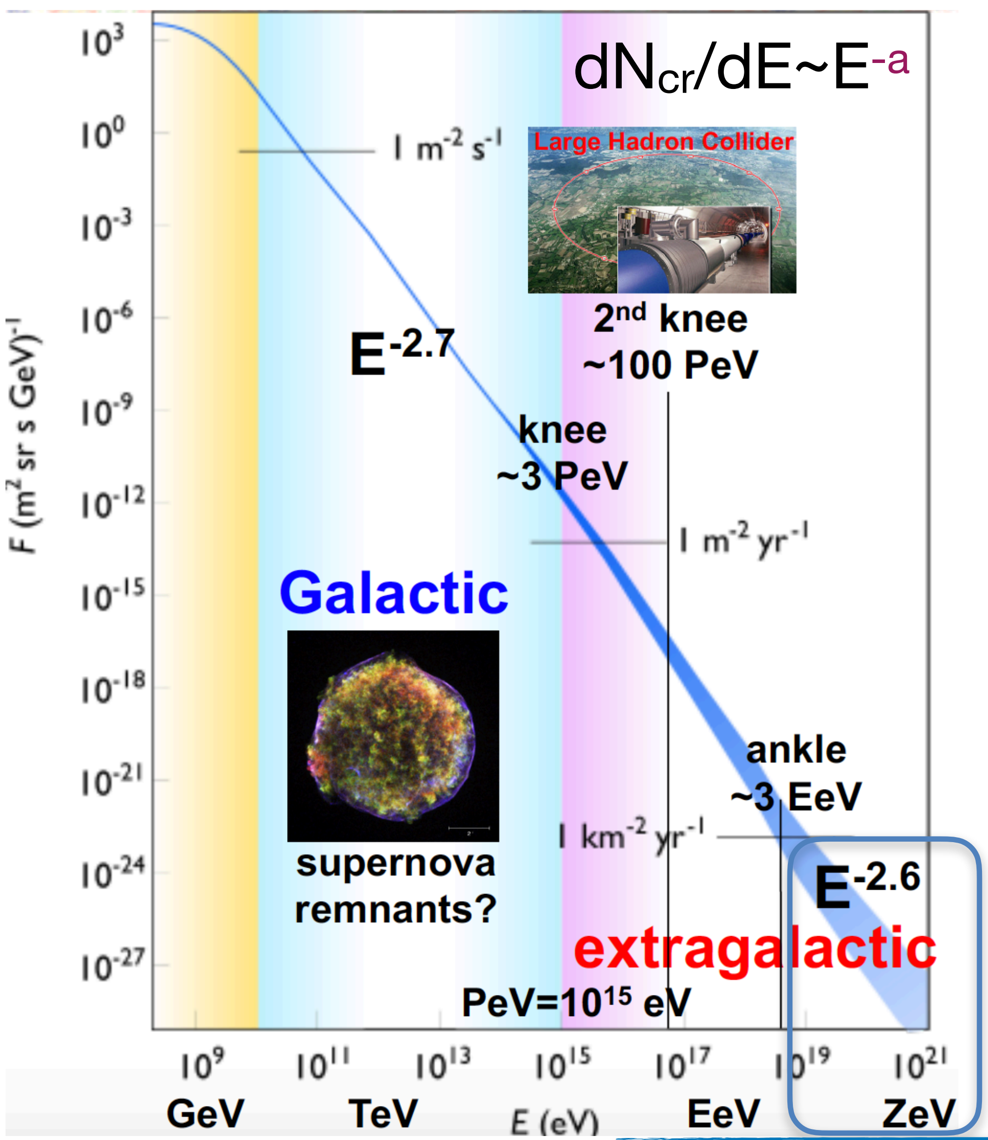

@Murase, 2018

1) How are cosmic rays accelerated?

bottom-up scenarios: *diffusive shock acceleration (a~2)*, Espresso models, acc. via induced electric field

2) How do they propagate?

diffusive, rectilinear

3) Transition from Galactic to extragalactic?

4) Where are their sources?

UHE CRs: 10^{18} eV < E_{UHECR} (LHC 6.5x10^{12} eV/beam)

4) Where are the (UHE)CR sources?

A century years old puzzle

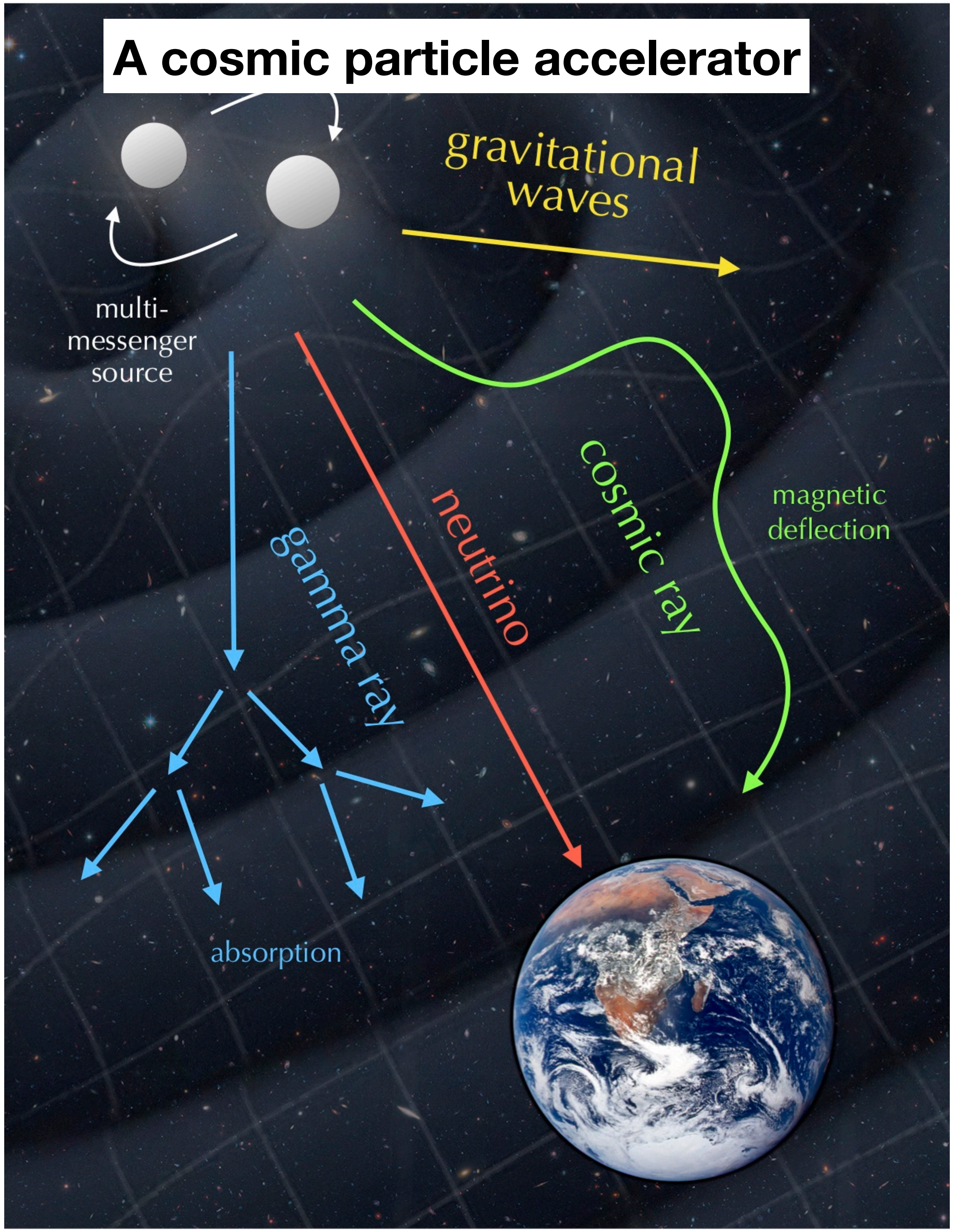

UHECRs

10^{18} eV < E_{UHECR} (LHC 6.5x10^{12} eV/beam)

Deflection by galactic and intergalactic magnetic fields

Greisen–Zatsepin–Kuzmin limit

The observed UHECR flux above ~ 5 x 10^{19} eV comes from sources within ~ 100 Mpc. It is z=0.024!

Gamma-rays make pairs with the EBL and CMB

The high-energy gamma-ray horizon at TeV energies is constrained to the universe at z < 1 and at PeV energies it is constrained to our Galaxy!

Pierre Auger Observatory (PAO):

One such event every four weeks in the 3000 km^2 area surveyed by the observatory

It is extremely difficult to find the sources of UHECRs

The observable Universe as function of the energy

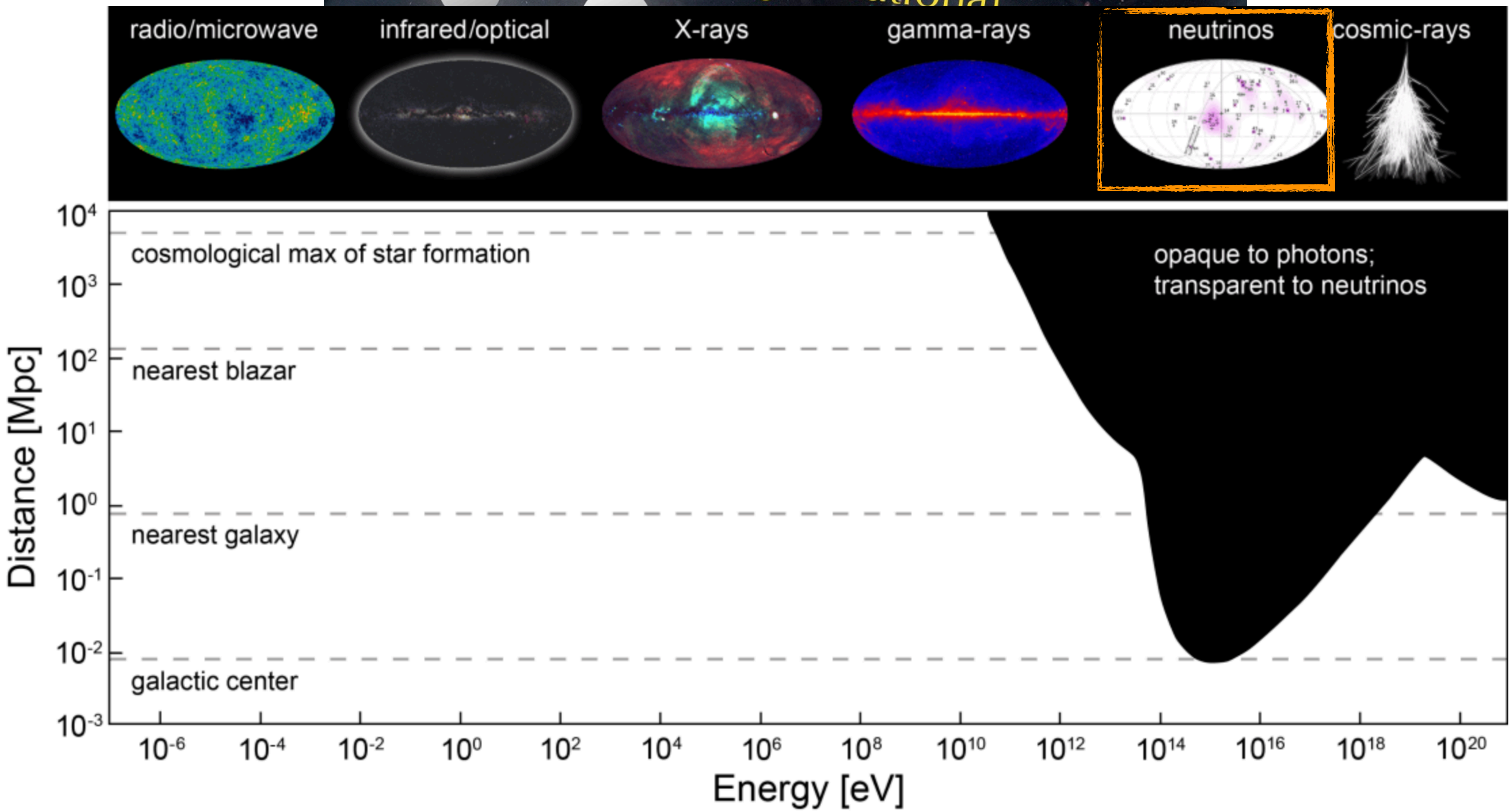

Neutrinos are **key messengers** to reveal an **unobstructed view of the universe** where it is opaque to light, and to the high-energy cosmic rays

Neutrinos from the cosmos

Cosmic neutrino-background (primordial neutrinos, diffuse SN- neutrino background)

Solar (and SN) neutrinos (nuclear processes)

E
n
e
r
g
y

The Sun in neutrinos,
Super-Kamiokande

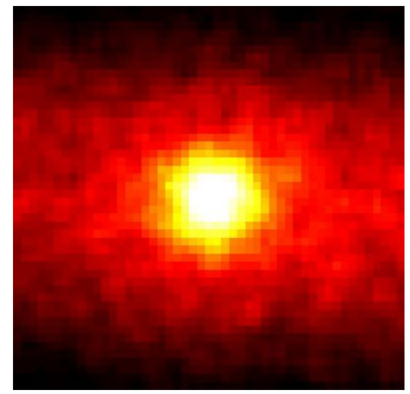

10^{-4} eV

>20 order of magnitudes

Cosmic neutrinos (meson decay in distant sources)

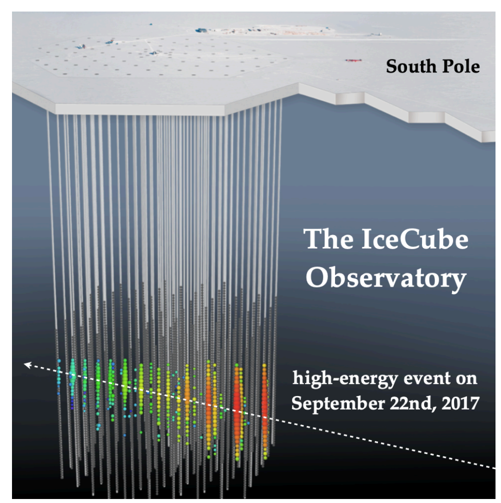

High-energy neutrino
from an active galaxy

10 PeV<

Cosmogenic neutrinos (UHECRs+CMB, GZK cutoff)

The rest-mass energy of a muon neutrino is <0,17 MeV
10 PeV is 10^{11} times this

1 eV=1,6x10^{-19} J
10 PeV=1,6x10^{-3} J

Extremely efficient acceleration

Cosmic neutrinos

Galactic

- SNII supernovae
- Binary neutron stars
- Microquasars
- Magnetars
- Anomalous X-ray pulsars
- Molecular clouds

Extragalactic

- Active galactic nuclei
- Starburst galaxies
- Tidal disruption events
- Gamma-ray bursts

What we observe might be a cumulative signal of all sources (or more)
What are the dominant sources?

AGN are extremely efficient particle accelerators

The most powerful permanent particle accelerators in the Cosmos

- The particles flow onto central supermassive black hole
- Some of the gravitational energy is released
- η measures how much of the rest mass will be converted to energy
- The efficiency η will depend on the spin (a) of the black hole:
  - for a=0 (Schwarzschild) we have η =6%
  - for a=1 (extreme Kerr) we have η =40%!

a* has a maximum at 0.89 for rotating black holes with accretions disk

for the hydrogen fusion η is about 0.7%

- The binding energy is transformed into the acceleration of protons or heavier nuclei

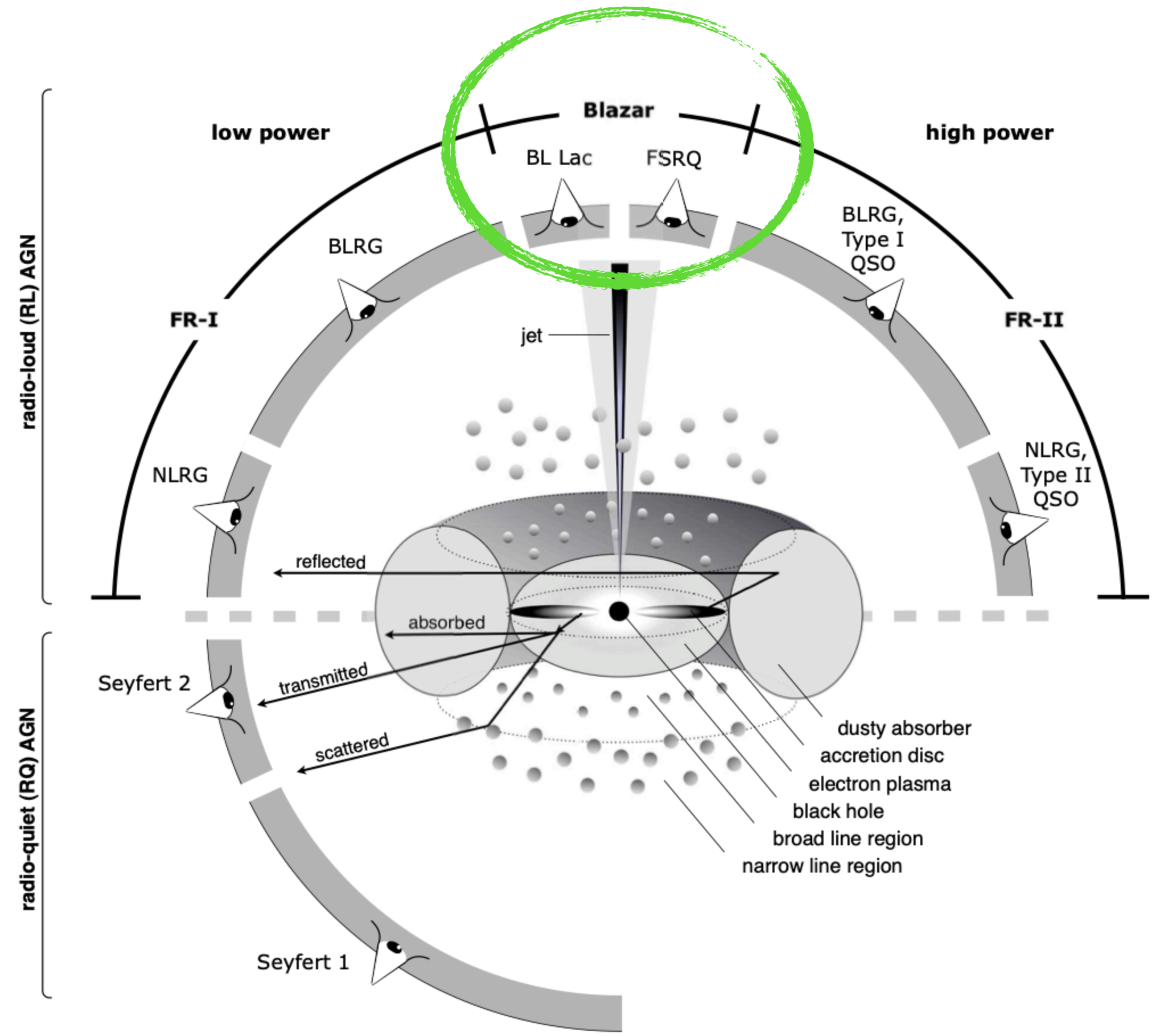

Urry&Padovani, 1995, PASP,107, 803
Beckmann & Shrader, 2012
illustration by Marie-Luise Menzel, 2012

Other prime candidates: starburst galaxies, TDEs

High-energy neutrinos from extragalactic UHECR sources?

A large part of the signal might come!

- HE neutrinos are isotropically distributed
- Their intensity is compatible with expectations
- No significant correlation between nearby UHECR sources and neutrinos

IceCube Neutrino Detector
~10 detections per year

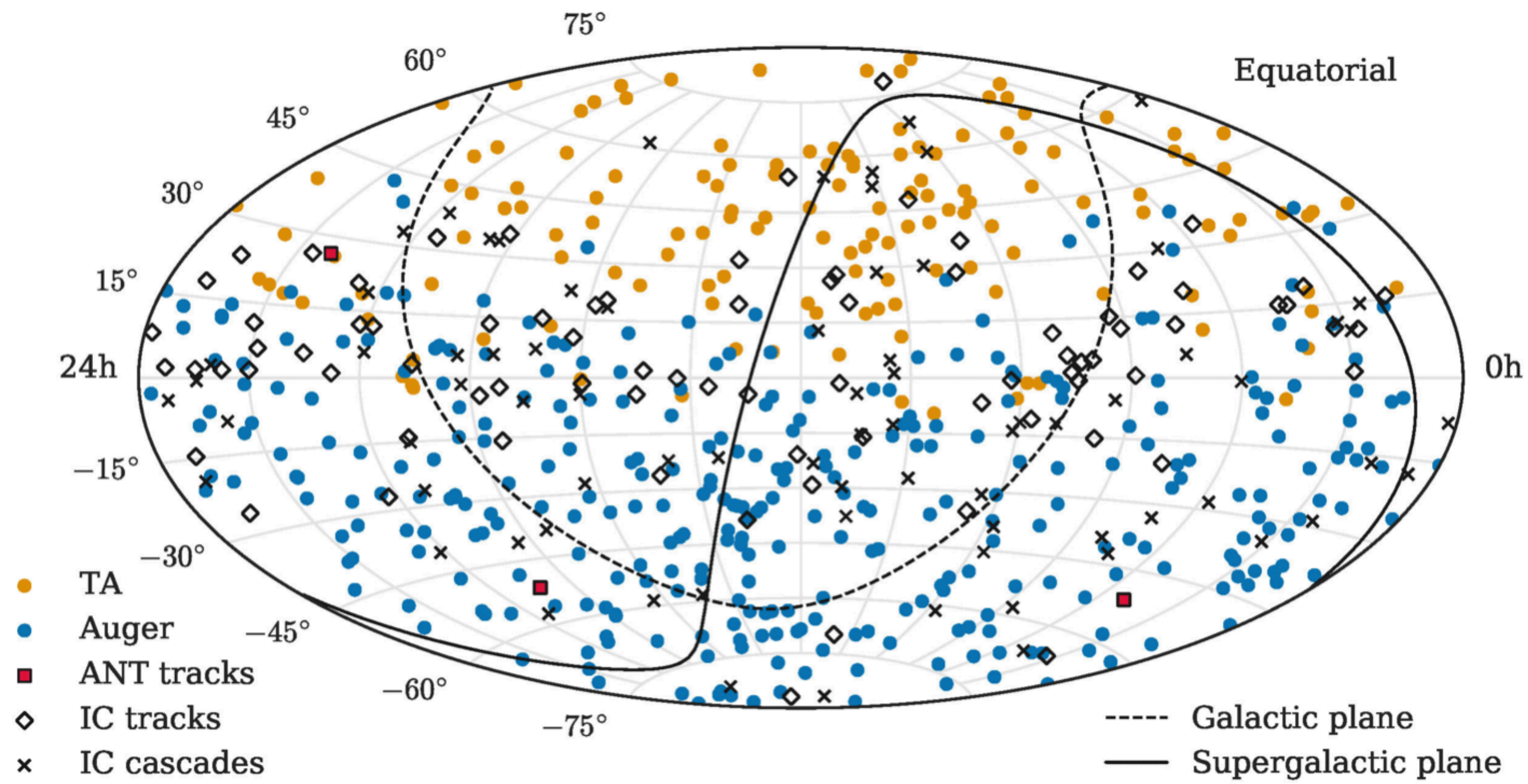

Sky map of the arrival directions of UHECR events from the Pierre Auger Observatory and the Telescope Array and high-energy neutrinos from IceCube and ANTARES. Credit: The ANTARES, IceCube, Pierre Auger and Telescope Array collaborations.

ANTARES, IceCube, Pierre Auger and Telescope Array Collaborations: M.G.Aartsen et al. Submitted to *Astrophysical Journal.* arxiv.org/abs/2201.07313

High-energy neutrinos from extragalactic UHECR sources?

A large part of the signal might come!

Catalogue of $z \geq 4$ AGNs

(Perger 2020, doi: 10.15476/ELTE.2020.161)

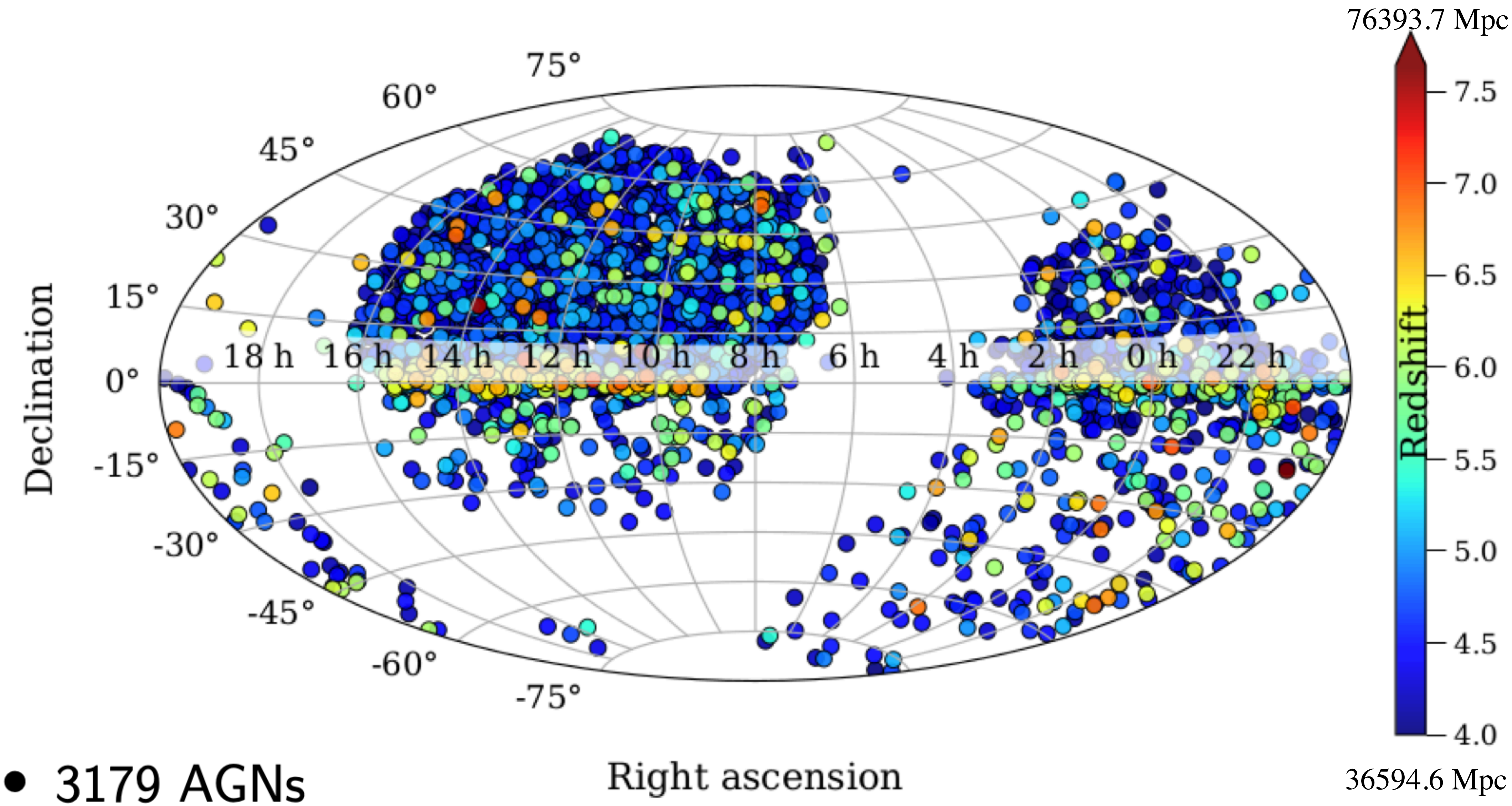

- 3179 AGNs

Sky map of the arrival directions of UHECR events from the Pierre Auger Observatory and the Telescope Array and high-energy neutrinos from IceCube and ANTARES. Credit: The ANTARES, IceCube, Pierre Auger and Telescope Array collaborations.

ANTARES, IceCube, Pierre Auger and Telescope Array Collaborations: M.G.Aartsen et al. Submitted to *Astrophysical Journal*. arxiv.org/abs/2201.07313

Radio emission from active galaxies

- Charged particles gyrating about the magnetic field
- Synchrotron radiation: primary process to generate the radio continuum of jetted AGN
- Low energy component of the blazar SEDs
- method 1: search correlations between astro neutrinos and <u>individual radio sources</u> or source catalogs

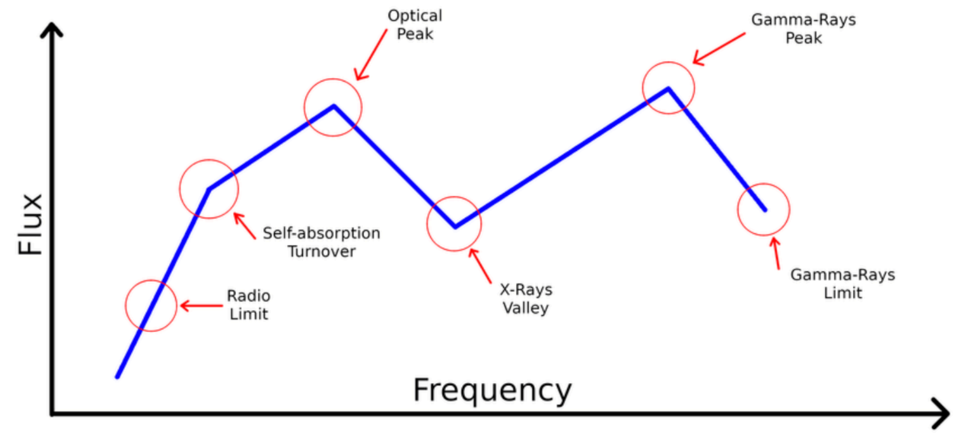

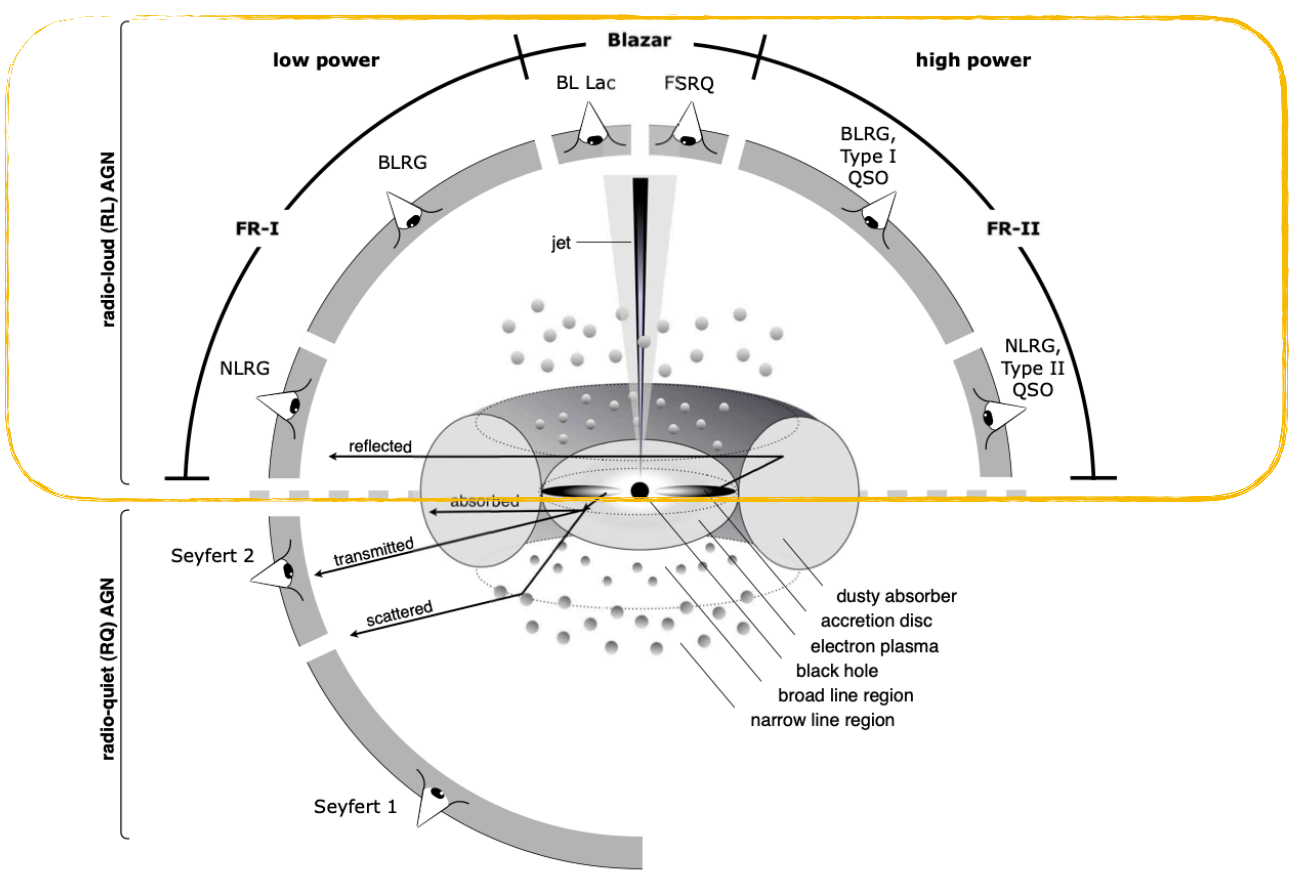

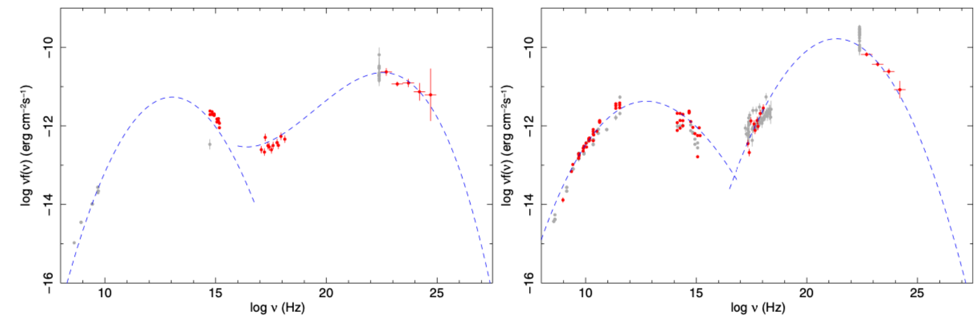

Figure 8. SED of 0FGL J0516.2−6200 = MC4 0516-621 (left) and of 0FGL J0531.0+1331 = PKS 0528+134 (right).
(A color version of this figure is available in the online journal.)

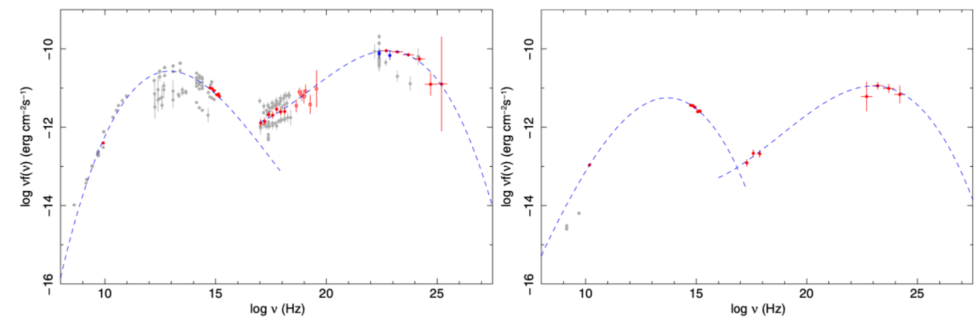

Figure 9. SED of 0FGL J0538.8−4403 = PKS0537-441. (left) and of 0FGL J0712.9+5034 = GB6 J0712+5033 (right).
(A color version of this figure is available in the online journal.)

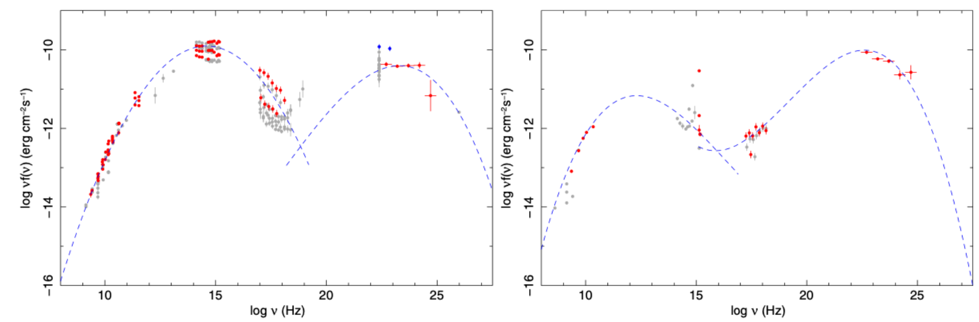

Figure 10. SED of 0FGL J0722.0+7120 = S50716+714 (left) and of 0FGL J0730.4−1142 = PKS0727-11 (right).
(A color version of this figure is available in the online journal.)

Radio observations+neutrinos

- method 1: search correlations between astro neutrinos and <u>individual radio sources</u> or source catalogs

Single-dish radio observation of individual sources

Examples: **TXS 0506+056 (OVRO, 15 GHz)**

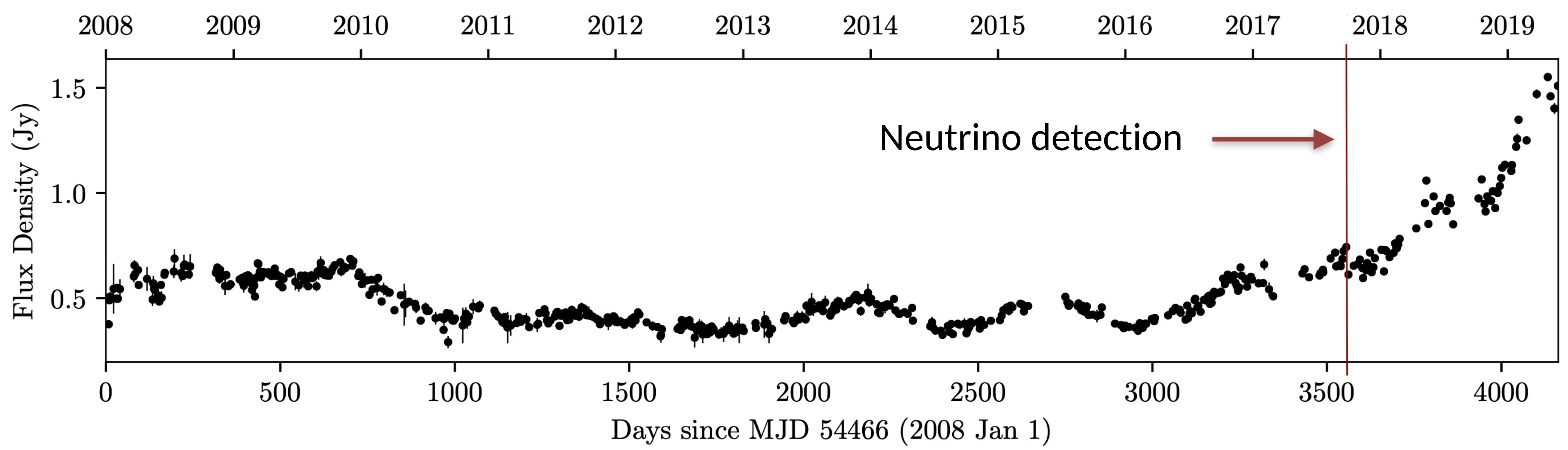

PKS 1502+106 (OVRO, 15 GHz)

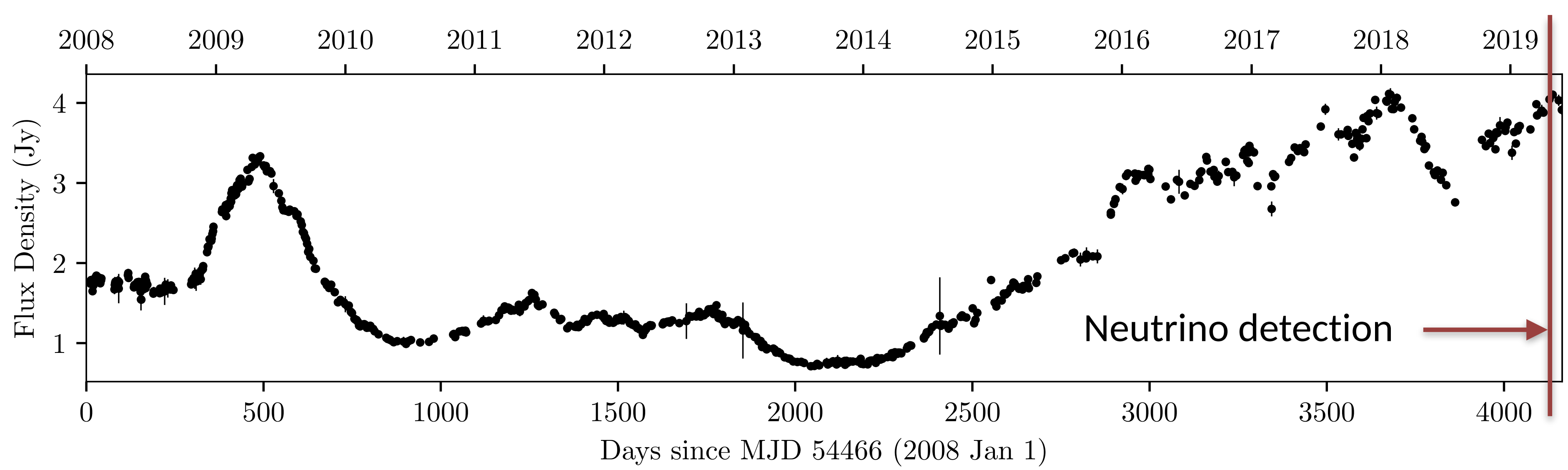

PKS 1502+106: gamma-ray flux vs radio flux density

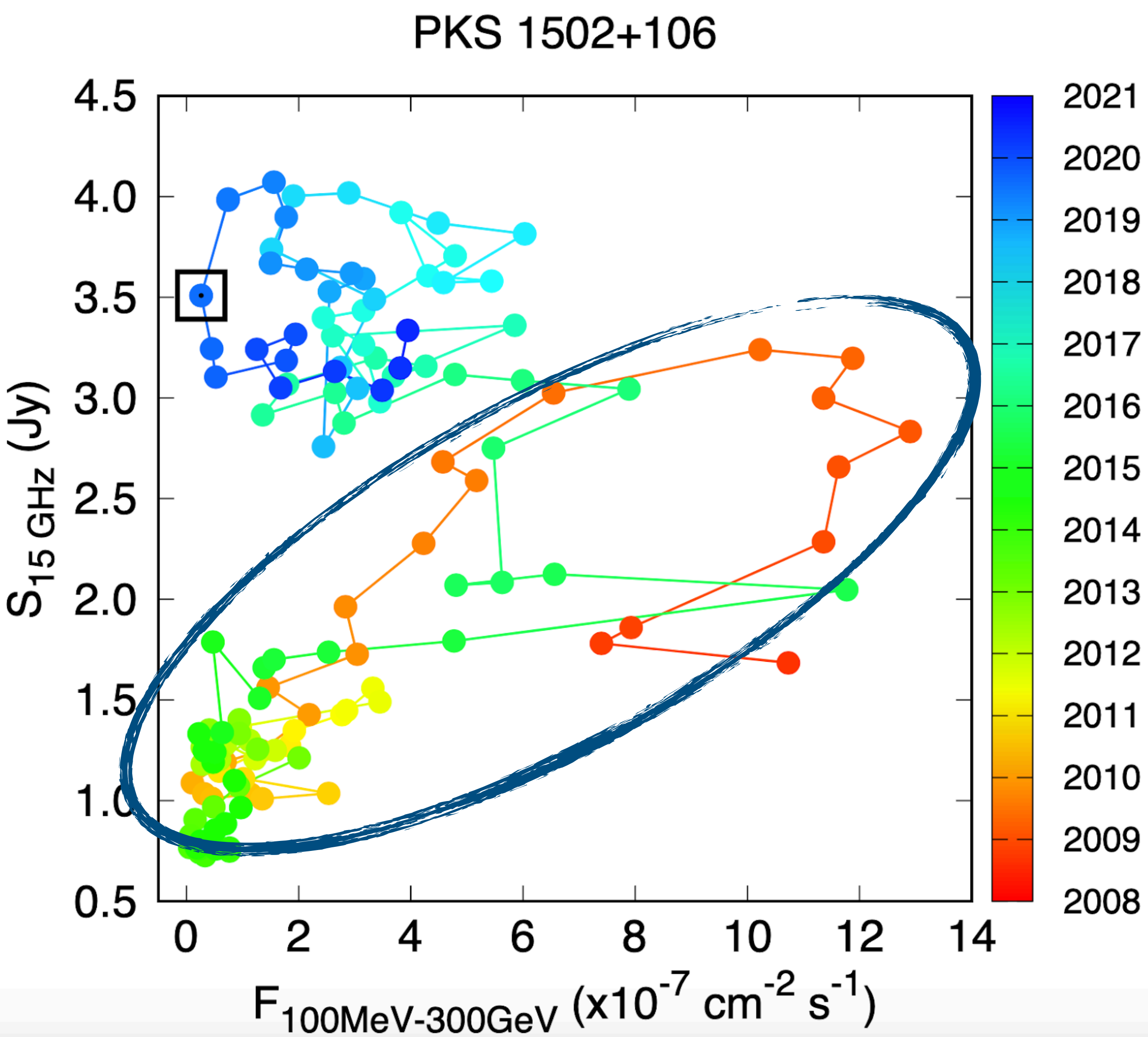

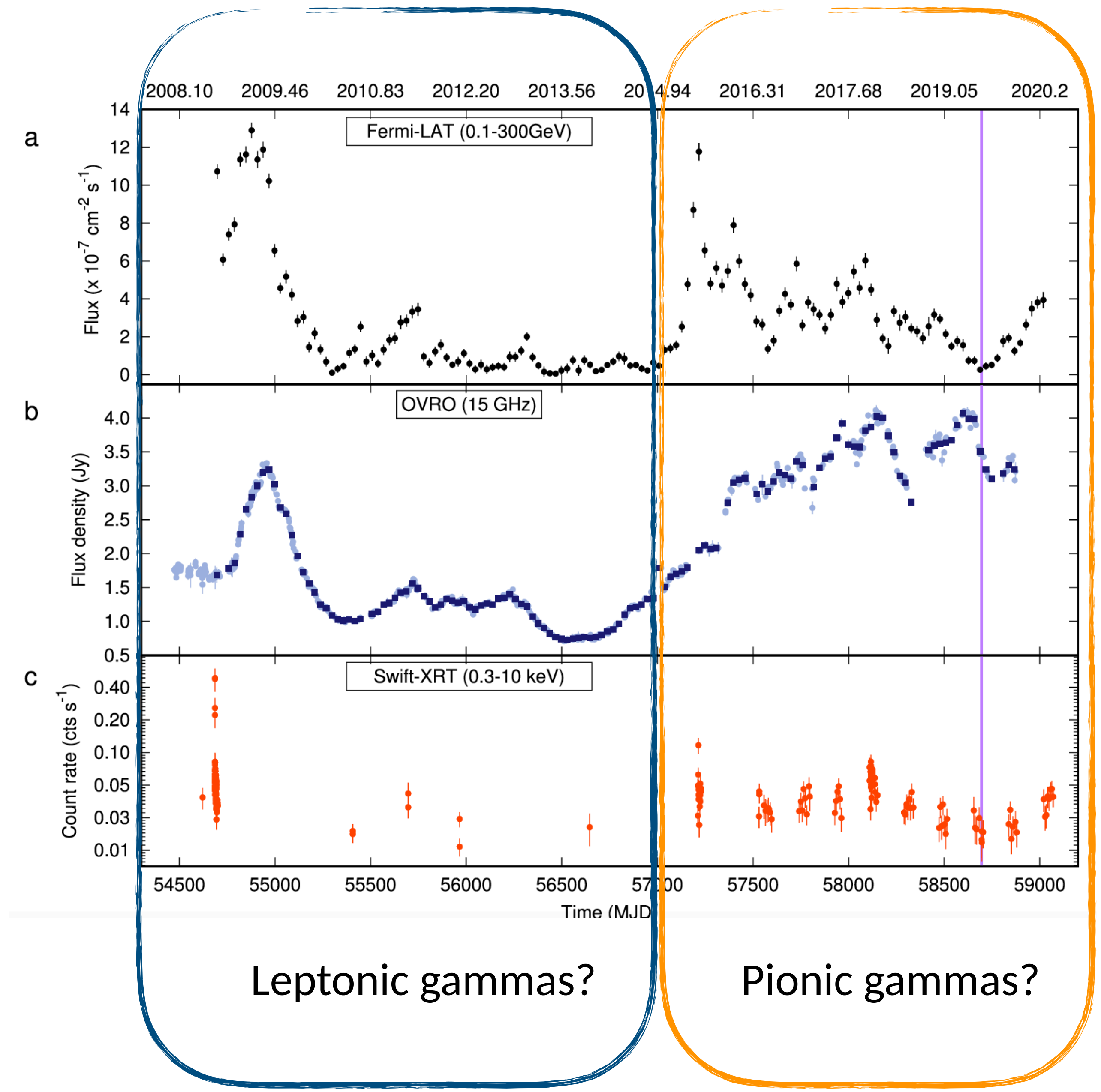

Mode1: gamma correlates with radio, the radio lagging behind the gamma flux (R=0.85, τ_c=59+-32 days)

Mode2: more complex connection

Kun, Bartos, Becker-Tjus, Biermann, Halzen, Mező, 2021, ApJL, 911, L18

What caused this switch?

We can pinpoint different components of the jet

Where are the acceleration sites? (do leptons and hadrons get co-accelerated?)

Radio brightening of TXS 0506+056

Kun, Biermann, Gergely 2019, MNRAS Letters, 483, 42

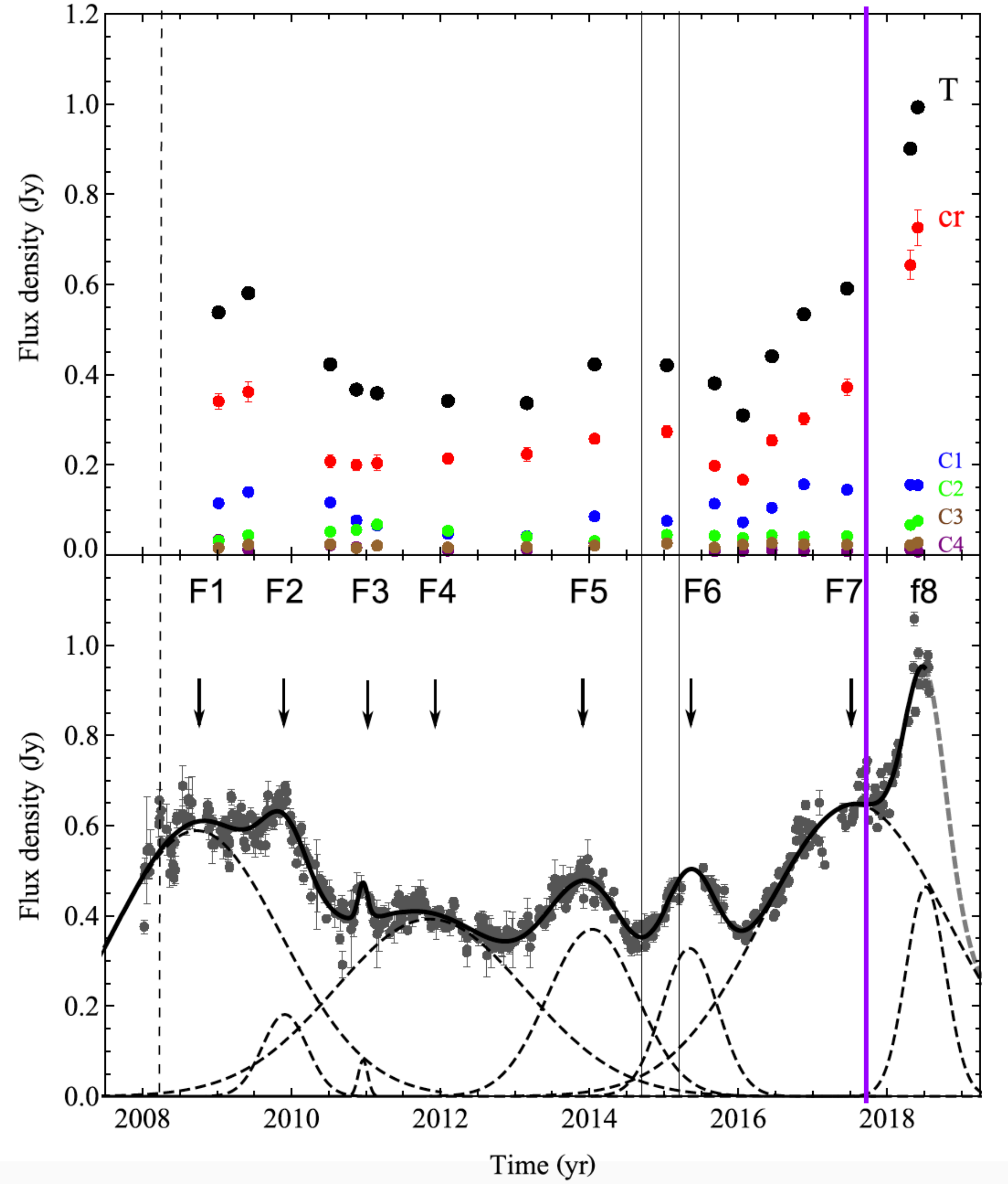

Flux density curve of the jet components (MOJAVE/VLBA at 15 GHz)

VLBI core is responsible for the brightening at 15 GHz

(same results at higher frequencies, e.g. Ros et al. 2019)

IceCube-170922A

Gaussian decomposition of the single dish flux density curve at 15 GHz measured with the OVRO 40m Telescope

VLBI of individual sources

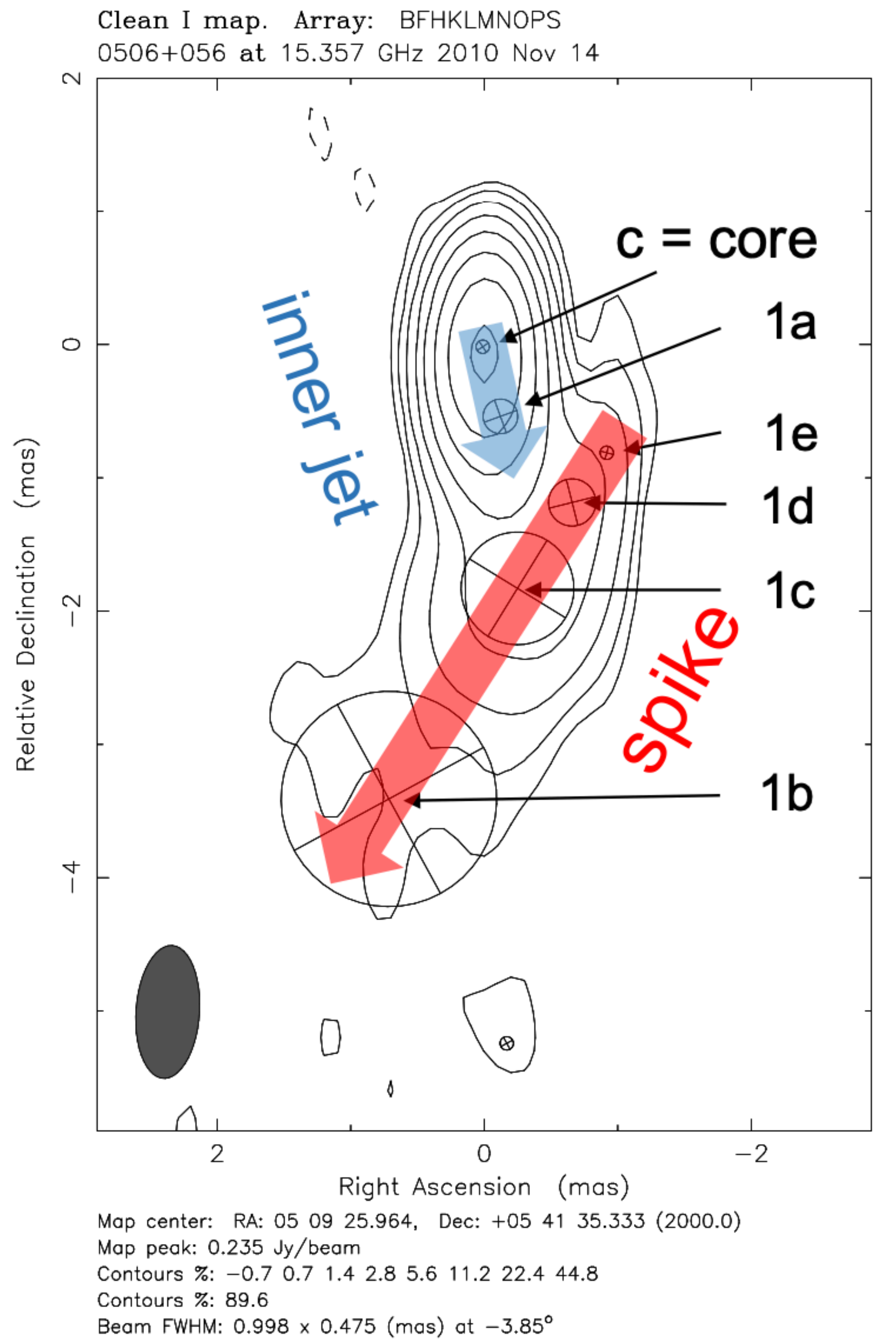

A cosmic collider: Was the IceCube neutrino generated in a precessing jet-jet interaction in **TXS 0506+056**?

Britzen et al. 2019

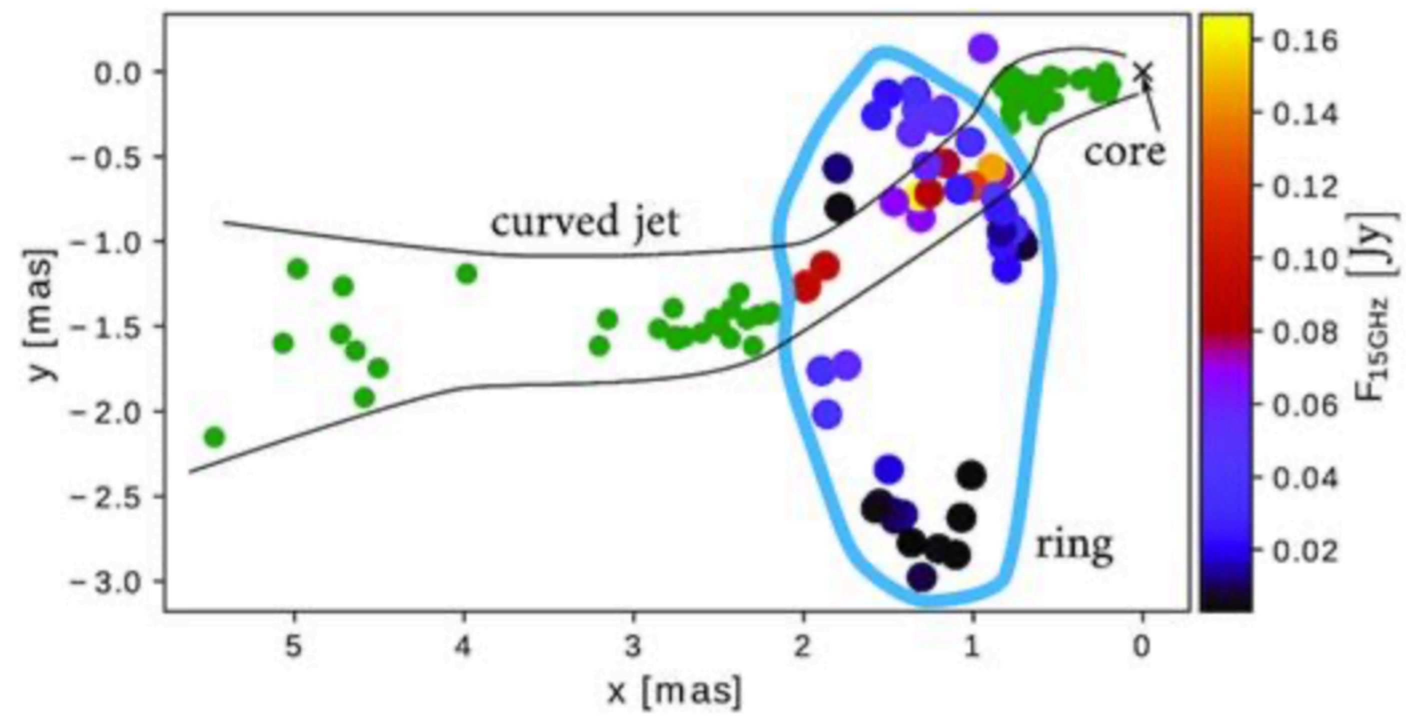

A ring accelerator? Unusual jet dynamics in the IceCube candidate **PKS 1502+106**

Britzen et al. 2021

Radio observations+neutrinos

- method 1: search correlations between astro neutrinos and individual radio sources or source catalogs
- 7 years of IceCube muon tracks, 8 GHz VLBI data of 3411 radio-loud AGN (Plavin et al 2020, 2021): 4.1 sigma connection
- OVRO (15 GHz) and Metsahovi radio observatories (36.8 GHz), IceCube tracks (Hovatta et al. 2021): radio flares in blazars at the same time as the neutrino event unlikely to be random coincidence at 2 sigma level

Radio observations+neutrinos

- method2: stacking analysis (Achterberg et al. 2006)
- 10 year of muon tracks 3,388 Radio Fundamental Cat. (Zhou et al. 2020): these AGN can account for at most 30% (95 CL) of the flux of neutrino tracks
- MOJAVE XV. Catalog (15 GHz, VLBA) 10 years of detector data (Desai et al 2021): no significant correlation

No significant findings, but there are promising results

CRATES 4.8 GHz and 8.4 GHz + 70 IceCube muon-tracks (2009-2019)

- Matched positions of point sources in the CRATES 8.4 GHz catalog (also 4.8 GHz) with 70 track-type IceCube neutrinos (2009-2019) from Giommi et al. (2020)
- Found 87 (96) CRATES sources at 4.8 GHz (8.4 GHz) within the 90 C.L. error ellipse of the neutrinos

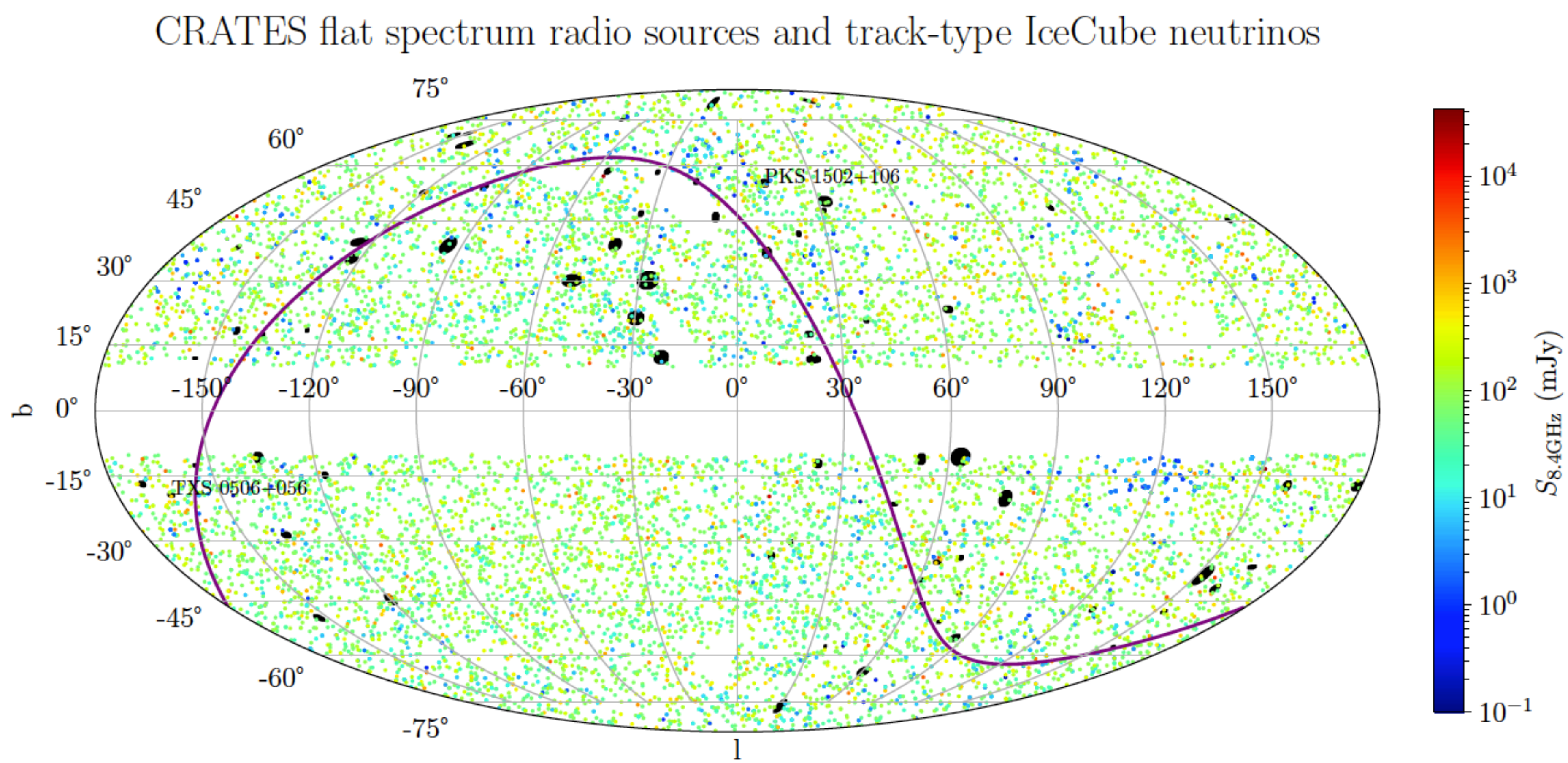

Figure 3. Galactic sky-position (l,b) and 8.4 GHz flux density of the CRATES radio sources (colored dots) and track-type neutrino detections of the IceCube Neutrino Detector (black filled ellipses) published by Giommi et al. (2020). The maps are shown in Mollweide projection. The equator is plotted by a purple continuous line. TXS 0506+056 and PKS 1502+106 are marked on the map.

Kun et al. 2022, submitted

CRATES 4.8 GHz and 8.4 GHz + 70 IceCube muon-tracks (2009-2019)

- Matched positions of point sources in the CRATES 8.4 GHz catalog (also 4.8 GHz) with track-type neutrinos from Giommi et al. (2020)
- Found 87 (96) CRATES sources at 4.8 GHz (8.4 GHz) within the 90 C.L. error ellipse of the neutrinos

CRATES flat spectrum radio sources and track-type IceCube neutrinos

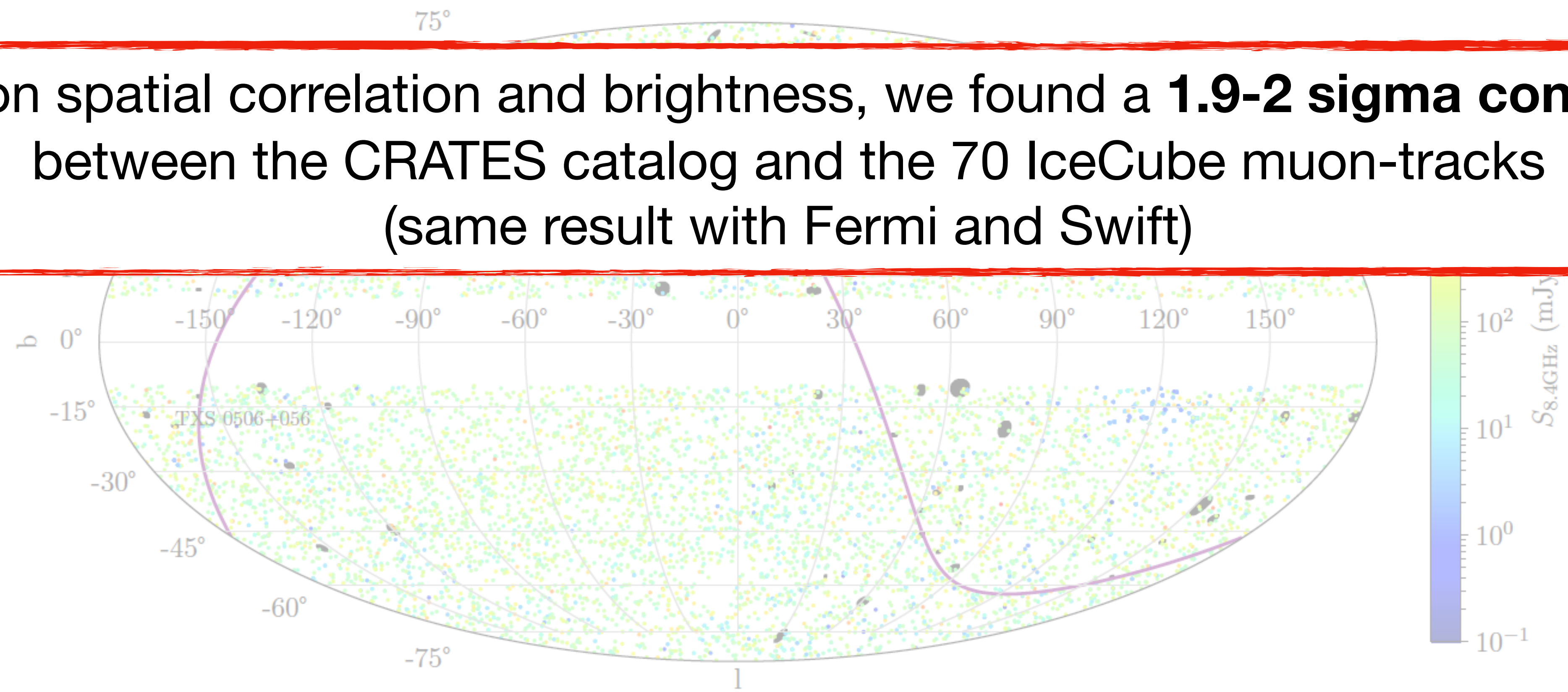

Based on spatial correlation and brightness, we found a **1.9-2 sigma connection** between the CRATES catalog and the 70 IceCube muon-tracks (same result with Fermi and Swift)

Figure 3. Galactic sky-position (l,b) and 8.4 GHz flux density of the CRATES radio sources (colored dots) and track-type neutrino detections of the IceCube Neutrino Detector (black filled ellipses) published by Giommi et al. (2020). The maps are shown in Mollweide projection. The equator is plotted by a purple continuous line. TXS 0506+056 and PKS 1502+106 are marked on the map.

Kun et al. 2022, submitted

CRATES + neutrinos

- Made a complete sample of CRATES (complete in luminosity redshift plane)
- Calculated how many neutrinos could be explained with this complete sample, if the probability of to detect a neutrino is proportional to the (k-corrected) radio flux
- Results: the **CRATES 4.8 GHz (8.4 GHz)** complete sub-sample **can explain between 4% and 53% (3% and 42%) of the neutrinos (90% C.L.)**.

Kun et al. 2022, submitted

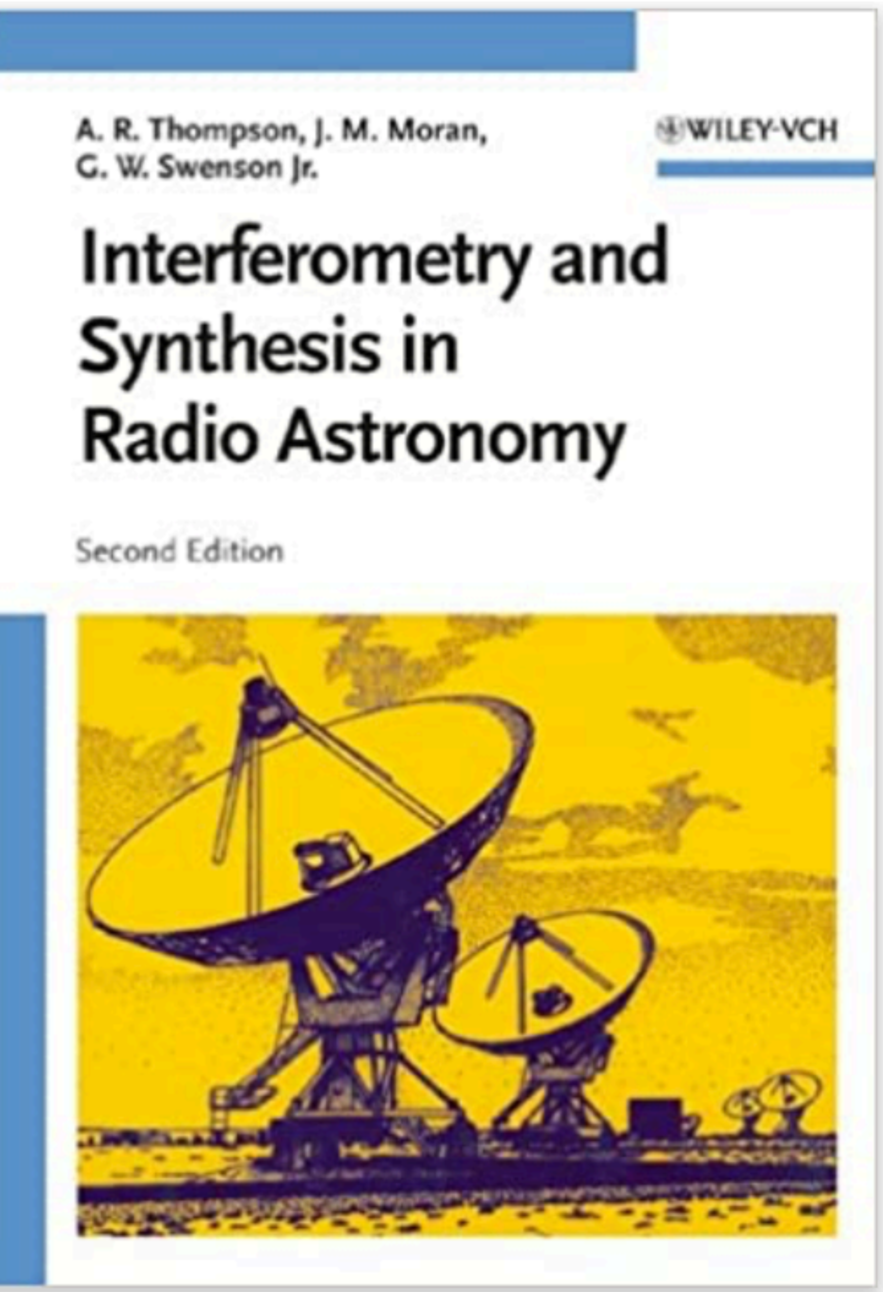

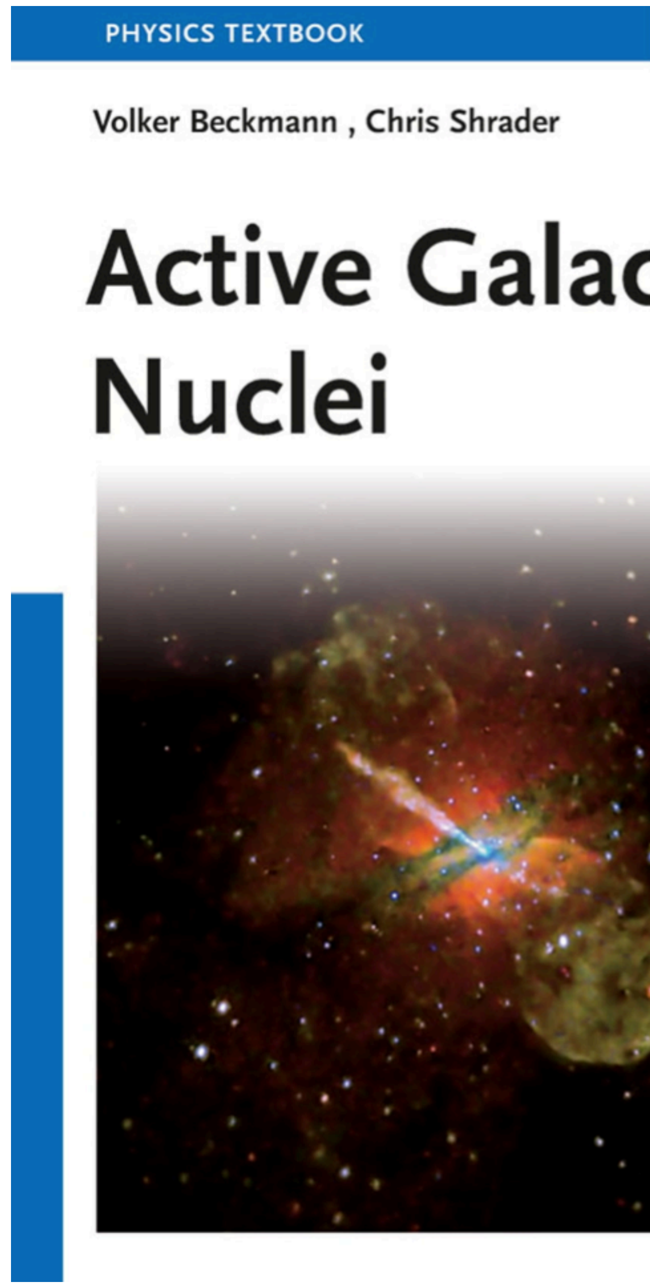

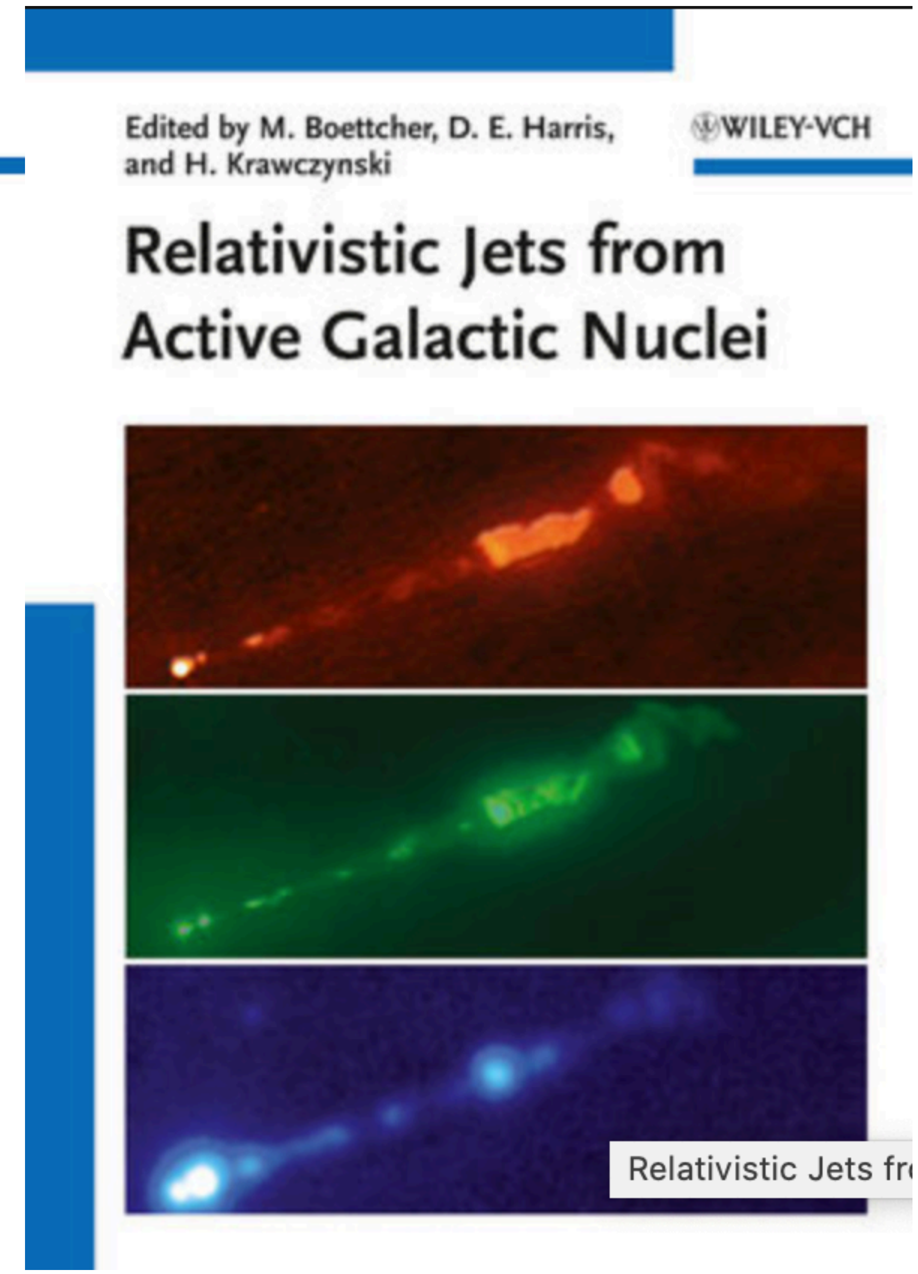

Recommended books

Thank you for your attention!

Questions?

If you are too shy or need help: kun.emma@csfk.org

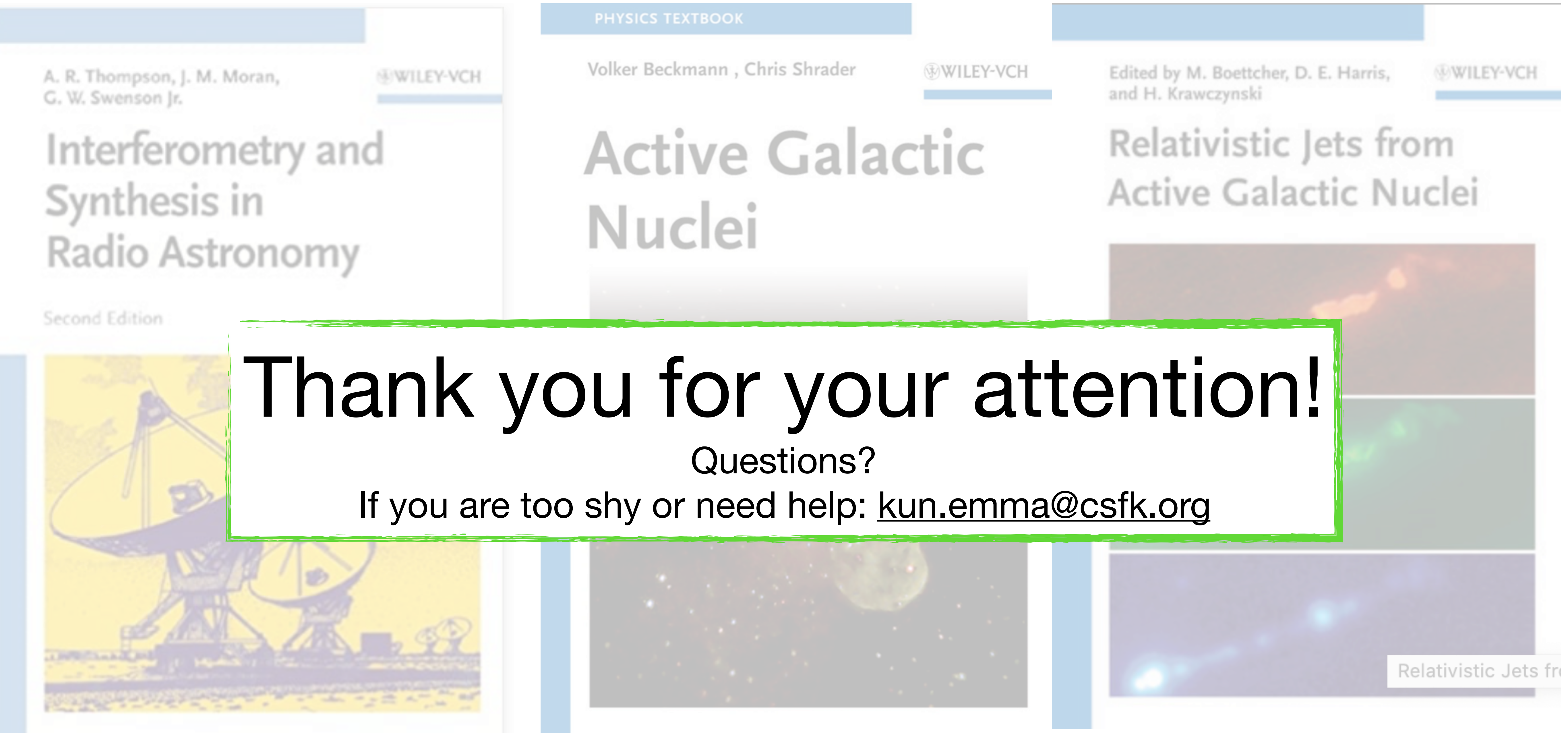

Recommended books